

Leveraging 6G Technologies to Optimize Information Freshness for Time-Sensitive Applications

Ali Muhammad

A Thesis
In
The Department of
Electrical & Computer Engineering

Presented in Partial Fulfillment of the Requirements
For the Degree of
Doctor of Philosophy (Electrical and Computer Engineering)
Concordia University
Montréal, Québec, Canada

September 2022

© Ali Muhammad, 2022

CONCORDIA UNIVERSITY
School of Graduate Studies

This is to certify that the thesis prepared

By: **Ali Muhammad**

Entitled: **Leveraging 6G Technologies to Optimize Information
Freshness for Time-Sensitive Applications**

and submitted in partial fulfillment of the requirements for the degree of

Doctor of Philosophy (Electrical and Computer Engineering)

complies with the regulations of this University and meets the accepted standards
with respect to originality and quality.

Signed by the final examining committee:

Dr. Yuhong Yan	Chair
Dr. Abdallah Shami	External Examiner
Dr. Roch Glitho	External to Program
Dr. Dongyu Qiu	Examiner
Dr. Anjali Agarwal	Examiner
Dr. Chadi Assi	Supervisor

Approved _____
Chair of Department or Graduate Program Director

_____ 2022 _____

Mourad Debbabi, Dean
Gina Cody School of Engineering and Computer Science

ABSTRACT

Leveraging 6G Technologies to Optimize Information Freshness for Time-Sensitive Applications

Ali Muhammad, Ph.D.

Concordia University, 2022

Next-generation wireless networks (Beyond 5G, 6G) aim to provide tremendous improvements over previous generations by promising a massive connectivity, ultra-reliable and low-latency communications, and soaring broadband speeds. Such transformation will give rise to a wide range of propitious Internet-of-Things (IoT) applications such as intelligent transportation systems (ITS), tactile internet, augmented/virtual reality, industry 4.0, etc. These applications possess stringent requirements of fresh and timely information updates to make critical decisions. Outdated or stale information updates are highly undesirable for these applications as they may call forth unreliable or erroneous decisions. The conventional performance metrics such as delay and latency may not fully characterize the freshness of information for time-critical IoT applications. Recently, information freshness has been investigated through defining a new performance metric termed as Age of Information (AoI). AoI offers a rigorous way to quantify the information freshness as compared to other performance metrics and is deemed suitable for real-time IoT applications.

In reality, the limited energy and computing resources of IoT devices (IoTDs) is a significant challenge towards realizing the timely delivery of information updates. To address this challenge, the first aim of this dissertation is to examine the capability of multi-access edge computing (MEC) towards minimizing the AoI. In fact, MEC offers an expedited computation of resource-intensive tasks, which, if processed locally at the IoTDs, may experience excessive computational latency. In this context, an optimization problem is setup to determine the optimal scheduling policy with the goal of minimizing the expected sum AoI of multiple IoTDs, while considering the combined impact of unreliable channel conditions and random packet arrivals.

Another acute challenge is the high randomness and uncontrollable behaviour of wireless communication environments, which may severely impede the timely and reliable delivery of information updates. Towards addressing this challenge, reconfigurable intelligent surface (RIS) is leveraged to mitigate the propagation-induced impairments of the wireless environment and enhance the quality of wireless links to preserve the information freshness. First, a wireless network consisting of a base station (BS) that is forwarding information updates of multiple real-time traffic streams to their destinations is studied. The considered multiple access technique is frequency division multiple access (FDMA), which is an orthogonal multiple access (OMA) technique. A joint user scheduling and phase-shift matrix (passive beamforming) optimization problem is formulated with the objective of minimizing the expected sum AoI of the coexisting multiple traffic streams. The resulting problem is a mixed integer non-convex optimization problem. To evade the high coupling of the invoked optimization variables, the bi-level optimization technique is utilized, where the original problem is decomposed into an outer traffic stream scheduling problem and an inner RIS phase-shift matrix problem. Owing to the stochastic nature of packet arrivals, a deep reinforcement learning (DRL) solution is employed to solve the outer problem. To do so, the traffic stream scheduling is modeled as a Markov Decision Process (MDP) and Proximal Policy Optimization (PPO) is invoked to solve it. On the other hand, the inner problem that determines the RIS configuration is solved through semi-definite relaxation (SDR).

Due to the limitations of OMA techniques in terms of the number of served IoT devices and the spectral efficiency, the focus of this dissertation shifts to explore non-orthogonal multiple access (NOMA) scheme towards achieving the goal of minimizing the AoI in an uplink setting. In this context, an optimization problem is formulated to optimize the RIS configuration, the transmit power of IoT devices and their clustering policy. To solve this mixed-integer non-convex problem, the RIS configuration is obtained first by resorting to difference-of-convex (DC) along with successive convex approximation (SCA). On the other hand, the bi-level optimization is used to solve the power allocation and the clustering problems. Optimal closed-form expressions are derived for the power control scheme and the one-to-one matching is employed to solve the clustering problem. Aiming to further improve the information freshness in time-critical IoT applications, an extended version of NOMA, termed as

Cooperative-NOMA (C-NOMA), is adopted. In C-NOMA, the cooperation between IoTDS through device-to-device (D2D) communication and full-duplex (FD) relaying is invoked within the NOMA scheme. In this context, the integration of RIS and C-NOMA is investigated towards achieving the goal of minimizing the average sum AoI. Precisely, it is investigated how much performance gain in terms of AoI reduction can be brought by the RIS-enabled uplink C-NOMA system compared to the conventional C-NOMA and NOMA schemes, both with and without RIS. Results elucidate the superiority of our proposed approaches against other baseline schemes. The findings in this dissertation shed light on the choice of effective design of wireless communication networks leveraging the core future enabling technologies.

Acknowledgments

Praise be to Allah Almighty, the Lord of the worlds. I can look back with pride and vividly recount the toiling days and sleepless nights in the journey to meet the deadlines.

Submitted with special thanks to my supervisor, Dr. Chadi Assi, for giving me the life-changing opportunity to join his lab. His invaluable leadership, boundless passion and incredible work ethic has been a constant source of inspiration. I am profoundly grateful for having had the privilege to work closely with him.

I would also like to thank Dr. Long Qu, Dr. Ibrahim Sarkhouh, Mohamed Amine Arfaoui, Mohamed Elhattab, Dr. Dariush Ebrahimi, and Dr. Ahmed Al-Hilo, for their technical feedback and cooperation. A big thank goes to Dr. Moataz Shoukry for his support and guidance both personally and work-wise. I am particularly grateful to my friend Dr. Hamed Abdzadeh Ziabari for always being there for me, through good and bad times.

I would like to express my sincere appreciation to the members of my Ph.D. advisory committee: Dr. Roch Glitho, Dr. Dongyu Qiu, and Dr. Anjali Agarwal for their valuable comments and constructive feedback which have helped me to improve the quality of this dissertation. I would also like to thank Dr. Abdallah Shami for accepting to be my external examiner.

I dedicate this accomplishment to my Parents; Syed Shabahat Hussain Naqvi (late) and Syeda Shahnaz Fatima, who took great pain for our wellbeing and success. Also, I am indebted to my siblings for their constant encouragement and support in thick and thin. Finally, I cannot help admiring patience of my wife and my daughters for their sacrifices and enduring broken promises as I undertook this work.

To my loving family!

Contents

List of Figures	xi
List of Tables	xiii
Abbreviations	xiv
1 Introduction	1
1.1 Motivation	2
1.2 State of the Art: Overview and Limitations	3
1.2.1 AoI Based Data Transmissions	3
1.2.2 MEC-Assisted Networks	5
1.2.3 RIS-Assisted Networks	6
1.2.4 NOMA/Cooperative-NOMA Enabled RIS Networks	8
1.3 Contributions	9
1.3.1 AoI Optimization in MEC-Assisted IoT Networks	9
1.3.2 AoI Optimization in RIS-Assisted IoT Networks	10
1.3.3 AoI Optimization in RIS-Assisted NOMA/ C-NOMA Based IoT Networks	11
1.4 List of Publications	12
1.4.1 Publications Related to the Dissertation	12
1.4.2 Publications Not Related to the Dissertation	13
1.5 Thesis Organization	14
2 Background	15
2.1 Background	16
2.1.1 Age of Information	16

2.1.2	Multi-Access Edge Computing	17
2.1.3	Reconfigurable Intelligent Surfaces (RIS)	19
2.1.4	Non-Orthogonal Multiple Access (NOMA)	22
3	AoI Optimization in MEC-Assisted IoT Networks	26
3.1	Motivation and Contributions	27
3.2	System Model	28
3.3	Illustrative Example	32
3.4	Problem Formulation	35
3.4.1	Preliminary Definitions	35
3.4.2	Scheduling Constraints	36
3.4.3	Computation Offloading Constraint	38
3.4.4	Mathematical Definition of Age of Information	38
3.5	Algorithmic Methods	42
3.5.1	Alternating Dual Minimization Algorithm	42
3.5.2	Age-Based Modified Greedy Algorithm (AMG)	46
3.5.3	Deep Reinforcement Learning (DRL) Based Solution	47
3.6	Simulation and Numerical Analysis	49
3.6.1	Simulation Setup	49
3.6.2	Simulation Parameters	49
3.6.3	Benchmark Schemes	50
3.6.4	Results and Discussions	51
3.7	Conclusion	58
4	AoI Optimization in RIS-Assisted IoT Networks	60
4.1	Motivation and Contributions	61
4.2	System Model	62
4.2.1	Network Model	62
4.2.2	Channel Model and SNR Analysis	64
4.3	Age of Information	67
4.4	Problem Formulation	69
4.4.1	Problem Formulation	69
4.4.2	Solution Approach	71
4.5	Simulation and Numerical Analysis	77

4.5.1	Simulations Setup	77
4.5.2	Benchmark Schemes	78
4.5.3	Results and Discussions	80
4.6	Conclusion	88
5	AoI Optimization In RIS-Assisted NOMA/C-NOMA Based IoT Networks	89
5.1	Motivation and Contributions	90
5.2	AoI optimization in RIS-assisted NOMA based IoT networks	91
5.2.1	System Model	91
5.2.2	Problem Formulation and Solution Approach	96
5.2.3	Simulation and Numerical Analysis	102
5.2.4	Extension to Multi-RIS Setting	105
5.2.5	Results and Discussions	108
5.2.6	Conclusion	110
5.3	AoI Optimization In RIS-Assisted C-NOMA Based IoT Networks	110
5.3.1	System Model	110
5.3.2	Problem Formulation and Solution Approach	114
5.3.3	Simulation Results	119
5.3.4	Conclusion	122
6	Conclusions and Future Research Directions	123
6.1	Conclusion	124
6.2	Future Research Directions	125
	Bibliography	128

List of Figures

2.1	AoI evolution vs. time.	17
2.2	MEC applications in wireless networks	18
2.3	RIS architecture	20
2.4	RIS applications in wireless networks	21
2.5	Multiple access techniques	22
2.6	Illustration of an uplink NOMA system	24
2.7	Illustration of a C-NOMA system.	25
3.1	An illustration of the system model.	30
3.2	The evolution of AoI.	33
3.3	Expected sum AoI for different arrival rates λ	52
3.4	Accumulated reward over time.	54
3.5	Impact of number of IoTDS on expected sum AoI.	55
3.6	Expected sum AoI for different arrival rates λ	56
3.7	AoI comparison under different channel conditions.	57
4.1	An illustration of our system model.	63
4.2	An illustration of the proposed solution.	70
4.3	Distance model.	78
4.4	Accumulated reward vs. iterations.	81
4.5	Impact of number of RIS elements on the AoI.	82
4.6	Impact of arrival rate on the AoI.	84
4.7	Impact of the position of RIS on the AoI	85
4.8	The performance comparison of different algorithms for a sample of three traffic streams.	86
5.1	An illustration of the system model.	92
5.2	Problem decomposition and solution flow.	95
5.3	Performance evaluation.	104

5.4	An illustration of the system model.	106
5.5	Performance evaluation.	108
5.6	RIS-assisted uplink C-NOMA based IoT network.	111
5.7	Performance evaluation	120

List of Tables

3.1	Table of notations.	32
3.2	The calculation of AoI.	34
3.3	An example to demonstrate the evolution of AoI.	42
3.4	Simulation parameters.	50
3.5	Execution time (msec) ($\lambda = 1, p = 1$)	58
4.1	Simulation parameters.	79
5.1	Simulation parameters.	119

Abbreviations

AoI	Age of Information
AR	Augmented Reality
AWGN	Additive White Gaussian Noise
B5G	Beyond Fifth-Generation
BS	Base Station
CSI	Channel State Information
CSMA	Carrier-Sense Multiple Access
C-NOMA	Cooperative Non Orthogonal Multiple Access
CT	Cooperative Transmission
DC	Difference of Convex
DRL	Deep Reinforcement Learning
D2D	Device-to-Device Communication
DT	Direct Transmission
DF	Decode and Forward
ESA	Expected Sum Age of Information
FCFS	First-Come-First-Serve
FPGA	Field-Programmable-Gate-Array
FD	Full-Duplex
HD	Half-Duplex
IoT	Internet of Things
IoTDs	Internet of Things Devices
ITS	Intelligent Transportation System
LoS	Line of Sight

LP	Linear Programming
MEC	Multi-Access Edge Computing
MDP	Markov Decision Process
MIMO	Multiple Input Multiple Output
MRC	Maximum-Ratio Combination
MINLP	Mixed Integer Non Linear Program
MRC	Maximum-Ratio Combination
NFV	Network Function Virtualization
NLoS	Non Line of Sight
NOMA	Non Orthogonal Multiple Access
OFDMA	Orthogonal Frequency Division Multiple Access
OMA	Orthogonal Multiple Access
PSD	Positive Semi-Definite
PPO	Proximal Policy Optimization
QoS	Quality of Service
RIS	Reconfigurable Intelligent Surface
SCA	Successive Convex Approximation
SDN	Software-Defined Networking
SNR	Signal to Noise Ratio
SDR	Semi-definite relaxation
TDMA	Time Division Multiple Access
UAVs	Unmanned Aerial Vehicles
UE	User Equipment
VNF	Virtual Network Function
VR	Virtual Reality

Chapter 1

Introduction

1.1 Motivation

Future generations of wireless communication networks are envisioned to provide tremendous improvements over previous generations by offering soaring broadband speeds (up to 1 Tb/s), a super-low latency (less than 1 msec), and a massive connectivity [1]. Such transformation is anticipated to bring forward a myriad of disruptive services, such as intelligent transportation systems (ITS), tactile internet, and industry 4.0 to name a few, which are enabled by a plethora of Internet of Things (IoT) devices. The crux of these applications is the critical decisions that rely on real-time information updates. For example, in cooperative autonomous driving systems, which is a potential ITS application, information updates, such as speed and vehicle position, along with other sensory data must be timely disseminated to other vehicles so that decisions, such as changing lanes or merging maneuvers, must be taken. Similarly, in remote surgery applications [2], the position of surgical tools and hand movements of the surgeon are the information updates that must be delivered in real-time otherwise may have serious consequences. Likewise, other related examples can be extracted from monitoring and control systems in smart industry [3], where fleet of collaborative robots (cobots) update the control center to carry out task assignment and other decisions. The above examples show that status updates must be disseminated in a timely manner to ensure that fresh data is always available at the receivers when critical decisions are made. Thus, reliability and timeliness in delivering status updates are of primordial importance for these real-time applications. Out-dated information updates are undesirable as being inconsistent with the current state of the system and may provoke unreliable/erroneous decisions. Unfortunately, the conventional performance metrics, such as delay and throughput, may not fully characterize the freshness of information for time-critical applications [4][5].

Information freshness has been investigated recently through defining a new performance metric, termed as Age of Information (AoI) [6–10]. AoI quantifies the freshness of status updates from the perspective of a destination and it is defined as the elapsed time since the most recent delivered status message was generated. AoI has brought a sheer novelty in specifying the information freshness against other metrics, such as delay and latency, for time-critical applications. Motivated by this, information freshness should be deeply investigated through the AoI metric in real time wireless networks, such as IoT networks [11], vehicular ad hoc networks (VANETs) [6], flying ad hoc networks (FANETs) [7], and mobile edge computing assisted networks [9], which is the focus of this dissertation. Specifically, the objective of this thesis is to propose novel solutions and frameworks to optimize the information freshness for real time applications through the AoI metric by leveraging 6G enabling technologies, such as non-orthogonal multiple access (NOMA), cooperative communication, reconfigurable intelligent surface (RIS), and multi-access edge computing (MEC). These technologies will be defined in details in the Background chapter 2.

1.2 State of the Art: Overview and Limitations

1.2.1 AoI Based Data Transmissions

AoI metric, owing to its applications in time-sensitive systems, has widely attracted the research community. The AoI problem has been addressed for a variety of applications, such as vehicular networks [6][12], Unmanned Aerial Vehicle (UAV) assisted communications [13, 14], edge caching [8, 15, 16], device-to-device (D2D) communications [17, 18], etc. The studies that investigated AoI minimization problem with stochastic arrivals are more relevant to this research and are briefly discussed in this section. In [10], a lower bound on the average age of information performance

is derived for networks with stochastic arrivals under three queuing systems: i.e., i) No queue, ii) Single packet queue and ii) First-in first-out queue. However, the remote processing of computation intensive tasks was not considered. The authors of [19] investigated the AoI in a carrier-sense multiple access (CSMA) based system employing the stochastic hybrid systems technique. They aimed to optimize the average AoI by adjusting the back-off time for each link. The authors of [20] discussed a system model where multiple sources update a single destination and the update frequency was optimized to minimize the age in first-come, first-served queueing system. In [21], the authors proposed near-optimal solution to address the optimization of AoI in wireless communication networks wherein Whittle’s index was used to capture the transmission urgency of terminals. The authors of [22] considered various sampling periods and sample sizes for each source node and proposed a low-complexity scheduling algorithm that achieves near-optimal performance when there is no synchronization among the nodes during the sampling process. The authors of [7] investigated AoI problem in the context of cellular Internet of UAVs and formulated a joint sensing, transmission time, UAV trajectory and scheduling optimization problem. The problem, being NP-hard, was decoupled into two subproblems and was solved using an iterative algorithm and a dynamic programming approach. The authors of [23] investigated the impact of first-come-first-serve (FCFS) and last-come-first serve with preemption (LCFS-PR) protocols under an ALOHA channel access scheme. It was observed that LCFS-PR outperforms FCFS in terms of minimizing both the peak and average AoI. The impact of channel access control (ALOHA) on age were monitored in both dense and sparse networks.

1.2.2 MEC-Assisted Networks

Recent years have seen a large number of studies dedicated to MEC systems as they provision computation resources in close proximity to end users. This approach results in better computation and improves the capabilities of end devices to run real-time applications [24]. Different objectives well studied in the literature are minimizing total energy consumption in a multi-user MEC system [25], the power-delay trade off [26], minimizing the execution latency by leveraging the load balancing between the mobile device and the server [27]. Nevertheless, the quality of service and quality of experience of the real-time applications highly depend on the freshness of information. Whereas, the computation offloading policies with conventional metric such as delay, cannot capture the timeliness of status update messages. Consideration of information freshness or AoI adds another dimension to the traditional MEC resource optimization problems. The studies that have addressed the challenges pertaining to age of information in the context of MEC systems are particularly relevant to this dissertation. For example, in [28], the AoI for computation intensive messages was studied with status update scenarios in MEC system. However, a single-source-single-destination system was considered and the closed-form average AoI was derived for exponentially distributed computing time. The authors of [29] studied the joint task generation and computation offloading policy and proposed a lightweight structure-based status update algorithm. Further, a Q-learning-based status update algorithm is proposed for unknown channel conditions. The authors of [30] studied the AoI minimization problem under energy constraints. Considering that prior knowledge of network dynamics is unavailable, an online algorithm based on stochastic gradient descent is proposed by jointly considering the randomness in energy arrivals, and the stochasticity of transmission and computing processes. In [31], the joint optimization

of energy spectral efficiency and average age of information of the network was investigated. The authors of [32] studied the AoI in MEC network and demonstrated that remote computing outperforms local computing when edge server has much higher computation capacities than that of the local device. The authors of [9] discussed MEC infrastructure utilization and provided a lower peak age of information for vulnerable road user information messages. The authors of [33] investigated the benefits of utilizing MEC in a medical IoT system. The task offloading problem with AoI and energy consumption constraints was modelled as a weighted game considering the cost of computation for each user and nash equilibrium is achieved among users in a decentralized manner. The authors of [34] studied the AoI in UAV-aided IoT network where UAVs were deployed as MEC servers for task computation. A one-node multi-source FCFS queuing model was presented where the AoI depends on the arrival rate of packets and the computation time of MEC node.

Most of the works in the literature for AoI in MEC systems either consider the deterministic arrivals or assumed that the communication channel is reliable between BS and destinations. This motivates us to study the AoI for computation intensive messages in an MEC system and concentrate on addressing the link scheduling optimization with stochastic packet arrivals under unreliable transmission conditions.

1.2.3 RIS-Assisted Networks

Due to its effectiveness, integration of RIS for enhancing the wireless communication has recently drawn a significant attention from the research community. In [35], the authors addressed the minimization problem of total transmit power at the transmitter by jointly optimizing the transmit beamforming through the active antenna array of the transmitter and the passive beamforming through the phase-shift elements of the RIS. The authors of [36] developed different free-space path-loss models

for RIS-assisted wireless communications, with the goal of enhancing the network coverage in a cost-effective and energy-efficient way through optimizing the phase-shifts of the RIS elements. Considering the potential challenges pertaining to spectrum and energy usage in D2D communication, the authors in [37] focused on an RIS-assisted uplink D2D-enabled cellular networks and investigated the joint power allocation and RIS phase-shift optimization problem with an objective to maximize the sum rate. The authors of [38] investigated the resource allocation problem for multi-user communication leveraging the RIS. More specifically, the total transmit power is minimized through an optimal design of the transmit power at the base station (BS) and the passive beamforming at the RIS. In [39], the authors proposed a two-way communication model assisted by an RIS, where the objective was to maximize the minimum received signal-to-interference-plus-noise ratio (SINR) at the cellular users by optimizing the RIS configuration. The paramount security performance of multi-input and multi-output wireless communication systems is probed by invoking the RIS in [40], where the aim was maximizing the secrecy rates through a proper design of the RIS configuration and the transmit power. However, none of these works studied the effect of the RIS on improving the AoI.

Recently, the authors of [41] addressed the AoI problem in UAV-assisted RIS networks with an objective to minimize average sum AoI by optimizing the altitude of UAVs, the RIS configuration and the scheduling decisions. Although the work in [41] is the first that studied the AoI minimization problem through the use of RIS, it considered the scheduling of only a single user within a given time-slot and ignored the direct channels from the BS to the users. To the best of our knowledge, the integration of RIS in time-sensitive applications, where the freshness of information is of critical importance, is still far from being mature. This motivated us to investigate the integration of RIS towards optimizing the information freshness in IoT networks.

1.2.4 NOMA/Cooperative-NOMA(C-NOMA) Enabled RIS Networks

The integration of RIS in NOMA-based systems has recently drawn a significant attention from the research community. The authors of [42] studied the joint power allocation, RIS phase-shift and hybrid beamforming problem to maximize the sum-rate in RIS-assisted millimeter wave NOMA system. The authors of [43] investigated the joint active and passive beamforming for RIS aided system to minimize the total transmit power. The problem was investigated under the assumption of two-user NOMA clusters. The authors of [44] studied the problem of maximizing the minimum achievable rate in order to ensure user fairness through joint active and passive beamforming optimization. In [45], integration of RIS with mmWave-NOMA system was considered. The authors investigated the optimization of power allocation joint with active and passive beamforming. The resulting non-convex problem was decomposed into sub-problems which were solved by leveraging alternative optimization and SCA. The focus of other related works to explore the benefits of RIS in NOMA-based systems had been on maximizing the sum data rate [46], augmenting the spectral efficiency [47], improving the network coverage range [48], enhancing the secrecy performance [49], and boosting the energy efficiency [50]. Moreover, the investigation of integrating RIS with Cooperative-NOMA(C-NOMA) is still in its infancy [51, 52]. Specifically, the authors of [51, 52] have studied the integration of RIS in downlink C-NOMA systems with the objective of minimizing the total transmit power. However, the above proposed approaches may not be necessarily optimal neither for the freshness of information nor for uplink transmissions. This fact is the main motivation to study the impact of RIS on NOMA/C-NOMA based networks towards optimizing the information freshness.

1.3 Contributions

The main goal of this dissertation is to address the limitations of the state-of-the-art. In this context, the main contributions are summarized as follows:

1.3.1 AoI Optimization in MEC-Assisted IoT Networks

IoT applications such as Augmented/Virtual reality, tactile internet, immersive gaming, etc., are currently experiencing an unprecedented growth in their demand. IoT devices (IoTDs) are constrained by limited computation and power features and might experience excessive computational latency to support resource-intensive tasks. MEC appears to be a promising solution in this regard to expedite the computations of resource-intensive tasks by offloading them to the edge of the network. In this context, this contribution considers a scenario where a BS serves traffic streams from multiple IoTDs. The packets from each stream arrive at the BS (following a stochastic process) and then forwarded to their respective destinations after they are processed by the MEC node. The scheduling decisions are aimed to keep the information fresh at the destination and the information freshness is captured by AoI metric. We aim to minimize the expected sum AoI for the MEC-assisted IoT network and provide mathematically traceable expressions for the AoI. An optimization problem is formulated to find the optimal scheduling policy in order to minimize the expected sum AoI considering the joint impact of stochastic arrivals and unreliable channel conditions. We also propose low-complexity algorithms to obtain results for larger networks. Finally, through extensive simulations, we demonstrate the effectiveness of our proposed methods as compared to other existing strategies. Our finding for this aim were published in [53].

1.3.2 AoI Optimization in RIS-Assisted IoT Networks

In the previous contribution, we discussed the AoI problem evaluating the combined impact of stochastic packet arrivals, scheduling policy and unreliable channel conditions. As a next step, we aim to leverage the RIS to preserve the information freshness. In this regard, this contribution considers a wireless network consisting of a BS that is serving multiple real-time traffic streams forwarding information updates to their destinations. Since the wireless channels may be unreliable due to the impurities of the propagation environments, such as deep fading, blockages, etc., we integrate RIS to the wireless system in order to mitigate the propagation-induced impairments, enhance the quality of the wireless links, and ensure that the required freshness of information is achieved. For this network set-up, we investigate the joint optimization of the traffic streams scheduling and the RIS phase-shift matrix with the goal of minimizing the long-term average AoI. The formulated optimization problem is a mixed integer non-convex optimization problem, which is difficult to solve. To circumvent the high-coupled optimization variables, and with the aid of bi-level optimization, we decompose the original problem into an outer traffic stream scheduling problem and an inner RIS phase-shift matrix problem. For the outer problem, owing to its complexity and stochastic nature of packet arrivals, we resort to deep reinforcement learning (DRL) solution where the traffic stream scheduling is modeled as a Markov Decision Process (MDP), and Proximal Policy Optimization (PPO) is invoked to solve it. Whereas, the inner problem that determines the RIS configuration is solved through semi-definite relaxation (SDR). Finally, we show through extensive simulations that our approach evaluates the combined impact of scheduling policy and RIS configuration on the long term average AoI, where we demonstrate its superiority against other baseline schemes. Our finding for this aim in parts were published in [54] and are submitted for possible publication in [55].

1.3.3 AoI Optimization in RIS-Assisted NOMA/ C-NOMA Based IoT Networks

The previous contribution showed that RIS can counter the propagation-induced impairments of the wireless links and can enhance the channel quality to ensure that the required freshness of information is achieved. However, the considered system model focused on orthogonal multiple access (OMA) scheme, where a single traffic stream may transmit its information update on a particular resource block (time and/or frequency) [56]. Now that we have established an RIS-assisted system model, we want to explore the potential benefits of other multiple access schemes (i.e., NOMA and C-NOMA) towards the objective of minimizing AoI. This contribution first investigates the benefits of integrating RIS on minimizing the average sum AoI in uplink NOMA-based IoT networks. A problem is formulated to optimize the RIS configuration, the transmit power of IoTDs and their clustering policy. The formulated problem is a mixed-integer non-convex one, and in order to solve it, we obtain first the RIS configuration by resorting to difference-of-convex (DC) and successive convex approximation (SCA). Afterwards, the joint power allocation and clustering problem is solved using the concept of bi-level optimization and is decomposed into an outer IoTDs clustering problem and an inner power allocation problem. Optimal closed-form expressions are derived for the inner problem and the one-to-one matching is employed to solve the outer one. As a second part of this contribution, we investigate the potential of integrating RIS and C-NOMA scheme in preserving the freshness of information. In this setup, an optimization problem has been formulated to minimize the average sum AoI by optimizing the transmit power of the IoTDs and the RIS phase shift matrix. A closed-form solution has been derived for the power control sub-problem and the SDR approach is adopted for the RIS configuration sub-problem. Simulation results demonstrate that our proposed RIS-empowered uplink C-NOMA

scheme achieves higher AoI-reduction compared to all baseline schemes. Our finding for this aim were submitted for possible publication in [57], [58], [59].

1.4 List of Publications

This dissertation has led to the key publications enumerated in Section 1.4.1. Moreover, I investigated the problem of multi-source multi-cast resource optimization in softwarized networks and my publications within this research direction are enumerated in Section 1.4.2.

1.4.1 Publications Related to the Dissertation

Journal Publications

1. **Ali Muhammad**, Ibrahim Sorkhoh, Moataz Samir, Dariush Ebrahimi and Chadi Assi, "Minimizing Age of Information in Multi-Access Edge Computing-assisted IoT Networks," in *IEEE Internet of Things Journal*, Dec. 2021.
2. **Ali Muhammad**, Mohamed Elhattab, Mohamed Amine Arfaoui and Chadi Assi, "Optimizing Information Freshness in RIS-assisted NOMA-based IoT Networks," in *IEEE Transactions on Vehicular Technology*, Jan 2022 (second round revision).
3. **Ali Muhammad**, Mohamed Elhattab, Mohamed Amine Arfaoui, Ahmed-Al Hilo and Chadi Assi, "Age of Information Optimization in *RIS-Assisted Wireless Networks*," in *IEEE Transactions on Network and Service Management*, June 2022 (first round revision).
4. **Ali Muhammad**, Mohamed Elhattab, Mohamed Amine Arfaoui and Chadi Assi, "Optimizing Age of Information in RIS-Empowered Uplink Cooperative

NOMA Networks,” in *IEEE Communications Letters*, Mar 2022 (second round revision).

Conference Publications

1. **Ali Muhammad**, Mohamed Elhattab, Moataz Samir and Chadi Assi, ”Leveraging Reconfigurable Intelligent Surface To Minimize Age Of Information In Wireless Networks,” in *IEEE International Conference on Communications (ICC)*, Seoul, South Korea, 2022.
2. **Ali Muhammad**, Mohamed Elhattab, Mohamed Amine Arfaoui and Chadi Assi, ”Optimizing Information Freshness Leveraging Multi-RISs in NOMA-based IoT Networks,” submitted to *IEEE Global Communications Conference (GLOBECOM)*, Rio de Janeiro, Brazil, 2022.

1.4.2 Publications Not Related to the Dissertation

1. **Ali Muhammad**, Long Qu and Chadi Assi, ”Delay-Aware Multi-Source Multicast Resource optimization in NFV-Enabled Network,” in *IEEE International Conference on Communications (ICC)*, Dublin, Ireland, 2020, pp. 1-7.
2. **Ali Muhammad**, Ibrahim Sorkhoh, Long Qu and Chadi Assi, ”Delay-Sensitive Multi-Source Multicast Resource Optimization in NFV-Enabled Networks: A Column Generation Approach,” in *IEEE Transactions on Network and Service Management*, vol. 18, no. 1, pp. 286-300, March 2021.

1.5 Thesis Organization

This thesis is organized as follows. Chapter 2 presents a background of the emerging technologies. Chapter 3 provides our contribution of solving the AoI minimization problem in MEC-assisted IoT Networks. Chapter 4 discusses how the RIS can be leveraged to minimize AoI in wireless communication network. Chapter 5 provides our third contribution, where NOMA and C-NOMA schemes are investigated in uplink settings with and without RIS. Finally Chapter 6 concludes this thesis with future directions.

Chapter 2

Background

This chapter succinctly discuss related concepts and notions that are used in this thesis. We present the concepts of age of information, multi-access edge computing, reconfigurable intelligent surface, and non-orthogonal multiple access scheme.

2.1 Background

2.1.1 Age of Information

Emerging IoT applications require efficient, timely and reliable delivery of information updates to make necessary decisions. Referring to an IoT network, where a single or multiple IoTDs are deployed to monitor and sense some physical processes e.g., environment monitoring in sensor networks [60]. Then, the sensed information updates are sent to the respective destinations to extract useful information from these updates to make critical decisions. Indeed, the accuracy and correctness of these decisions largely depend on the freshness of the information at the destination. However, depending on the application, the duration over which the information can still be considered as fresh could vary. For example, applications that are directly related to human safety, such as lane changing in autonomous driving system, will have this duration much smaller than the ones dedicated to temperature monitoring [61].

AoI is fundamentally different from other performance metrics such as the delay or latency as the latter measure the information freshness from the perspective of individual packets. However, AoI quantifies the information freshness from the destination's perspective where the timeliness is counted from the time, the information is generated (or sampled) until its delivery to the destination. More precisely, AoI measures the time elapsed since the most recent delivered status message was generated, whereas the delay measures the time elapsed from the generation of a packet to its delivery. Figure 2.1 illustrates the evolution of AoI of a single IoTd, which

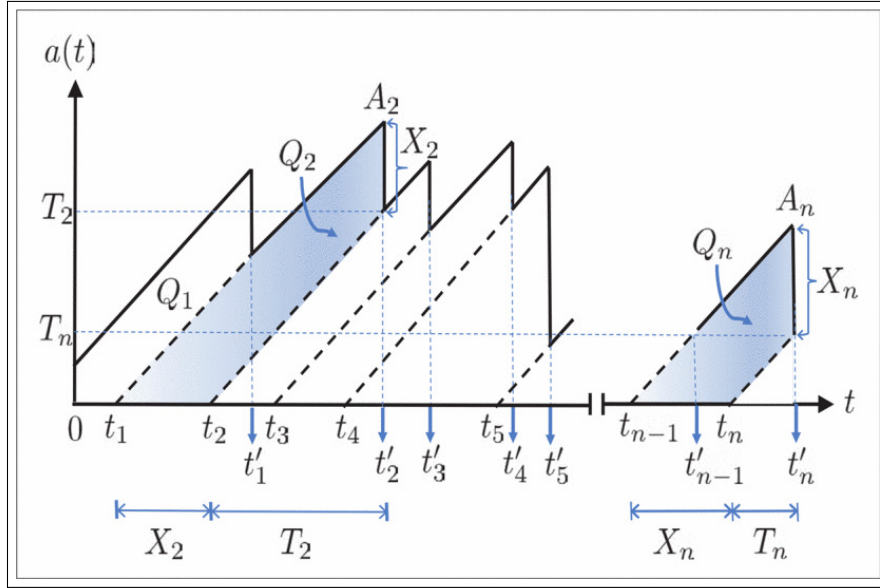


Figure 2.1: AoI evolution vs. time. [61]

is given by a solid line, whereas the dashed line denotes the elapsed time since the status update of the IoT device was generated. In this illustration, it is assumed that a single packet can be transmitted in a given time-slot and IoT device transmits n packets towards a destination. X_n denotes the inter-arrival time between packets n and $n - 1$, t_n and t'_n denote the transmission and reception time instances of a packet n , whereas, T_n represents the time elapsed since the packet n was generated until it is received at the destination. It can be observed from the Figure 2.1 that AoI linearly increases in each time-slot until the successful delivery of a packet, where the AoI is decreased.

2.1.2 Multi-Access Edge Computing

Multi-access Edge Computing (MEC)[62], previously termed as Mobile Edge Computing, is a paradigm that extends the cloud computing resources to the edge of the network. MEC was introduced by European Telecommunications Standards Institute (ETSI) realizing the mobile communication, but since then its benefits reach

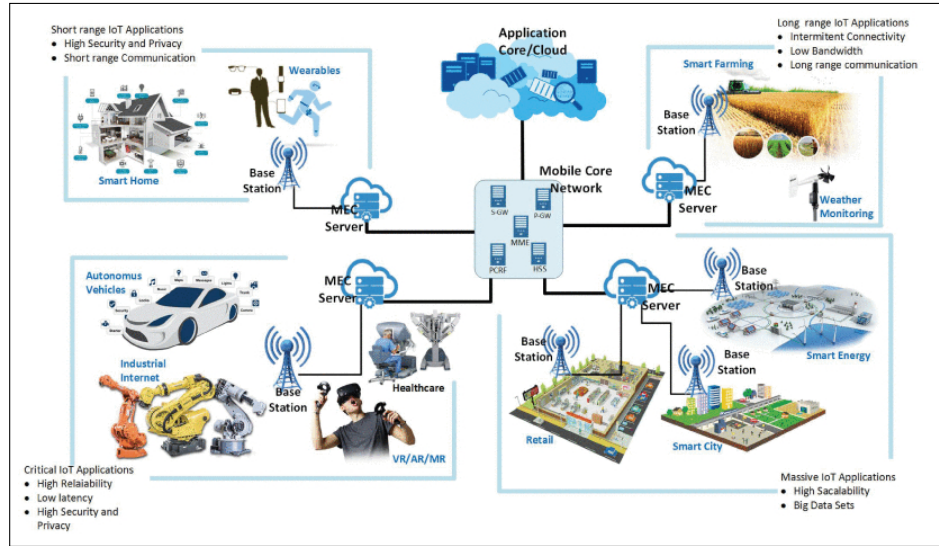


Figure 2.2: MEC applications in wireless networks [63].

beyond mobile and into the fixed access technologies [63]. The main idea of MEC is to bring computation and data storage closer to the user devices. Imagine a video surveillance camera connected with a Long Term Evolution (LTE) network that is forwarding the video streams to MEC server in order to perform real-time processing and anomaly detection. The MEC operation is indeed beneficial for both users and network operators. From a user’s perspective, resource-constrained devices could be free from running computation-intensive and delay-constrained applications locally. On the other hand, a network operator may reduce its core network congestion by moving applications on the network edge. MEC enhances the capabilities of end devices and allows them to offload their computation intensive tasks onto the edge of the network. The MEC servers are equipped with intelligent functions to process the resource-intensive tasks which are offloaded by the IoT devices. This can be achieved by first assigning a processing task of an IoT device to an MEC server through an uplink channel. Then, the required computing resources are allocated at the MEC server for the resolution of the task. Once done, the computation result is fed back to the IoT device through a downlink channel. This three step process is termed as ”offloading”

and this task-offloading may result in significant reduction of computing time of the tasks, which, if processed locally at IoT devices, may experience excessive computational latency. However, optimal resource assignment is a key challenge towards realizing the potentials of MEC [64]. Precisely, the core benefits of MEC architecture are reduced network congestion, enhanced bandwidth utilization, and lower latency-communication. Figure 2.2 illustrates different use cases of MEC in critical IoT applications, massive IoT applications, long range IoT applications and short range IoT applications, where the benefits of MEC such as low latency communication, improved reliability, enhanced security and privacy of IoT devices can be fully realized.

2.1.3 Reconfigurable Intelligent Surfaces (RIS)

RIS has been proposed as a new paradigm that will enable the next-generation networks by achieving smart and reconfigurable wireless channel propagation environments [65]. Generally, the wireless propagation suffers from impurities such as deep fading, blockages, etc. In this regard, the RIS has been envisioned as a revolutionizing technology to circumvent the impairments of the wireless propagation environments and enhance the spectrum and/or energy efficiency of the wireless communication networks. This can be achieved by reshaping and re-configuring the wireless environment, i.e., constructing a strong channel between the source and destination by recognizing the alternative propagation routes through which the information-bearing signal can be received at the point-of-interest [66]. From the construction's aspect, a typical architecture of RIS consists of three layers and a controller as shown in Figure 2.3. The outermost layer is composed of passive elements which are printed on a dielectric substrate to interact with the incident signals. The intermediate layer is composed of a copper plate which aims to minimize the signal energy leakages. The innermost layer is a control circuit board which is responsible for tuning and exciting

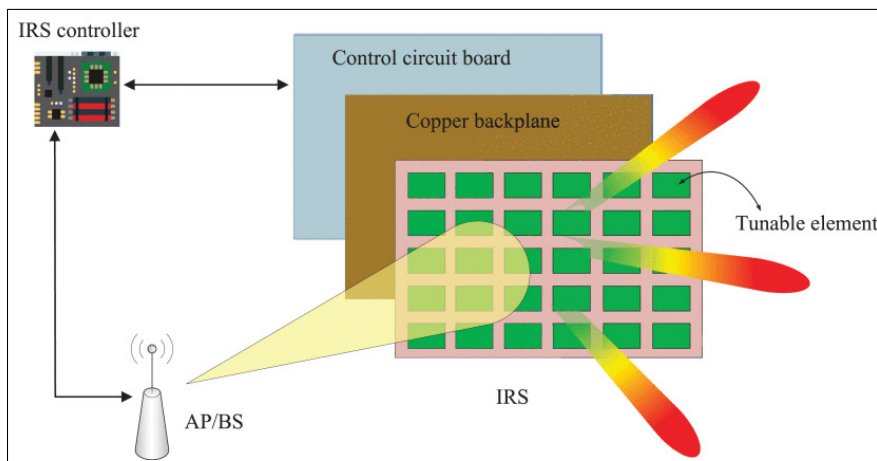


Figure 2.3: RIS architecture [67].

the reflective elements triggered by a smart controller attached to RIS. The controller can be implemented by a field-programmable gate array (FPGA) and considered as a gateway to coordinate/communicate with other components such as base station, access point, or a user terminals [67]. Precisely, RIS is a planar surface consisting of an array of passive elements. Each element receives the superposed multi-path signals from the BS (transmitter) and the combined signal is then scattered with adjustable phase and/or amplitude leading to a multiplicative channel model. Therefore, the signals transmitted within the wireless propagation environments can be controlled, and through a proper adjustment of the phase shifts of all the RIS elements, the desired signals at the points of interest can be enhanced [68]. RIS carry several practical advantages as compared to contemporary technologies such as active relay and backscatter communication, which are briefly discussed here. First, the RIS reflecting elements do passively reflect the impinging signals without the need of any active transmit module (i.e., power amplifier). Second, the RIS operates in full-duplex mode where it is free of any noise amplification/processing and self-interference. Third, the RIS has lightweight and low profile structures which can be easily mounted on walls and facades of buildings [67].

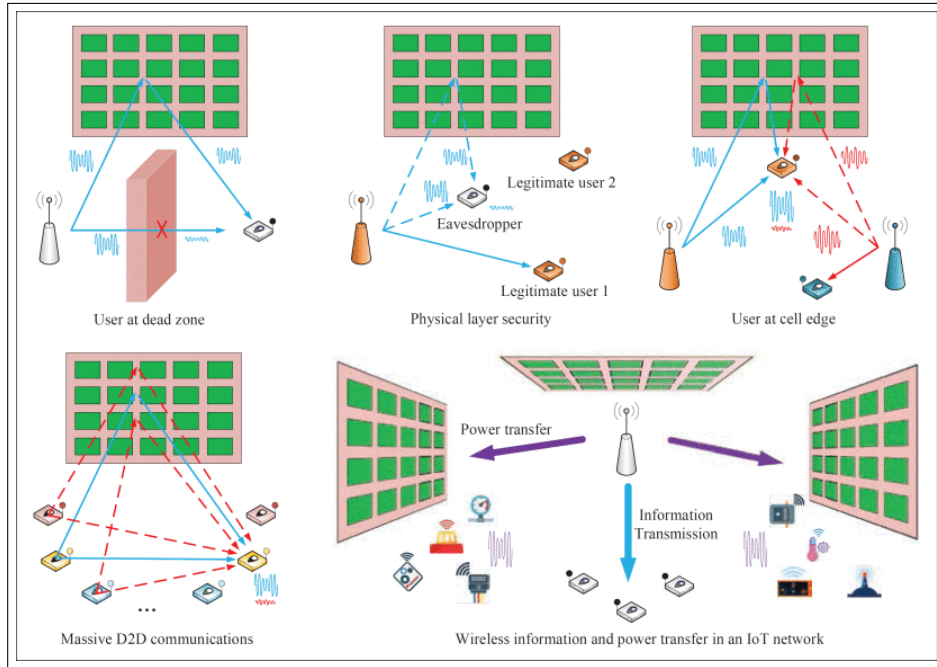
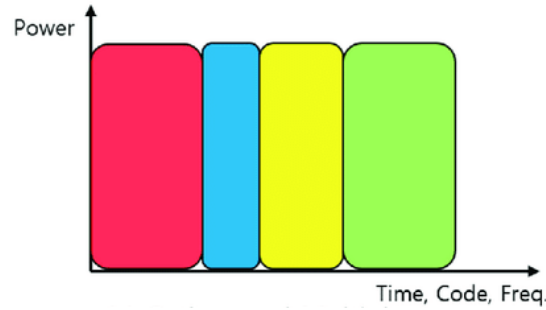


Figure 2.4: RIS applications in wireless networks [69].

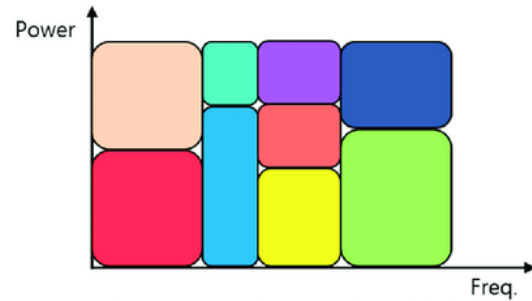
Figure 2.4 depicts that RIS can be used to support various applications, for example, consider a user at a dead zone with no coverage as the direct link between the user and its serving base station is blocked due to an obstacle. In this case, RIS can be deployed at a place where it has clear links between the user and the BS and it will help to create a virtual line of sight link through smart reflection to bypass the obstacle. Another application is physical layer security, where RIS can be used to reduce information leakage by canceling out the impact of the reflected signals of the eavesdropper. Moreover, in another application RIS can help the cell-edge user to not only enhance the desired signal power but may also reduce the interference from the neighbouring BS. In the light of the above discussion, it is evident that RIS can empower wireless communication networks for bypassing obstacles, improving coverage extension, reducing information leakage, enabling massive communication, and improving the power transfer efficiency. For more details on RIS, interested readers are referred to [70] [71].

2.1.4 Non-Orthogonal Multiple Access (NOMA)

NOMA is deemed as a promising multiple access scheme for future wireless networks due to its ability to allow multiple users to simultaneously access the same wireless resources. Contrary to OMA schemes, where only a single user can transmit its information on a specific resource block, NOMA empowers multiple users to utilize the same time/frequency resource to transmit their information and achieves superior spectral efficiency performance [72]. Figure 2.5(a) illustrates OMA scheme, where each user's information is transmitted over the available time/frequency resource in an orthogonal manner (resource allocated to different users is colored differently). Despite that, there is no interference among users, the total number of served users is limited. Figure 2.5(b) depicts that with NOMA, different user's information can be multiplexed in the same time/frequency resource by assigning different power levels.



(2.5.a) OMA.



(2.5.b) NOMA.

Figure 2.5: Multiple access techniques [73].

However, this is achieved by adopting a superposition coding (SC) at the transmitter side with proper power allocation and by performing a successive interference cancellation (SIC) at the end receivers to cancel the inter-NOMA user interference [74]. For example, in downlink setting, the BS schedules different users on the same resource but the messages of different users are transmitted using different power levels. In order to decode its own message, each user can apply SIC by exploiting the power differences. The operation of NOMA in uplink and downlink are different, relevant to this dissertation, we now discuss the working of uplink NOMA.

In uplink NOMA systems, each user transmits its own message over the same resource as other users towards the BS. All the signals despite causing interference to each other, are the desired signals for the BS. In order to decode each user's individual signal, BS adopts SIC. In this context, the signal from the user with the highest channel gain is likely the strongest one and decoded first. Hence, the user with the highest channel gain experiences the interference from rest of the users. Next, the user with the second highest channel gain will be decoded and so forth. Consequently, the user with the lowest channel gain will experience no interference.

Figure 2.6 demonstrates a 3-user uplink NOMA system where x_1, x_2, x_3 denote the messages and h_1, h_2, h_3 denote the channel gains of user1, user2, and user3 respectively, where $h_1 > h_2 > h_3$ and w_0 denotes the additive white Gaussian noise. As discussed earlier, the user's signal with the highest channel gain will be decoded first and will experience interference from the remaining users. Being said that, the achievable data rate for each user i can be given as:

$$R_i = \omega B \log_2 \left(1 + \frac{P_i \gamma_i}{\sum_{j=i+1}^3 P_j \gamma_j + \omega} \right), \quad (2.1)$$

where $\gamma_i = \frac{h_i}{N_0 B}$ is the normalized channel gain, N_0 is the noise spectral density, ω is the total number of channels, B is the transmission bandwidth of each channel,

and P_i is the transmission power of user i . The power allocation primarily depends on the performance metric, such that rate maximization, AoI minimization, etc., and the corresponding operating constraints.

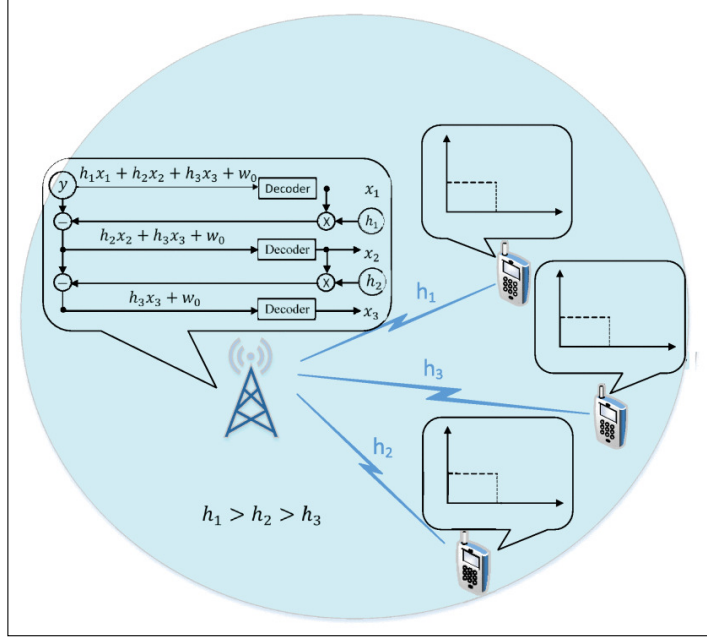


Figure 2.6: Illustration of an uplink NOMA system [75].

To further enhance the performance of NOMA systems and realizing the demanding requirements of 6G wireless networks [76] [77], the integration of NOMA, cooperative relaying techniques and device-to-device (D2D) communication, which is known as cooperative NOMA (C-NOMA), has been proposed [78]. In C-NOMA, the user with typically good channel conditions may act as a relay to aid the transmission of the user with the bad channel conditions. Figure 2.7 illustrates a system which consists of one BS, one far user and one near user. There are three links in the presented system model, first one is the direct transmission (DT) link from near user to the BS, second DT link is between far user and the BS. The third one is a cooperative transmission (CT) link between the far and near user. In the presented uplink C-NOMA system, the far user transmits its signal to the BS and to the near user

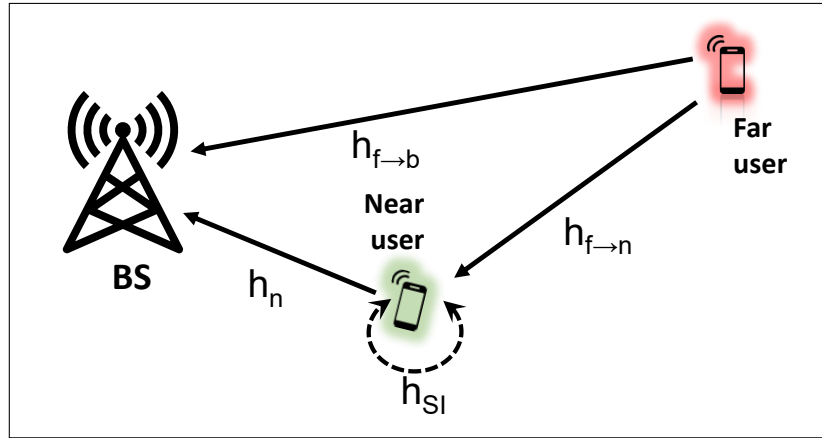


Figure 2.7: Illustration of a C-NOMA system.

simultaneously, while the near user, upon receiving the signal of far user decodes it first and then forwards this decoded signal of far user along with its own signal using SC to the BS. Generally, there are two possible decode and forward (DF) relaying modes that near user can adopt, either a half-duplex (HD) relaying mode or a full-duplex (FD) relaying mode. In HD mode, the DT phase and the CT phase occur in two consecutive time-slots, whereas, in FD mode, the direct transmission and the cooperative transmission both occur in the same time slot.

According to NOMA principle, both users will be served simultaneously within the same time/frequency resource block to provide their information to the BS. There are two possible decoding orders at the BS, either decode the far user first or decode the near user first. Assume that decoding order is to decode the far user first. In this case, the BS will employ maximum-ratio combination (MRC) to combine the signal that is directly transmitted by far user with the superimposed signal that is directly transmitted by near in order to decode far user. Once achieved, the signal of the far user will be subtracted from the total received signal at the BS to obtain the signal of near user[79]. For more details, readers are refer to [80], [81].

Chapter 3

AoI Optimization in MEC-Assisted IoT Networks

3.1 Motivation and Contributions

Real-time applications demand intensified computing capabilities to process status update messages but IoT devices are usually on low-budget for energy and computing resources. This might cause excessive computational delays to process resource-intensive tasks which may inversely impact AoI. MEC [62] appears to be a promising solution in this regard to enhance the capabilities of end devices by allowing them to offload their computation intensive tasks onto the edge of the network. The MEC servers are equipped with intelligent functions to process the resource-intensive tasks which are offloaded by the IoT devices. This task-offloading may result in significant reduction of computing time of the tasks, which, if processed locally at IoT devices, may experience excessive computational latency.

In this chapter, we study scheduling algorithms that attempt to minimize the expected sum AoI in a network with multiple traffic streams of IoT devices (deployed for critical applications). The packets from these traffic streams arrive to the base station following a stochastic process and are forwarded to their respective destinations over unreliable channels after they get processed by an MEC host. Note that an application in the MEC host executes compute-intensive functions with much higher performance on behalf of IoT users. The time is divided into time-slots and at each time-slot, the algorithm performs two scheduling decisions, i.e., schedule a packet from its queue to the MEC node, and schedule a processed packet from its queue to its relative destination with a goal to keep the information fresh at each destination. In short, we aim to answer the following questions: How the expected sum AoI can be minimized in this computation-intensive information-update system under probabilistic arrivals? How to properly allocate the packets of input streams to the MEC node and in which order? How to efficiently schedule packets to their respective destinations under unreliable transmission conditions?

We can summarize the main contributions as:

- Formulation of an optimization problem to find the optimal scheduling policy under single packet queue system with an objective to minimize the expected sum AoI by jointly considering the stochastic arrivals, processing at MEC node and unreliable channel conditions.
- Following that the optimization problem is difficult to solve, we provide a more traceable expression for the expected sum AoI and propose two low-complexity algorithms, (i) Alternating Dual Minimization algorithm (ADM), and (ii) Age-based Modified Greedy algorithm (AMG).
- The proposed solution is assessed by comparing it with other existing approaches. Through experimental analysis, we verify that a careful scheduling of the streams results in a lower expected sum AoI.

3.2 System Model

We consider a wireless network with a BS that serves packets from I traffic streams down-link to I destinations as shown in Figure 3.1.¹ The time is slotted with time-slot index $t \in \{1, 2, \dots, T\}$ where T is the time-horizon of this discrete-time system. At the beginning of every time-slot t , a packet from the stream $i \in \{1, 2, \dots, I\}$ arrives at its respective in-queue (i.e., Q_i) with probability $\lambda_i \in (0,1], \forall i$. This arrival of packets follows a Bernoulli process which is independent and identically distributed over time, and independent across different streams. The packet from stream i stays in the in-queue until the BS schedules it for processing at the MEC node. In each time-slot t , the BS either idles or schedules a packet from queue i to be processed

¹In this work, each information update message generated by a source is represented as a packet [32] [82][83] and once processed by MEC node can be successfully transmitted in a given time-slot to the respective destination if the channel is ON.

by the MEC node. The packets scheduled by the BS are processed by a softwarized network function hosted by the MEC node that is co-located with the BS. (Note that according to 5G system architecture and MEC [84], there are multiple options for physical deployment of the MEC hosts which are based on different operational, performance or security related requirements. Out of the several possible options, MEC is considered feasible to be collocated with the BS). The processed packet from stream i stays in the out-queue (i.e., \hat{Q}_i) before it is scheduled for transmission to the destination. The \hat{Q}_i is a single packet queue, hence a packet waiting in \hat{Q}_i would be pre-empted by a new processed packet.

We assume a single packet queue system such that when a new status packet is arrived in the queue, the older one is replaced by the new one. The reason being that destination will not benefit from receiving an outdated status update. So, at any time, if there are two status update packets in the system, one packet carrying the most recent state and the other one with old information. The packet with the recent information must be delivered. The similar approach has been adopted in [85–87]. We consider that MEC node can process one packet at a time. However, at any time-slot more than one packets of a traffic stream i could be available in the system; e.g., one packet of stream i available in Q_i (i.e., $a_i^t = 1$, where a_i^t indicates the arrival of a packet) while another packet after completing its processing at MEC node arrives to \hat{Q}_i to get transmitted to the destination.

The processed packets are transmitted to their respective destination nodes by the BS. The channel between BS and the destinations is unreliable and hence loses packets, which indeed demands the BS to hold the outgoing packet in its queue until the successful reception of the packet at the destination, otherwise the packet is replaced by a new processed packet. In this work, it is assumed that we have a statistical description of the channel gain rather than having a deterministic fixed

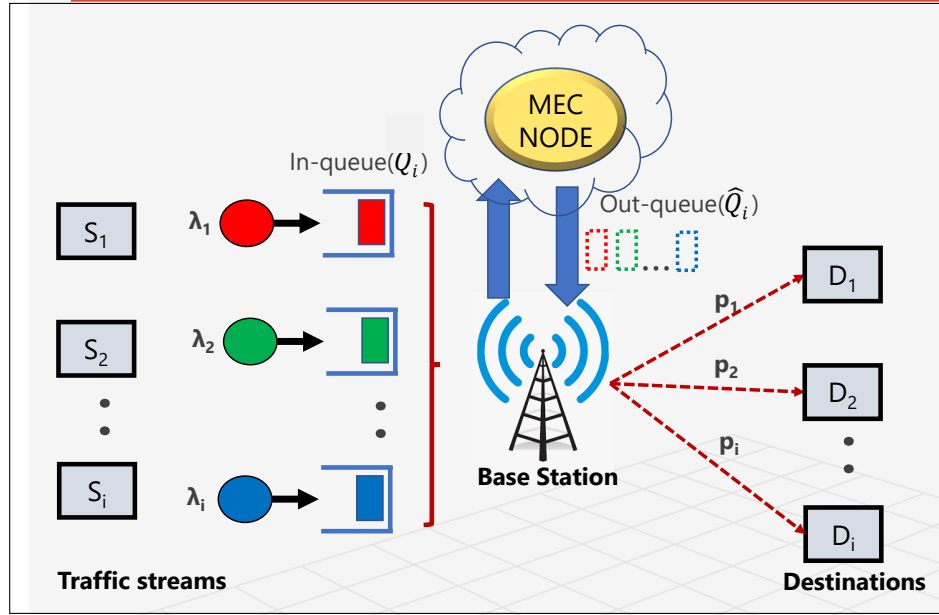


Figure 3.1: An illustration of the system model.

value. The channel gain here is random variable that follows a certain probability distribution which is known. With this assumption, our channel is considered as an ON-OFF channel [83, 88–90] and that reliability of transmission medium is depicted by the probability of successful transmission at each time unit. In this ON-OFF channel, the channel is considered to be ON, if the SNR is above the predefined threshold and OFF otherwise. Precisely, a packet is successfully received at the destination with probability $p_i = Pr[SNR_i \geq \gamma]$, where γ is a predefined threshold. Please note that any small scale fading channel (Rayleigh, Rician, Nakagami) can be mapped to an ON-OFF channel. The only thing that we need to know is the distribution of the channel. For example, Rayleigh channel is widely used in LTE networks [91][92] can be mapped to an ON-OFF channel, which can be obtained as follows. First, we need to find the SNR, which is as follows.

$$SNR_i = \frac{P \times |h_i|^2 \times d_i^{-\alpha}}{N_0}, \quad (3.1)$$

where P is the transmission power of the BS, d_i is the distance between the BS and the destination i , the h_i is the channel gain between the BS and the destination i , α is the path loss factor and N_0 is the thermal noise. Note that h_i is a random variable that follows an exponential distribution with a mean equals to 1 and we use it to determine the Bernoulli random variable which is the channel state. As we know the packet size, the threshold as well as the distance between the BS and the destination is fixed. We then need to find P_r as:

$$p_i = Pr[\text{channel is on}] = Pr[SNR_i \geq \gamma] = Pr\left[\frac{P \times |h_i|^2 \times d_i^{-\alpha}}{N_0} \geq \gamma\right] = e^{-\frac{\gamma \times N_0 \times d_i^{-\alpha}}{P}} \quad (3.2)$$

Given, all these configuration parameters (P, γ, N_0, α and d_i) are fixed, we can conclude that P_r is fixed through the time. It is noteworthy that the same assumption to consider the ON-OFF channel has been largely utilized in the literature [88][83] [89] [90].

The AoI measures the time that elapsed since the generation of the freshest packet that is received by the destination. Let A_i^t be the AoI associated with the destination i at the beginning of the time t . Let τ_i^t be the time-stamp of the recent packet received at the destination i by the time t . Then, the AoI is defined as $A_i^t := t - \tau_i^t$. In the context of MEC assisted network discussed here, this time is composed of waiting time in the first queue + waiting time in the second queue + computation time at the MEC node. The value of A_i^t increases linearly over time when no fresh packet is arrived at the destination which represents that the information is getting older. The moment a packet arrives at the destination, the value of τ_i^t is updated and the Age is reduced accordingly. For convenience, all symbols used throughout this chapter are summarized and defined in Table 3.1.

Symbol	Explanation
I	Set of traffic streams
T	Time horizon
λ_i	Probability with that a packet from stream i arrives to the system.
p_i	Probability that the channel is ON for destination i
a_i^t	Indicator that a packet from traffic stream i arrives in slot t in the queue.
\hat{a}_i^t	Indicator that a processed packet of stream i arrives in slot t at the queue \hat{Q}_i .
z_i^t	System time of the packet in Q_i of user stream i at the beginning of slot t .
β_i^t	Indicator with value 1 if the selected stream has a non-empty queue.
I_i^t	Inter-arrival time of currently scheduled packet and the last scheduled packet of stream i at time-slot t
c_i^t	Channel state associated with the destination i during slot t with value 1 if the channel is ON and 0 otherwise
$t_i[m]$	Index of the time-slot in which m^{th} packet of stream i arrives to the system
x_i^t	1: if traffic stream i is scheduled by BS to MEC in slot t and 0 otherwise.
\hat{x}_i^t	1: if processed packet of stream i is scheduled by BS to destination i in slot t and 0 otherwise.
$\hat{\beta}_i^t$	Indicator with value 1 if the selected stream from the \hat{Q}_i has a non-empty queue.
\hat{z}_i^t	System time of the packet in \hat{Q}_i of stream i at the beginning of slot t .
A_i^t	Age corresponding to destination i .

Table 3.1: Table of notations.

3.3 Illustrative Example

To better understand the definition of AoI and how it is calculated, we provide an example in Figure 3.2. The figure illustrates the evolution of AoI associated with traffic stream i represented by solid purple line; the evolution of \hat{z}_i^t (the system time of a packet of stream i in the out-queue, defined in section 3.4) represented by a red dotted line; and the evolution of z_i^t (the system time of a packet of stream i since its

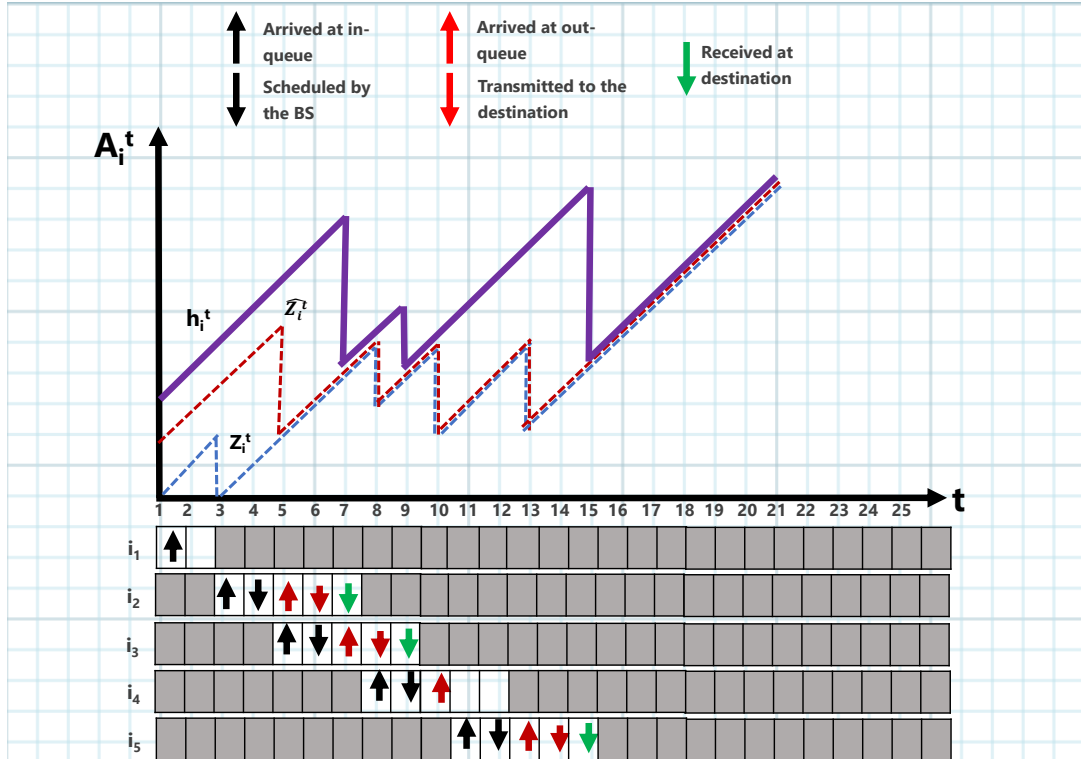


Figure 3.2: The evolution of AoI.

arrival in the in-queue, defined in section 3.4) shown by blue dotted line. Keeping a track of age is not trivial in this case due to multiple challenges: (i) Different arrival times of the packets must be carefully realized. (ii) The status of in-queue must be considered upon arrival of a fresh packet that would lead to discard any existing packet. (iii) The status of out-queue must be considered upon arrival of a fresh packet that leads to dropping any existing packet in the queue. (iv) The status of the out-queue must be checked upon the failure of the delivery of a packet. In this example, we consider five packets i_1 to i_5 that arrive in the system at different times and that the system is running for some time already (i.e., \hat{z}_i^t and A_i^t have initial values 2 and 3 respectively). A complete record of the events along with the evolution of age in each time-slot is demonstrated by Table 3.2.

The first packet i_1 arrives at Q_i when there was no other packet in the system. (i.e., \hat{Q}_i is empty and $x_i^{t-1} = 0$). The value of z_i^t is hence 0 at time-slot 1. At $t = 2$,

t	Event	I_i	z_i^t	\hat{z}_i^t	A_i^t
1	i_1 arrives at Q_i .	0	0	2	3
2	i_1 is waiting in Q_i .	0	1	3	4
3	i_2 arrives at Q_i (i_1 is dropped)	0	0	4	5
4	i_2 is scheduled.	$3-0 = 3$	1	5	6
5	i_2 arrives at \hat{Q}_i i_3 arrives at Q_i	3	2	2	7
6	i_3 is scheduled i_2 sent to dst	$5-3 = 2$	3	3	8
7	i_2 is delivered i_3 arrives at \hat{Q}_i	2	4	4	4
8	i_4 arrives at Q_i i_3 sent to dst	2	3	3	5
9	i_4 is scheduled i_3 is delivered	$8-5 = 3$	4	4	4
10	i_4 arrives at \hat{Q}_i	3	2	2	6
11	i_5 arrives at Q_i .	3	3	3	7
12	i_5 is scheduled.	$11-8 = 3$	4	4	8
13	i_5 arrives at \hat{Q}_i (i_4 is dropped)	3	2	2	9
14	i_5 is sent to dst	3	3	3	10
15	i_5 is delivered	0	4	4	4

Table 3.2: The calculation of AoI.

i_1 was waiting in the Q_i to get scheduled by the BS. At $t = 3$, a fresh packet i_2 arrives at Q_i . The arrival of i_2 causes i_1 to get discarded from the system since we are using a single packet queue and we assume that when a new packet is arrived, the existing packet is discarded. According to the definition of z_i^t , its value becomes 0 when a new packet arrives and there is no other packet in the system belonging to the same stream. Hence at $t = 3$, the value of z_i^t becomes 0. Even so, A_i^t and \hat{z}_i^t increase linearly. At $t = 4$, i_2 is scheduled and gives rise to the value of I_i that is the inter-arrival time between the recent scheduled packet and the last scheduled packet. The value of I_i changes to 3 as i_2 arrives at $t = 3$ and the value of I_i for last scheduled packet is 0. At $t = 5$, i_2 arrives at \hat{Q}_i and results in \hat{z}_i^t getting equal to z_i^t . We observe that whenever a packet is scheduled, the value of I_i is updated. At $t = 6$, I_i becomes equal to 2. At $t = 7$, i_2 gets delivered, hence, the value of A_i^t drops to the value of \hat{z}_i^t . The values of z_i^t and \hat{z}_i^t are updated in the next time-slot in which a packet is delivered. As we can see, at $t = 8$ and $t = 10$, the value of z_i^t and

\hat{z}_i^t is decreased by I_i . Moreover, when a new packet arrives at the non-empty \hat{Q}_i , the values of z_i^t and \hat{z}_i^t are decremented by I_i as shown at $t = 13$ (upon arrival of i_5 , i_4 is dropped). At $t = 15$, A_i^t gets a value 4 and I_i drops to 0. To summarise, we can say that AoI increases linearly at every time-slot between two successfully received updates and drops down to the elapsed time, \hat{z}_i^t , when the update is received by the destination. The inter-arrival time I_i helps to update the elapsed time, z_i^t and \hat{z}_i^t , in order to obtain the correct value of age.

3.4 Problem Formulation

This chapter aspires to solve the problem of minimizing AoI in MEC-assisted IoT networks. Two scheduling decisions give a concise account of this problem. The first defines the scheduling of computation-intensive packets from BS to the MEC node and the later entails the scheduling of processed packets from BS to the destination nodes. Given that packet arrival follows a stochastic process and the channel from BS to the destinations is unreliable and undergoes random packet loss, we derive the expression for the expected sum AoI under the single packet queue system. The detailed formulation is given as follows:

3.4.1 Preliminary Definitions

Let a_i^t be the indicator that a packet from traffic stream i arrives at Q_i in time-slot t and $a_i^t = 0$ otherwise. Let x_i^t be the indicator that is equal to 1 when the BS schedules a packet from stream i during slot t , and $x_i^t = 0$ otherwise. Let \hat{x}_i^t be the indicator that is equal to 1 when the BS transmits a packet from \hat{Q}_i to its respective destination during time-slot t , and $\hat{x}_i^t = 0$ otherwise. Let β_i^t be a binary variable that is equal to 1 if the selected stream from Q_i has a non-empty queue at the beginning

of time-slot t and 0 otherwise. Let $\hat{\beta}_i^t$ be a binary variable that is equal to 1 if the selected stream of \hat{Q}_i has a non-empty queue in time-slot t and 0 otherwise. If a packet of stream i arrives at Q_i in time-slot t (i.e., $a_i^t = 1$), then $\beta_i^t = 1$. Besides, the value of β_i^t changes to 0 only when the packet of stream i is scheduled to the MEC node (i.e., $x_i^t = 1$) and there is no newly arrived packet in the same queue (i.e., $a_i^t = 0$). The β_i^t can be written as.

$$\beta_i^{t+1} = \begin{cases} 1 & \text{if } a_i^{t+1} = 1, \\ 0 & \text{if } x_i^t = 1 \wedge a_i^{t+1} = 0, \forall i, t, \\ \beta_i^t & \text{otherwise.} \end{cases} \quad (3.3)$$

3.4.2 Scheduling Constraints

The adopted access technique in this paper is time division multiple access (TDMA) which means that only one transmission can be occurred per time-slot. Moreover, different traffic streams may have at most one fresh update packet at any time slot available for transmission. That's why at any time-slot, BS is assumed to transmit a single packet. Considering that BS can schedule at most one packet at any given time-slot t from the in-queue to MEC node. We have:

$$\sum_{i=1}^N x_i^t \leq 1, \forall t. \quad (3.4)$$

Moreover, a packet of stream i cannot be scheduled (i.e., $x_i^t = 0$) if the Q_i is empty (i.e., $\beta_i^t = 0$). This is given as following:

$$x_i^t \leq \beta_i^t, \forall i, t. \quad (3.5)$$

The BS can transmit at most one packet at any given time-slot t from out-queue

to the destination. Hence, we have:

$$\sum_{i=1}^N \hat{x}_i^t \leq 1, \quad \forall t. \quad (3.6)$$

Also, a packet of stream i cannot be transmitted to its destination if \hat{Q}_i is empty (i.e., $\hat{\beta}_i^t = 0$). This is given as follows:

$$\hat{x}_i^t \leq \hat{\beta}_i^t, \quad \forall i, t. \quad (3.7)$$

Recall that a packet processed by MEC node of stream i (i.e., $x_i^{t-1} = 1$) arrives at \hat{Q}_i in time-slot t (i.e., $\hat{a}_i^t = 1$), then $\hat{\beta}_i^t = 1$, as given below.

$$\hat{\beta}_i^t \geq \hat{a}_i^t, \quad \forall i, t. \quad (3.8)$$

The value of $\hat{\beta}_i^t$ changes to 0 only when the packet is successfully delivered to the destination (i.e., $\hat{x}_i^t \cdot c_i^t = 1$) and there is no newly arrived packet (i.e., $\hat{a}_i^t = 0$) in the same queue (i.e., no packet was scheduled to MEC node in the previous time-slot). The $\hat{\beta}_i^t$ can be written as.

$$\hat{\beta}_i^{t+1} = \begin{cases} 1 & \text{if } \hat{a}_i^{t+1} = 1, \\ 0 & \text{if } \hat{x}_i^t \cdot c_i^t = 1 \wedge \hat{a}_i^{t+1} = 0, \quad \forall i, t. \\ \hat{\beta}_i^t & \text{otherwise.} \end{cases} \quad (3.9)$$

The channel state process is independent and identically distributed over time and independent across different destinations, with $P(c_i^t = 1) = p_i, \forall i, t$. Note that, the probability p_i is fixed in time but may differ across destinations.

3.4.3 Computation Offloading Constraint

We consider that each packet scheduled to MEC node takes 1 time-slot of processing time before it arrives at \hat{Q}_i . Let \hat{a}_i^t be the indicator that a packet of traffic stream i processed by MEC node arrives at \hat{Q}_i in time-slot t and $\hat{a}_i^t = 0$ otherwise. The \hat{a}_i^t is defined as follows:

$$\hat{a}_i^{t+1} = x_i^t, \forall i, t. \quad (3.10)$$

3.4.4 Mathematical Definition of Age of Information

Let $t_i[m]$ be the index of the time-slot at which m^{th} packet of stream i arrives at the system. We define $I_i := t_i[m] - t_i[m-1]$ as the inter-arrival time of the currently scheduled packet m and the last scheduled packet $m-1$ of stream i with $t_i[0] = 0$. The value of I_i is only updated when a packet is scheduled in time-slot t (i.e., $x_i^t = 1$). I_i is set to 0 in two potential cases:

Case1: When there are no packets of stream i in the system (Q_i and \hat{Q}_i are empty).

Case2: A packet of stream i is delivered in time-slot t (i.e., $d_i^t = 1$) and a new packet is arrived (i.e., $a_i^t = 1$). This case is realized when (i) a packet is delivered in slot t , (ii) a new packet arrives at Q_i in the same slot (i.e., $\beta_i^t = 1$), and (iii) \hat{Q}_i is empty (i.e., $\hat{\beta}_i^t = 0$). Note that when $I_i = 0$, $t_i[m-1] = 0$, the inter-arrival time is given as follows:

$$I_i^t = \begin{cases} 0 & \text{if } (\beta_i^t = 0 \wedge \hat{\beta}_i^t = 0) \vee (\beta_i^t = 1 \wedge \hat{\beta}_i^t = 0 \wedge \hat{x}_i^t c_i^t = 1), \\ t_i[m] - t_i[m-1] & \text{if } x_i^t = 1, \forall i, t. \\ I_i^{t-1} & \text{otherwise.} \end{cases} \quad (3.11)$$

We define z_i^t as the system time of a packet in queue i at the beginning of slot t . By definition, we have $z_i^t = t - \tau_i^t$, where τ_i^t is the arrival time of the packet in the in-queue i . The value of z_i^t becomes 0 when: (i) a new packet of stream i arrives in Q_i (i.e., $a_i^t = 1$) when no other packet exists in \hat{Q}_i (i.e., $\bar{\beta}_i^t = 0$) and also no packet was scheduled to MEC node in the previous time-slot (i.e., $x_i^{t-1} = 0$), (ii) a new packet of stream i arrives in Q_i (i.e., $a_i^t = 1$) when there exists another packet in Q_i (i.e., $\beta_i^t = 1$). The value of z_i^t in time-slot t is dropped by the inter-arrival time when: (i) a packet had been successfully delivered to its destination in the previous time-slot (i.e., $\hat{x}_i^{t-1}c_i^{t-1} = 1$) or (ii) a new packet arrives in \hat{Q}_i (i.e., $\hat{a}_i^t = 1$) when \hat{Q}_i is not empty (i.e., $\hat{\beta}_i^t = 1$), otherwise the value of z_i^t is linearly increased by 1 in each subsequent time-slot. The evolution of z_i^t is given as following:

$$z_i^t = \begin{cases} 0 & \text{if } a_i^t = 1 \wedge \hat{\beta}_i^t = 0 \wedge \hat{x}_i^{t-1} = 0, \\ z_i^{t-1} + 1 - I_i^t & \text{if } (\hat{\beta}_i^{t-1} = 1 \wedge \hat{a}_i^t = 1 \wedge \hat{x}_i^{t-1} = 0), \forall i, t. \\ z_i^{t-1} + 1 & \text{otherwise.} \end{cases} \quad (3.12)$$

We define \hat{z}_i^t as the total system time for a packet i until it is processed and queued in the \hat{Q}_i at the beginning of time-slot t . The moment when (i) a packet arrives to \hat{Q}_i (i.e., $\hat{a}_i^t = 1$), or (ii) a packet was delivered in the previous time-slot (i.e., $\hat{x}_i^{t-1}c_i^{t-1} = 1$), the value of \hat{z}_i^t becomes equal to z_i^t , otherwise its value linearly increases in each time-slot. The evolution of \hat{z}_i^t can be written as:

$$\hat{z}_i^t = \begin{cases} z_i^t & \text{if } \hat{a}_i^t = 1, \forall i, t. \\ \hat{z}_i^{t-1} + 1 & \text{otherwise.} \end{cases} \quad (3.13)$$

We define A_i^t as the AoI associated with destination i in time-slot t . Some studies in literature, [93] [94], considered a certain threshold of AoI, which is termed as *risk level* such that the system's AoI should not be exceeded by this threshold value.

However, in this work, we consider that whenever a successful packet is received at the destination, the AoI is updated by \hat{z}_i^t . Similarly, if no fresh packet is received in time-slot t , the information gets one time-slot older, which is represented by $A_i^{t+1} = A_i^t + 1$. The evolution of A_i^t of destination i can be written as:

$$A_i^{t+1} = \begin{cases} \hat{z}_i^t + 1 & \text{if } \hat{x}_i^t c_i^t = 1, \forall i, t. \\ A_i^t + 1 & \text{otherwise.} \end{cases} \quad (3.14)$$

Let us denote $\mathbf{X}_1 = \{x_i^t, \forall i, t\}$, $\mathbf{X}_2 = \{\hat{x}_i^t, \forall i, t\}$, the optimization model to minimize the expected AoI is given as follows.

$$\begin{aligned} \mathcal{OP1}: \quad & \min_{\mathbf{X}_1, \mathbf{X}_2} \frac{1}{I} \frac{1}{T} \mathbb{E} \left[\sum_{t=1}^T \sum_{i=1}^I A_i^t | A_i^0 = 0 \right] \\ \text{s.t.} \quad & \mathcal{C1} : x_i^t \in \{0, 1\}, \forall i, t \\ & \mathcal{C2} : \hat{x}_i^t \in \{0, 1\}, \forall i, t \\ & \mathcal{C3}: \text{Eq. (3.1) - (3.12)} \end{aligned}$$

Problem $\mathcal{OP1}$ is an integer linear programming problem which is hard to be solved as a result of the intractability of the objective function, Eq. (3.3), Eq. (3.9), Eq. (3.11), Eq. (3.12) and Eq. (3.13), for which an exact derivation is difficult to obtain due to a large number of non linear terms. To overcome this issue, we will reformulate the problem in another fashion as follows. According to the definition of evolution of age, when a packet of stream i is received by its destination, the age is decreased by the factor of system time of the delivered packet. Otherwise, the age is increased by one. This condition can be modelled by constraint 3.16.

$$\mathbb{E}[A_i^{t+1}] = \mathbb{E}[(1 - \hat{x}_i^t)(A_i^t + 1) + \hat{x}_i^t c_i^t (t - H_i^t + 1) + \hat{x}_i^t (1 - c_i^t)(A_i^t + 1)] \quad (3.16)$$

The term H_i^t captures the system time of packet i at time-slot t . It ensures that the most recent packet is scheduled in each time-slot such that the expected age is minimized. The term $a_i^{t_2}$ is the indicator that gives the arrival time-slot of the most recent packet in the queue, whereas $y_i^{(t,t_1,t_2)}$ is a binary variable that ensures that in each time-slot the most recent packet is considered for each stream i .

$$\mathbb{E}[H_i^t] = \mathbb{E} \sum_{t_1 < t} \sum_{t_2 < t_1} [x_i^{t_1} y_i^{(t,t_1,t_2)} a_i^{t_2} \times t_2], \forall i, t. \quad (3.17)$$

$$\sum_{t_1 < t} \sum_{t_2 < t_1} y_i^{(t,t_1,t_2)} = 1, \quad \forall i, t. \quad (3.18)$$

Table 3.3 shows the evolution of AoI for the presented formulation. For demonstration purpose we consider that channel is always ON, i.e., $c_i^t = 1$ and $A_i^t = 1$ at $t = 1$. There are two packets of stream i i.e., i_1 and i_2 that arrive at the system during a time horizon of $T = 5$. As shown in Table 3.3, a packet arrives at time-slot 1 raises age to 2 in time-slot 2. However, another packet arrives in the same queue. As expected, the previous packet is discarded. At time-slot 3, the packet i_2 is scheduled to MEC node. At time-slot 4, this packet arrived at its respective queue and since this was the only packet in the queue, BS scheduled it in time-slot 4. Finally, at time-slot 5, i_2 was delivered and hence the age is dropped to 3.

t	Event	a_i^t	t_1	t_2	x_i^t	\hat{x}_i^t	H_i^t	A_i^t
1	i_1 arrives to Q_i .	1	0	0	-	0	0	1
2	i_2 arrives to Q_i (i_1 is dropped).	1	<1	0	-	0	0	2
3	i_2 is scheduled to MEC node	0	<2	<1	1	-	1	3
4	i_2 is scheduled to destination	0	<3	<2	-	1	2	4
5	i_2 is delivered	0	<4	<3	-	-	2	3

Table 3.3: An example to demonstrate the evolution of AoI.

3.5 Algorithmic Methods

We observe that the optimization problem presented in Section 3.4 is hard to solve due to the existence of binary variables x_i^t , \hat{x}_i^t and $y_i^{(t,t_1,t_2)}$. Moreover, the Linear Programming (LP) methods might be very expensive in terms of computing times for large scale problems. Hence, we provide different algorithmic solutions in search of the best policies to schedule the IoT traffic streams from in-queues to the MEC and between the out-queue and the destinations via BS.

3.5.1 Alternating Dual Minimization Algorithm

We propose an iterative scheme to solve the optimization problem by applying alternating dual minimization (ADM) algorithm. The ADM algorithm has two steps. The first step consists of dividing the set of optimization variables into two blocks of variables. The second step iteratively optimizes over each block of variables, while keeping the remaining variables fixed. The ADM algorithm is presented as Algorithm 1.

Following the steps of ADM algorithm, the expected sum AoI problem can be divided into two subproblems. In the first subproblem, the set of decision variables i.e., $x_i(t)$ is considered fixed and the optimization problem is solved considering the other set of decision variables i.e., $\hat{x}_i(t)$. Conversely, in the second subproblem, the set of decision variables $\hat{x}_i(t)$ is considered fixed and the optimization problem is solved

Algorithm 1 ADM Algorithm

- 1: **Input:** I, T, K (number of iterations), λ_i, p_i
 - 2: **Output:** Expected sum age of information
 - 3: $x_i(t) \leftarrow$ random
 - 4: **for** $k \leftarrow 1 : K$ **do**
 - 5: $\hat{x}_{i,k}(t) \leftarrow$ *Subproblem 1* ($x_{i,k}(t)$)
 - 6: $x_{i,k}(t) \leftarrow$ *Subproblem 2* ($\hat{x}_{i,k}(t)$)
 - 7: Obtain expected sum age from *Subproblem 2* ($\hat{x}_{i,K}(t)$)
-

considering $x_i(t)$. The two subproblems are defined as follows:

3.5.1.1 Subproblem 1

$$\mathcal{OP}2: \min_{\mathbf{x}_2} \frac{1}{I} \frac{1}{T} \mathbb{E} \left[\sum_{t=1}^T \sum_{i=1}^I A_i^t \right]$$

$$\mathcal{C}1 : \hat{x}_i^t \in \{0, 1\}, \forall i, t$$

$$\mathbb{E}[A_i(t+1)] = \mathbb{E}[(1 - \hat{x}_i^t)(A_i^t + 1) + \hat{x}_i^t c_i^t (t - H_i^t + 1) + \hat{x}_i^t (1 - c_i^t)(A_i^t + 1)] \quad (3.20)$$

$$\mathbb{E}[H_i^t] = p_i \lambda_i \sum_{t_1 < t} \sum_{t_2 < t_1} x_i^{t_1} y_i^{(t, t_1, t_2)} t_2, \forall i, t. \quad (3.21)$$

$$\sum_{t_1 < t} \sum_{t_2 < t_1} y_i^{(t, t_1, t_2)} = 1, \quad \forall t \leq T \quad i \in I. \quad (3.22)$$

$$\sum_{i \in I} \hat{x}_i^t \leq 1, \quad \forall t \leq T. \quad (3.23)$$

3.5.1.2 Subproblem 2

$$\mathcal{OP}3: \min_{\mathbf{x}_1} \frac{1}{I} \frac{1}{T} \mathbb{E} \left[\sum_{t=1}^T \sum_{i=1}^I A_i^t \right]$$

$$\mathcal{C}1 : x_i^t \in \{0, 1\}, \forall i, t.$$

$$\mathbb{E}[A_i^{t+1}] = \mathbb{E}[(1 - \hat{x}_i^t)(A_i^t + 1) + \hat{x}_i^t c_i^t (t - H_i^t + 1) + \hat{x}_i^t (1 - c_i^t)(A_i^t + 1)] \quad (3.25)$$

$$\mathbb{E}[H_i^t] = p_i \lambda_i \sum_{t_1 < t} \sum_{t_2 < t_1} k_i^{(t, t_1, t_2)} t_2, \forall i, t. \quad (3.26)$$

$$\sum_{t_1 < t} \sum_{t_2 < t_1} y_i^{(t, t_1, t_2)} = 1, \quad \forall t \leq T \quad i \in I. \quad (3.27)$$

$$\sum_{i \in I} x_i^t \leq 1, \quad \forall t \leq T. \quad (3.28)$$

Both optimization sub-problems are non-linear and will be linearized by introducing new variables. The r_i^t , s_i^t and $k_i^{(t, t_1, t_2)}$ are the new variables that are introduced to linearize the products $\hat{x}_i^t h_i^t$, $\hat{x}_i^t A_i^t$, and $x_i^t * y_i^{(t, t_1, t_2)}$ respectively. Equation 3.16 can be simplified as follows:

$$\mathbb{E}[A_i^{t+1}] = \mathbb{E}[(1 + A_i^t) + c_i^t \{\hat{x}_i^t * t - H_i^t \hat{x}_i^t - A_i^t \hat{x}_i^t\}] \quad (3.29)$$

where $\mathbb{E}[\hat{x}_i^t] = \hat{x}_i^t$. Also we have a non linear term here: $\hat{x}_i^t * \mathbb{E}[A_i^t]$, where the first term is binary and the second term is continuous. The linearization is given as follows: Suppose we can give a finite upper bound for $\mathbb{E}[A_i^t]$ called M . Then this constraint can be linearized by using the so-called big M method. We introduce a new variable r that should take the same value as the product $\hat{x}_i^t * \mathbb{E}[A_i^t]$. The linearization is given as follows:

$$r_i^t \leq \hat{x}_i^t M \quad (3.30)$$

$$r_i^t \geq 0 \quad (3.31)$$

$$r_i^t \leq \mathbb{E}[A_i^t] \quad (3.32)$$

$$r_i^t \geq \mathbb{E}[A_i^t] - (1 - \hat{x}_i^t) M \quad (3.33)$$

$$\mathbb{E}[H_i^t] = \sum_{t_1 < t} \sum_{t_2 < t_1} x_i^{t_1} y_i^{t, t_1, t_2} \mathbb{E}[a_i^{t_2} \times t_2] \quad (3.34)$$

$$\mathbb{E}[H_i^t] = \lambda_i \sum_{t_1 < t} \sum_{t_2 < t_1} x_i^{t_1} y_i^{t, t_1, t_2} t_2 \quad (3.35)$$

we have a non linear term here: $x_i^t y_i^{t, t_1, t_2}$ as a product of two binary variables. The linearization can be performed by introducing a new variable k_i^{t, t_1, t_2} .

$$k_i^{t, t_1, t_2} \leq x_i^{t_1} \quad \forall i, t \quad (3.36)$$

$$k_i^{t, t_1, t_2} \leq y_i^{t, t_1, t_2} \quad \forall i, t \quad (3.37)$$

$$k_i^{t, t_1, t_2} \geq y_i^{t, t_1, t_2} + x_i^{t_1} - 1 \quad \forall i, t \quad (3.38)$$

The ADM is an iterative algorithm. In the beginning of the first iteration, the x_i^t values are randomly generated and given as input to the subproblem 1. The optimization problem is solved and \hat{x}_i^t values are collected from the solution. These resultant values are now provided as input to the subproblem 2 and the optimization problem is solved such that x_i^t values are collected from the solution. The two optimization problems are solved iteratively to improve the overall objective value.

3.5.1.3 ADM Complexity Analysis

For the ADM algorithm, the complexity of the $\mathcal{OP}1$ problem largely depends on the solver that is used to solve this problem. Realizing that $\mathcal{OP}1$ is a convex problem any interior-point solver can be used to solve it. We take on a number of Newton steps, denoted by C_s to measure its complexity. The Newton steps rely on two main aspects, (i) number of recursive iterations till convergence from a given initial point, and (ii) the problem size. As given in [95], the worst-case C_s to obtain a local solution in $\mathcal{OP}1$ can be written as:

$$C_s \sim \sqrt{\text{problem size}} \quad (3.39)$$

where problem size is the total number of variables of the $\mathcal{OP}1$ problem. As given, the $\mathcal{OP}1$ is divided into two subproblems and each subproblem in every iteration will update IT variables in the worst case. This results in the overall complexity of $K\sqrt{IT + IT}$ where K is the finite number of iterations.

The complexity of ADM algorithm as shown above, directly depends on the number of iterations. In order to achieve a better solution, the two subproblems must be solved for reasonable number of times. The ever-increasing demands of real-time applications require high quality solutions that take smallest possible computation time to satisfy the latency constraint of these applications. Keeping that in mind, we present a low-complexity algorithm in the quest of obtaining high quality solution with small computation time.

3.5.2 Age-Based Modified Greedy Algorithm (AMG)

In AMG approach as given by Algorithm 2, the BS iteratively checks the instantaneous age of all the traffic streams in each time slot and selects the stream that can potentially achieve the highest drop of age in subsequent time-slot. This is shown by line 4 of Algorithm 2. Once, the stream with the largest age reduction is identified, the age of the rest of the streams will be increased by one in the next time-slot as given by line 5-7. Following this, the age of the identified stream can be easily determined from the expected drop of age as shown by line 8. The next step is to calculate generation time of the most recent packet in the out-queue for each traffic stream as given by lines 9-11. The generation time, once calculated, helps to determine the stream with the most recent packet available as shown by line 12. Finally, the lines 13-16 signify that the stream with the highest drop of age by generation time should be scheduled to transmit its packet to the destination.

Algorithm 2 AMG Algorithm

```
1: Input:  $I, T, \lambda_i, p_i (i \in I), A_i(0) \leftarrow 0$ 
2: Output: Expected sum age of information
3: for  $t \leftarrow 1 : T$  do
4:    $max_i \leftarrow \operatorname{argmax}_i A_i^t + 1 - p_i * (t - H_i^t + 1) - (1 - p_i) * (A_i^t + 1)$ 
5:   for  $i \leftarrow 1 : I$  do
6:      $A_i^{t+1} \leftarrow A_i^t + 1$ 
7:    $A_{max_i}^{t+1} \leftarrow p_{max_i} * (t - H_{max_i}^t + 1) + (1 - p_{max_i}) * (A_{max_i}^t + 1)$ 
8:   for  $i \leftarrow 1 : I$  do
9:      $GT_i \leftarrow (t - 1) * \lambda_i$ 
10:   $max_i \leftarrow \operatorname{argmax}_i A_i^{t+1} + 1 - p_i * (t - GT_i + 2) - (1 - p_i) * (A_i^{t+1} + 1)$ 
11:  for  $i \leftarrow 1 : I$  do
12:     $H_i^{t+1} \leftarrow H_i^t$ 
13:   $H_{max_i}^{t+1} \leftarrow GT_{max_i}$ 
```

3.5.3 Deep Reinforcement Learning (DRL) Based Solution

We present our approach where the problem is first modelled as an MDP and then a DRL based on Proximal Policy Optimization (PPO) algorithm is leveraged to determine the policy that governs the two scheduling decisions for traffic streams in each timeslot. An MDP is a 4-tuple $(\mathbf{S}, \mathbf{V}, \mathbf{R}, \mathbf{P})$, where: \mathbf{S} is a finite set of states s^t at any time-slot t , where $s^t \in \mathbf{S}$; \mathbf{V} is a set of all actions v^t at any time-slot t , where $v^t \in \mathbf{V}$; \mathbf{R} is the reward distribution, given by a measurable function $P(r^t | s^t, v^t)$, to give immediate reward $r^t \in \mathbf{R}$ after an action $v^t \in \mathbf{V}$ is taken in a state $s^t \in \mathbf{S}$ at time-slot t ; \mathbf{P} is a Markovian transition model, where $P(s^{t+1} | s^t, v^t), s^t, s^{t+1} \in \mathbf{S}, v^t \in \mathbf{V}$ represents the probability of advancing to state s^{t+1} from state s^t when an action v^t is taken.

The state, action and reward functions under the MDP framework are given as follows:

- **State \mathbf{S} :** The system state is defined as $s(t) = (\mathbf{A}^t, \boldsymbol{\nu}^t, \boldsymbol{\rho}^t, \boldsymbol{\chi}^t, \boldsymbol{\kappa}^t)$ at time t , where $s^t \in \mathbf{S}$. The $\mathbf{A}^t = (A_1^t, A_2^t, \dots, A_I^t)$ is a vector of size I for the AoI of all traffic streams at time-slot t , $\boldsymbol{\nu}^t = (\beta_1^t, \beta_2^t, \dots, \beta_I^t)$ is a vector of size I

Algorithm 3 Proposed DRL for Minimizing the expected sum AoI

- 1: **Input:** Number of users (I), Number of time-slots (T), Learning Rate, Episodes K .
 - 2: **Output:** Scheduling policy.
 - 3: Initialize policy π with random parameter θ
 - 4: **for** $k \leftarrow 1 : K$ **do**
 - 5: **for** $t \leftarrow 1 : T$ **do**
 - 6: Get $(\mathbf{A}^t, \boldsymbol{\nu}^t, \boldsymbol{\rho}^t, \boldsymbol{\chi}^t, \boldsymbol{\kappa}^t)$ from the environment.
 - 7: sample action $v^t \sim \pi_{\theta_{old}}$.
 - 8: Take action v^t that specifies the two scheduling decisions.
 - 9: Obtain the sum AoI, r^t and new state s^{t+1} .
 - 10: Store (s^t, a^t, r^t, s^{t+1}) as one transition in the experience replay.
 - 11: Compute advantage estimate \hat{A} for all epochs.
 - 12: Optimize surrogate loss function using Adam optimizer.
 - 13: Update current policy $\pi_{\theta_{old}} \leftarrow \pi_{\theta}$.
-

containing the status of queue Q_i , $\forall i \in I$ at time-slot t , $\boldsymbol{\rho}^t = (\hat{\beta}_1^t, \hat{\beta}_2^t, \dots, \hat{\beta}_I^t)$ is a vector of size I containing the status of \hat{Q}_i , $\forall i \in I$ at time-slot t , $\boldsymbol{\chi}^t = (z_1^t, z_2^t, \dots, z_I^t)$ is the vector of time spent in the queue Q_i $\forall i \in I$ related to the I streams at time slot t . and $\boldsymbol{\kappa}^t = (\hat{z}_1^t, \hat{z}_2^t, \dots, \hat{z}_I^t)$ is the vector of size I containing the time spent in the queue \hat{Q}_i associated with all traffic streams at time slot t .

- **Action \mathbf{V}** : An action v^t is executed by BS at each time-slot t denoted by $v^t \in \mathbf{V}$ consists of scheduling decisions. The current composite action v^t is denoted by $v^t = (\boldsymbol{\omega}^t, \boldsymbol{\eta}^t)$, where $\boldsymbol{\omega}^t = [x_1^t, x_i^t, \dots, x_I^t]$, where x_i^t represents the scheduling decision for traffic stream towards MEC and each element $x_i^t = 1$ shows that traffic stream i is scheduled to transmit its packet to MEC in time-slot t , whereas $x_i^t = 0$ means that traffic stream i is not scheduled in time slot t to transmit its packet. The row vector $\boldsymbol{\eta}^t = [\hat{x}_1^t, \hat{x}_i^t, \dots, \hat{x}_I^t]$, where \hat{x}_i^t represents the scheduling decision of streams from \hat{Q}_i to the respective destinations and each element $\hat{x}_i^t = 1$ shows that a processed packet from out-queue i is scheduled to be transmitted to its respective destination in time-slot t , whereas $\hat{x}_i^t = 0$

means that traffic stream i is not scheduled in time slot t to transmit its packet.

- **Reward \mathbf{R} :** The immediate reward r^t at time slot t is the negative summation of AoI, $r^t = -\sum_{i=1}^I A_i^t$, where $r^t \in \mathbf{R}$. Considering the objective of minimizing the expected sum AoI, the RL-agent aims to optimize the scheduling decisions that lead to minimize the AoI.

3.6 Simulation and Numerical Analysis

3.6.1 Simulation Setup

We evaluate the performance of proposed algorithms by conducting a series of simulations. We compare the expected age obtained by the ILP and AMG algorithm with ADM, DRL, and other benchmarks, i.e., round robin and random policy. We use CPLEX to solve the ILP solution, C++ to simulate the proposed algorithms and Python to implement DRL model. The experiments are run on a machine with Intel Xeon (R) X5670 2.93 GHz CPU, 12-GB RAM and 64-b operating system.

3.6.2 Simulation Parameters

Figure 3.3 shows the simulation results with varying arrival rate, in particular, $\lambda \in \{0.1, 0.2, 0.4, 0.6, 0.8, 1\}$ with $p \in \{0.1, 0.5, 0.9\}$. Figure 3.5 presents the results on network with different number of IoT devices, namely, $I \in \{10, 15, 20, 25, 30, 35, 40\}$, whereas $T = 250$ and $\lambda = p = 0.7$. In the simulation of Figure 3.6, we set the $I = 15$ and $T = 250$. Figure 3.7 simulates the network with $p \in \{0.1, 0.3, 0.7, 1\}$, $\lambda = 0.75$, $T = 500$, and $I \in \{3, 15\}$. Other simulation parameters related to DRL are given by Table 3.4.

Table 3.4: Simulation parameters.

Parameter	Values
Activation functions	Softmax and Tanh
Number of Neurons	64
Number of Hidden layers for Networks	3
Learning Rate	0.002
Optimizer technique	Adam
Clip function, ϵ	0.2
Total number of Epochs	3000
Reward Discount	0.9

3.6.3 Benchmark Schemes

To the best of our knowledge, there is no existing approach that solves the similar problem of minimizing AoI in MEC-assisted IoT network considering the impact of stochastic arrivals and unreliable channel conditions. Thus, for the sake of comparison, we develop two other baseline approaches:

3.6.3.1 Round Robin scheduling scheme (RR)

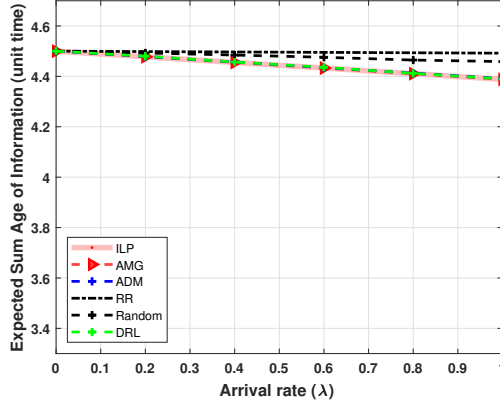
In the RR scheme, at each time-slot, the BS alternately selects an input stream $i \in I$ (starting from the first stream and so on) to upload its status update packet to the MEC node. This is done irrespective of the knowledge that the selected stream has any status update packet available or not. In case, if there is no status update packet in the selected stream's in-queue, a time-slot is lost. The same approach is adopted for the out-queue scheduling from BS to each destination.

3.6.3.2 Random scheduling scheme

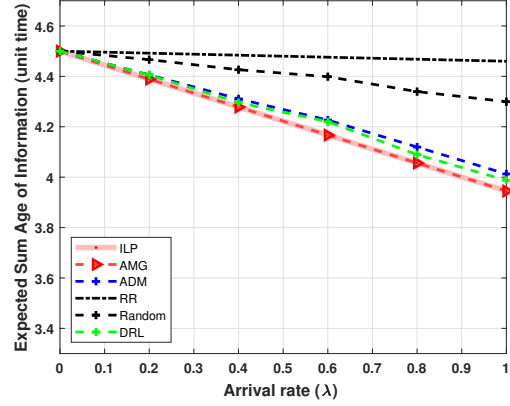
In the random scheme, instead of alternatively selecting the streams, at each time-slot, the BS randomly selects a stream to upload its status update packet to the MEC node. Similar to the RR approach, the scheduling decision is taken irrespective of the knowledge that the queue of the selected stream is empty or has a packet to deliver.

3.6.4 Results and Discussions

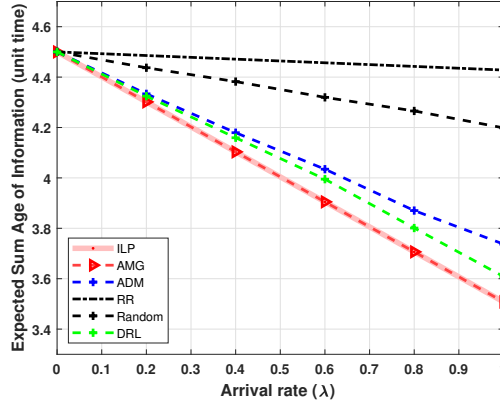
We start by analyzing the impact of variable network load on the age of information. Figure 3.3 delineates the impact of increasing network load on AoI and compares the proposed heuristic algorithm against the optimal solution and benchmark methods. The impact of increasing the load is simulated by varying arrival rate of the packets from 0 to 1 with an increasing factor of 0.2. The results are plotted for the expected sum age of information versus the arrival rate with five traffic streams competing for system resources to update their respective destinations with the fresh information. The time-horizon used for this experiment is 10. We observed a significant improvement in the expected age of information with the proposed AMG algorithm as compared to the other methods. The AMG algorithm outperforms other algorithms by obtaining the same solution as obtained with the ILP method. However, the computation time of AMG is significantly lower than the computation time of ILP (results given by Table 3.5). The system first runs to capture the expected sum age of information by varying the network load with a very low channel reliability value, i.e., $p = 0.1$ as shown by Figure 3.3(a). We observe that when the channel is highly unreliable, the expected age for all the methods increases. This is because, if channel conditions are not favorable, the number of re-transmissions will increase and packets will spend more time in queues, waiting to get scheduled to their respective destinations. This will increase the staleness of packets and that would eventually lead to an increase in the expected age. However, as the arrival rate is increased, more fresh packets will arrive to the system. This increases the chance of getting scheduled and delivered to the destination. It can be observed from Figure 3.3(a) that, when $\lambda = 1$, the expected age is minimum for all the methods. Nonetheless, the AMG solution is better than the baseline methods. The performance of round-robin approach was the worst in this experiment. The reason is its policy to schedule the



(3.3.a) Results for $p = 0.1$.



(3.3.b) Results for $p = 0.5$.



(3.3.c) Results for $p = 0.9$.

Figure 3.3: Expected sum AoI for different arrival rates λ .

streams sequentially without taking into account if there is an update packet available at the selected stream. The ADM method performs better than random and round robin approaches in this experiment.

Figure 3.3(b) shows the impact of arrival rate on the expected age when the channel conditions get slightly better, i.e., $p = 0.5$. It is noticed that in this experiment, the expected age significantly decreased. Again, the AMG outperformed all the other methods by providing the same solution as the exact method. Finally, Figure 3.3(c) presents the results with $p = 0.9$ for the channel from BS to all the destinations. It can be seen that the curves of the expected age of information for all the schemes

decrease as the arrival rate increases. The reason being that more fresh packets are expected to arrive to the system and replace the old ones. For example when the arrival rate is increased from 0 to 0.8, the expected sum age is decreased by 17.63% for the AMG solution which has the same value as the ILP solution. We observe that the round robin and random both get close results for the small values of the arrival rates, but when the arrival rate reaches to 1, the random outperforms the round robin method. The reason being that, random method, instead of scheduling in-turns like round robin, selects one stream randomly in each time-slot and schedules it. However, the streams are selected without considering if they have any update packet available for transmission. It can be seen that when the arrival rate is 1, the ADM algorithm gives 6.13% worst performance than the AMG. This is because the number of iterations of ADM are set to 10 in this experiment. If the number of iterations is increased, the quality of ADM solution may increase but at the cost of large execution time which might make it unsuitable for real-time networks.

It can be observed from Figure 3.3 that DRL algorithm performs better than ADM and other baseline methods in all the experiments. This is understandable since, the DRL agent learns over the time how to schedule the traffic streams effectively such that the expected sum AoI is reduced considering the impact of arrival rate and channel quality. Obviously, the number of lost status-update packets is high with baseline approaches as the scheduling decisions are taken irrespective of the knowledge of the packets arrival and channel condition. For example, when $p = 0.9$ and arrival rate is 1, DRL achieves around 18.5%, 14.05%, 3.5% reduced expected sum AoI than the round robin, random, and ADM approaches respectively. On the other hand, in the same experiment, the DRL gets 2.86% higher expected sum AoI as compared to the proposed approach. To get insights, let's understand that action-space affects the performance of the DRL algorithm. The DRL agent, in this case, is trained for

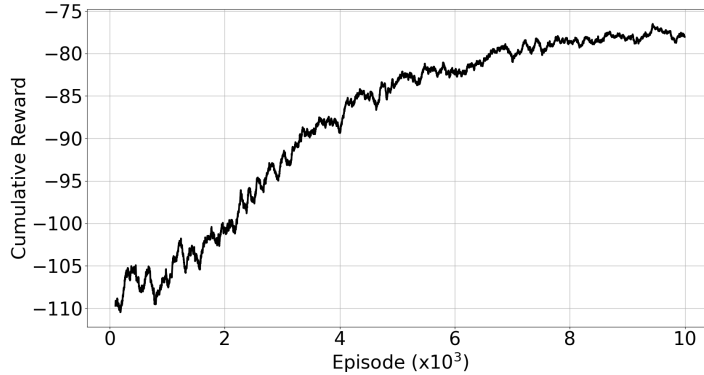


Figure 3.4: Accumulated reward over time.

multiple actions per time-slot. Due to the large action space, it is difficult for DRL agent to learn the value of each true action when multiple actions are to be taken per time-slot. Next, we study the behavior of DRL agent and verify the convergence of the proposed algorithm. As depicted in Figure 3.4, the cumulative reward, which is the opposite value of the minimum average sum AoI, is significantly improving as the number of episodes is increasing. Basically, it can be observed from this figure that the cumulative reward increases relatively quickly and then the increase gets relatively slow. The reason being that, in the beginning of episodes, many traffic streams are not properly scheduled to transmit their packets to the MEC node and from the out-queue to the destinations. However, as the agent gets trained and starts to efficiently adapt the scheduling policies, the improvements become less obvious.

Next, we studied the impact of a number of IoT devices on the expected sum age. This experiment was conducted with 250 time-slots and the arrival rate and channel reliability both are set to 0.7. As shown in Figure 3.5, the number of IoT devices is varied from 10 to 40 and the expected sum AoI is reported. It also depicts that AMG algorithm is able to minimize the expected sum AoI with higher performance as compared to the other schemes. As the number of IoT devices increases, the expected sum AoI also increases. This is to note that as the waiting time for arrived packets

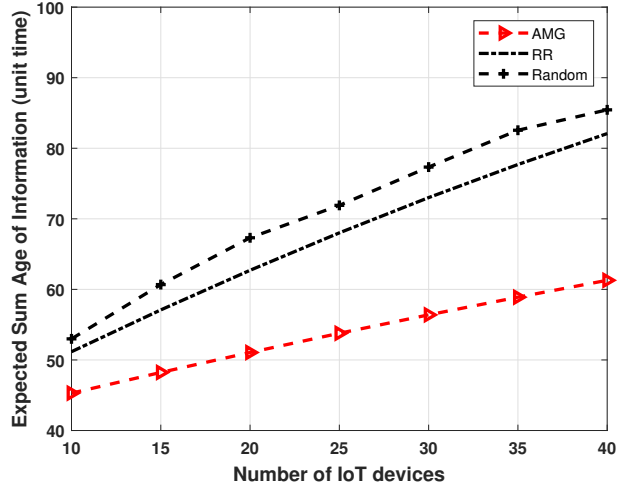
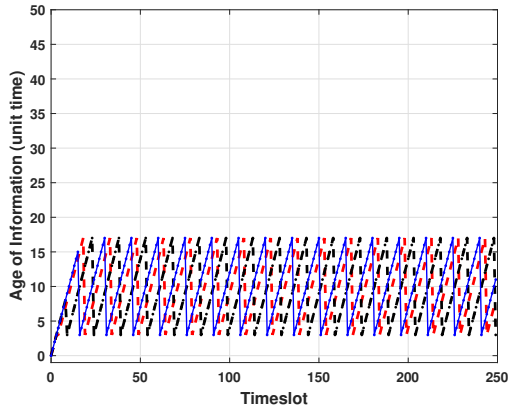


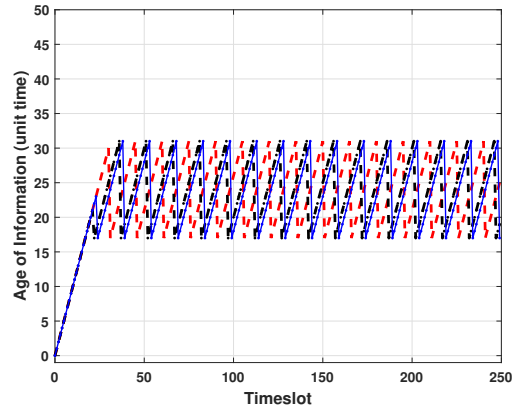
Figure 3.5: Impact of number of IoTDs on expected sum AoI.

increase, more scheduling is required to decrease the expected sum age. The round robin approach is shown to perform better than the random policy. This is because, the round robin approach handles scheduling in a circular order without any priority. Each IoT device gets scheduled turn by turn which results in decreasing the overall age. The random approach, in each iteration, selects a random traffic stream to be scheduled at both in-queue and out-queue and hence results in the worst performance as the number of traffic streams are increased.

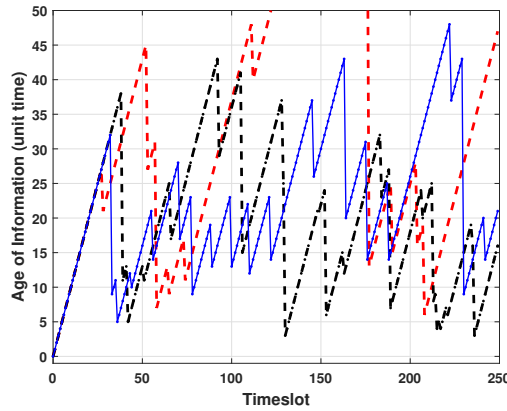
In Figure 3.6, the AoI evolution is presented for AMG, round robin and random approaches for a selected set of three IoT devices in a network of 15 IoT devices. Figure 3.6 depicts that the AoI evolution is substantially different for the different policies. It is observed that by leveraging AMG, the AoI of the three IoT devices is considerably smaller than that of the baseline methods. Due to the reason that AMG aims to minimize the expected age of all the streams by choosing the stream to be schedule in each iteration that gives the maximum drop in age by realizing generation time of the most recent packet in the out-queue. It is interesting to see that round robin policy gives better results than random as the number of time-slots



(3.6.a) AMG



(3.6.b) Round Robin Approach

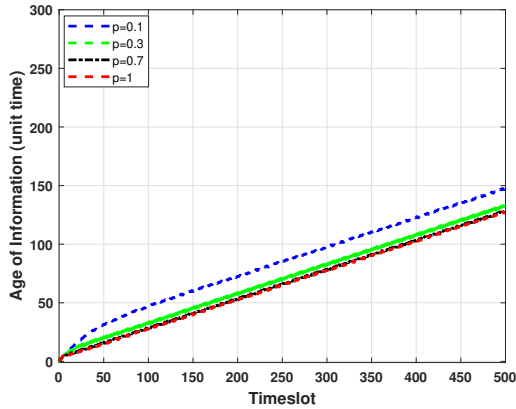


(3.6.c) Random Approach

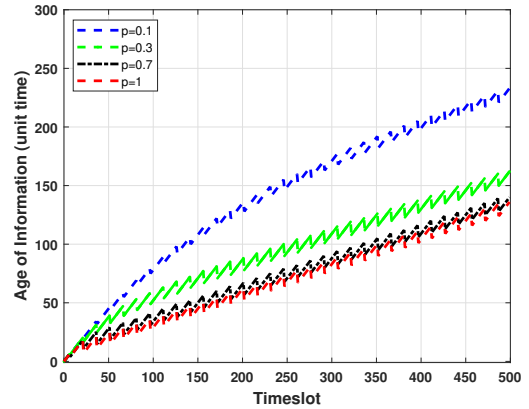
Figure 3.6: Expected sum AoI for different arrival rates λ .

are increased. The random scheme decreases age for some IoT devices. On the other hand, it significantly increases the age to maximum for other IoT devices. This is because random approach schedules the traffic streams from in-queue and out-queue irrespective of each other. As the name implies, the scheduling decisions are totally random and hence result in worst performance.

Figure 3.7 compares the curves of age of information for a single destination with a fixed arrival rate i.e., $\lambda = 0.75$ under different channel conditions. The two cases are presented in Figure 3.7(a) and 3.7(b) to evaluate the performance of AGM algorithm. In our first experiment as presented by Figure 3.7(a), three IoT devices are



(3.7.a) Case A: $I = 3$, $\lambda = 0.75$



(3.7.b) Case B: $I = 15$, $\lambda = 0.75$

Figure 3.7: AoI comparison under different channel conditions.

considered sending their information update messages to the destinations. We report the evolution of age with respect to a single destination which is randomly selected. It is observed that when the channel conditions are worst, i.e., $p = 0.1$, age has the largest value. This is true because when the channel conditions are bad, the number of re-transmissions will increase, and that will increase the overall age. It can be seen that when channel is considered fully reliable, i.e., $p = 1$, age attains the lowest possible value. The second experiment as shown by Figure 3.7(b) is performed on 15 IoT devices which are competing to get their resource-intensive information messages processed by an MEC node before they are sent to their respective destinations over unreliable channel. It can be observed that the age of information attains higher values in this experiment as compared to the one shown in Figure 3.7(a). This is understandable since, at any time-slot t , the BS can schedule a packet from a single traffic stream and rest of the streams will have their age of information increased by one. Similarly, BS can schedule a single stream to transmit its packet to the destination. Consequently, when the number of traffic streams are increased, the age of information will be increased. Nevertheless, a good scheduling policy will ensure that expected sum age of information is minimized.

Table 3.5: Execution time (msec) ($\lambda = 1, p = 1$)

I	T	ILP	AMG	ADM	RR	Random
2	10	644.88	<1	586.46	<1	<1
5	10	2599.9	<1	671	<1	<1
2	20	22765	<1	1522	<1	<1
5	20	> 7h	< 1	1108000	< 1	< 1
10	100	>7h	0.15	>7h	7.97	7.46
20	500	>7h	0.34	>7h	2043.68	2042.75

Finally, we report the computation times of the different approaches. Table 3.5 shows that the computation time for ILP grows exponentially as the time horizon increases. For example when $T=20$ for only 2 streams, the ILP takes around 22.76 seconds to execute while the computation time for AMG is negligible. Moreover, when the problem is solved for $I=5$ streams and 20 time-slots, the ILP runs for more than 7 hours. Besides, AMG obtains the same solution in fraction of milliseconds (negligible time). Interestingly, for large instances when $T=500$ and $I=20$, AMG only takes 0.34 milliseconds which makes our AMG algorithm eligible to solve real network problems.

3.7 Conclusion

This chapter studied the AoI for computation-intensive messages in an MEC-assisted IoT network where a BS serves multiple traffic streams to forward their messages to the destinations. The status-update messages arrive at the BS with a stochastic arrival process and are selected following a scheduling policy to be forwarded to the MEC node which is equipped with an intelligent function. The MEC node processes each packet which then arrives at its respective queue at the BS. The BS decides, in each time-slot, which stream to select in order to transmit its packet to the destination over an unreliable channel. The scheduling decisions are aimed to keep the information fresh at the destination. Our main contributions include:

(i) formulating an optimization problem to find the optimal scheduling policy under single packet queue system that minimizes the expected sum AoI evaluating combined impact of stochastic packet arrivals, scheduling policy and unreliable channel conditions. (ii) proposing an AMG algorithm that achieves a significant reduction of computation time which makes it a suitable candidate to solve the age minimization problem for real-time networks. Numerical results show the effectiveness of our proposed algorithm, that is also verified through extensive comparisons with other existing approaches.

Chapter 4

AoI Optimization in RIS-Assisted IoT Networks

4.1 Motivation and Contributions

In reality, the timely delivery of information update messages is challenging due to the behaviour of wireless communication environments, which may be highly random and uncontrollable. Typically, a strong communication link between a source and destination cannot be guaranteed due to channel impairments and blockages. Thus, the question that arises here is the following: *how can one guarantee reliable wireless communication links in highly random and uncontrollable environments?*. RIS technology has been envisioned as a key solution which provides the answer to this question. It is worth mentioning that the benefits of introducing RIS to enhance the QoS performance of communication networks have been unveiled in the literature for real-time applications. For example, in vehicle-to-everything (V2X) applications [96][97], RIS has proven to improve the QoS in harsh transmission environments. Similarly, in smart industry application [98], RIS offers promising signal strength and quality over longer distances. Motivated by these facts, it is foreseen that the information freshness can be significantly improved through the integration of RIS, especially for time-sensitive applications and services, which is indeed the focus of this chapter.

The main contributions of this chapter are summarized as follows:

- We formulate a joint user scheduling and phase-shift matrix (passive beamforming) optimization problem with the objective of minimizing the expected sum AoI of multiple traffic streams.
- Owing to the stochastic nature of arrival of packets, the combinatorial nature of the user scheduling task, and the non-convexity of the different system

constraints, it is extremely challenging to solve the formulated problem. Alternatively, with the aid of bi-level optimization, the original problem is reformulated into an outer user scheduling problem and an inner phase-shift matrix optimization problem. Owing to the complexity and stochastic nature of the packet arrivals, the outer problem is formulated as a MDP and solved through the DRL technique. For the inner problem, an efficient algorithm based on SDR is proposed.

- The performance of the proposed approach is assessed through extensive simulations, where different baseline methods were considered for comparison purposes. We demonstrate that our proposed scheme achieves the minimum expected sum AoI in contrast with the other considered methods.

4.2 System Model

4.2.1 Network Model

We consider a downlink wireless network consisting of one BS, equipped with a single antenna, that is serving I traffic streams to forward their status-update messages to I destinations as depicted in Figure 4.1. We assume that the BS is equipped with I virtual queues, within which the BS only stores the most recent packet of each stream. The time dimension is slotted into time-slots, where each is represented by a time-slot index $t \in [1, \infty)$. Let T denote the time horizon of this discrete-time system. In addition, let $\mathcal{T} = \{1, 2, \dots, T\}$ denote the set of time slot indices within the time interval $[1, T]$ and let $\mathcal{I} = \{1, 2, \dots, I\}$ denote the set of the traffic streams. In this setting, at the beginning of every time-slot $t \in \mathcal{T}$, a packet from stream $i \in \mathcal{I}$ arrives to the system with a probability $\lambda_i \in (0, 1]$. Accordingly, for all $t \in \mathcal{T}$ and $i \in \mathcal{I}$, let $u_i(t)$ be the binary variable that indicates whether a packet

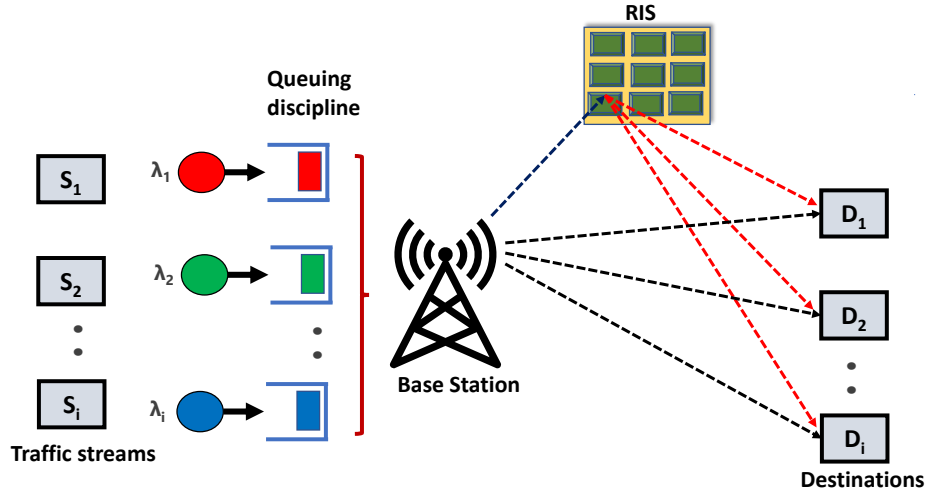


Figure 4.1: An illustration of our system model.

from the i th traffic stream arrives to the BS at the t th time-slot or not. Based on its definition, for all $i \in \mathcal{I}$, the arrival process $u_i(t)$ is a Bernoulli arrival process that is i.i.d over time, where $P(u_i(t) = 1) = \lambda_i$. Moreover, the arrival processes $(u_i(t))_{1 \leq i \leq I}$ are independent across the different streams.

Due to the obstacles of the wireless propagation environment, the existence of a strong direct line-of-sight (LoS) communication link between the BS and each destination is difficult to obtain. For this purpose, an RIS equipped with L reflecting elements is assumed to be deployed within the considered wireless network to assist the transmission from the BS by passively relaying the status update information to the destinations. The BS continuously controls the phase-shift of the reflecting elements in order to maintain the quality of service (QoS) required by the destinations. In this context, for all $t \in \{1, 2, \dots, T\}$, let $\Phi(t) = \text{diag}(\exp[\theta(t)]) \in \mathbb{C}^{L \times L}$ denotes the $L \times L$ phase-shift matrix of the RIS, where $\theta(t) = [\theta_1(t), \theta_2(t), \dots, \theta_L(t)]^T$ is the $L \times 1$ vector that contains the phase-shifts of the RIS, such that, for all $l \in \mathcal{L} \triangleq \{1, 2, \dots, L\}$, $\theta_l(t) \in [0, 2\pi)$ is the phase-shift of the l th reflecting element of the RIS.

The total bandwidth available at the BS is divided into N channels, where each

channel consists of one spectrum resource. The channel diversity exists between different channels and BS can schedule different traffic streams to at most N channels where each traffic stream is assumed to be allocated to only one channel [22]. Let $\mathcal{N} = \{1, 2, \dots, N\}$ denote the set of the N channels. Moreover, for all $t \in \mathcal{T}$, $i \in \mathcal{I}$ and $n \in \mathcal{N}$, let $x_{i,n}(t)$ be the indicator whether the i th stream has been scheduled by the BS on n th channel in the t th time-slot or not.

$$x_{i,n}(t) = \begin{cases} 1 & \text{if traffic stream } i \text{ is scheduled on channel } n \text{ in time-slot } t, \\ 0 & \text{otherwise,} \end{cases} \quad (4.1)$$

Based on this, the transmission scheduling constraints are given as follows.

$$\sum_{i=1}^I \sum_{n=1}^N x_{i,n}(t) \leq N, \quad \forall t \in \mathcal{T}. \quad (4.2)$$

$$\sum_{n=1}^N x_{i,n}(t) \leq 1, \quad \forall t \in \mathcal{T}, i \in \mathcal{I}. \quad (4.3)$$

4.2.2 Channel Model and SNR Analysis

For all $t \in \mathcal{T}$, $i \in \mathcal{I}$, and $n \in \mathcal{N}$, the channel coefficients between the BS and the RIS, the RIS and the i th destination, and between the BS and the i th destination on the n th spectrum resource are denoted, respectively, by $\mathbf{h}_{b \rightarrow R,n}(t) \in \mathbb{C}^{L \times 1}$, $\mathbf{h}_{R \rightarrow i,n}(t) \in \mathbb{C}^{L \times 1}$ and $h_{b \rightarrow i,n}(t) \in \mathbb{C}$. All channel coefficients consist of both the small-scale fading and the large-scale fading. In fact, for all $t \in \mathcal{T}$, $i \in \mathcal{I}$, and $n \in \mathcal{N}$, the channel coefficients $\mathbf{h}_{b \rightarrow R,n}(t)$, $\mathbf{h}_{R \rightarrow i,n}(t)$ and $h_{b \rightarrow i,n}(t)$ are expressed, respectively, as

$$\mathbf{h}_{b \rightarrow R,n}(t) = \hat{\mathbf{h}}_{b \rightarrow R,n}(t) \Delta_{b \rightarrow R} \quad (4.4)$$

$$\mathbf{h}_{R \rightarrow i,n}(t) = \hat{\mathbf{h}}_{R \rightarrow i,n}(t) \Delta_{R \rightarrow i} \quad (4.5)$$

$$h_{b \rightarrow i,n}(t) = \hat{h}_{b \rightarrow i,n}(t) \Delta_{b \rightarrow i} \quad (4.6)$$

where $\hat{\mathbf{h}}_{b \rightarrow R, n}(t)$, $\hat{\mathbf{h}}_{R \rightarrow i, n}(t)$ and $\hat{\mathbf{h}}_{b \rightarrow i, n}(t)$ represent the small-scale fading coefficients between the BS and the RIS, between the RIS and the i th destination, and between the BS and i th destination on the n th frequency resource, respectively, whereas $\Delta_{b \rightarrow R}$, $\Delta_{R \rightarrow i}$ and $\Delta_{b \rightarrow i}$ represent the large-scale fading coefficients between the BS and RIS, between the RIS and the i th destination, and between the BS and the i th destination respectively. Additionally, for all $i \in \mathcal{I}$, and $n \in \mathcal{N}$, the large-scale fading coefficients can be modeled as

$$\Delta_{b \rightarrow R} = \sqrt{\gamma_0 d_{B \rightarrow R}^{-\eta_{bR}}} \quad (4.7)$$

$$\Delta_{R \rightarrow i} = \sqrt{\gamma_0 d_{R \rightarrow i}^{-\eta_{Ri}}} \quad (4.8)$$

$$\Delta_{b \rightarrow i} = \sqrt{\gamma_0 d_{B \rightarrow i}^{-\eta_{bi}}} \quad (4.9)$$

where γ_0 is the path-loss average channel power gain at a reference distance $d_0 = 1\text{m}$, η_k is the path-loss exponent for the wireless link $k \in \{bR, Ri, bi\}$, $d_{R \rightarrow i}$ represents the distance between the RIS and i th destination, $d_{B \rightarrow i}$ represents the distance between the BS and i th destination, and $d_{B \rightarrow R}$ represents the distance between the BS and RIS. The small scale fading of the direct links between the BS and the destinations is modelled as a Rayleigh fading channel with zero mean and unit variance [52]. Meanwhile, the communication links between the BS and the RIS and between the RIS and the destinations are considered to have LoS components. These links experience small-scale fading that is modelled as Rician fading [52]. Accordingly, for all $t \in \mathcal{T}$ and $n \in \mathcal{N}$, the small-scale fading $\hat{\mathbf{h}}_{b \rightarrow R, n}(t)$ between the BS and the RIS on the n th frequency resource is defined as:

$$\hat{\mathbf{h}}_{b \rightarrow R, n}(t) = \sqrt{\frac{K_1}{K_1 + 1}} \tilde{\mathbf{h}}_{b \rightarrow R, n}(t) + \sqrt{\frac{1}{K_1 + 1}} \bar{\mathbf{h}}_{b \rightarrow R, n}(t), \quad (4.10)$$

where K_1 is the Rician factor, and $\tilde{\mathbf{h}}_{b \rightarrow R, n}(t)$ and $\bar{\mathbf{h}}_{b \rightarrow R, n}(t)$ are the deterministic LoS and Rayleigh fading components respectively. Similarly, for all $t \in \mathcal{T}$, $i \in \mathcal{I}$, and $n \in \mathcal{N}$, the small-scale fading $\hat{\mathbf{h}}_{R \rightarrow i, n}(t)$ between the RIS and the i th destination on the n th frequency resource is given as:

$$\hat{\mathbf{h}}_{R \rightarrow i, n}(t) = \sqrt{\frac{K_2}{K_2 + 1}} \tilde{\mathbf{h}}_{R \rightarrow i, n}(t) + \sqrt{\frac{1}{K_2 + 1}} \bar{\mathbf{h}}_{R \rightarrow i, n}(t), \quad (4.11)$$

where K_2 is the Rician factor and $\tilde{\mathbf{h}}_{R \rightarrow i, n}(t)$ and $\bar{\mathbf{h}}_{R \rightarrow i, n}(t)$ are the deterministic LoS and Rayleigh fading components respectively. Additionally, similar to other works in literature [44, 99, 100], we assume that the channel state information (CSI) of the considered wireless links is perfectly estimated at the BS. Although, obtaining the perfect CSI is quite challenging, recent studies [101, 102] have provided means to obtain efficient channel estimation techniques for RIS-enabled networks that can be embraced with our system model to obtain accurate CSI.

Based on the above discussion, and for all $t \in \mathcal{T}$, $i \in \mathcal{I}$, and $n \in \mathcal{N}$, the signal-to-noise ratio (SNR) at the i th destination at the t time-slot and for the n th channel can be expressed as

$$\gamma_{i, n}(\Phi(t)) = \frac{P |\mathbf{h}_{b \rightarrow R, n}^H(t) \Phi(t) \mathbf{h}_{R \rightarrow i, n}(t) + h_{b \rightarrow i, n}(t)|^2}{\sigma^2}, \quad (4.12)$$

where σ^2 is the noise power experienced at each destination and P is the transmit power of the BS. So far, we have discussed the main components related to the SNR at each destination. Next, we will discuss the main elements for the AoI problem.

4.3 Age of Information

The AoI illustrates how old the information is from a destination's perspective and is defined as the time elapsed since the most recent successful transmission of the valid information update [4]. For all $t \in \mathcal{T}$ and $i \in \mathcal{I}$, let $A_i(t)$ denote the AoI for a destination i in time-slot t . In addition, it is important to mention that a successful delivery of a packet at the destination in a given time slot t , for all $t \in \mathcal{T}$, is conditioned on two realizations:

1. The stream selected by the BS for scheduling in time-slot t has a packet available in its queue.
2. The SINR of the channel between the BS and the destination including the impact of both the direct and indirect links is above a given threshold.

Precisely, for all $i \in \mathcal{I}$ and $t \in \mathcal{T}$, if a packet of the i th traffic stream is scheduled by the BS and it is successfully delivered at the t th time-slot¹, then the corresponding AoI in the subsequent time-slot will be given by $A_i(t+1) = z_i(t) + 1$, where $z_i(t)$ represents the system time of the packet in queue i at the beginning of slot t . Conversely, if the transmission remained unsuccessful, then the AoI in the subsequent time-slot will be given by $A_i(t+1) = A_i(t) + 1$. Hence, for all $i \in \mathcal{I}$, the evolution of AoI of destination i [10] is given as

$$A_i(t+1) = \begin{cases} z_i(t) + 1 & \text{if } x_{i,n}(t) = 1, \beta_i(t) = 1, \text{ and } \gamma_{i,n}(\Phi(t)) \geq \gamma_{\text{th}}, \\ A_i(t) + 1 & \text{otherwise,} \end{cases} \quad (4.13)$$

where $A_i(0) = 0$ and $\beta_i(t)$ is a binary variable that indicates whether the i th stream has an available packet for transmission at the beginning of time-slot t or not. It is

¹In this work, we considered that the transmission of each packet occupies one time-slot from BS to each destination [103].

worth mentioning that, for all $i \in \mathcal{I}$, the value of z_i is reset to 0 when a new packet of the i th stream arrives in its queue. However, if no new packet is available at the i th queue, then the value of z_i is linearly increased by 1 in the subsequent time-slot. Based on this, for all $i \in \mathcal{I}$, the evolution of z_i [10] is given as

$$z_i(t+1) = \begin{cases} 0 & \text{if } u_i(t+1) = 1, \forall i, t. \\ z_i(t) + 1 & \text{otherwise.} \end{cases} \quad (4.14)$$

In addition, it is important to mention that, for all $i \in \mathcal{I}$, the value of $\beta_i(t)$ changes to 0 only when the packet of stream i is scheduled and successfully delivered and there is no new arrival in the same queue, i.e., $u_i(t) = 0$. Based on this, for all $i \in \mathcal{I}$, the evolution of $\beta_i(t)$ [104] can be written as:

$$\beta_i(t+1) = \begin{cases} 1 & \text{if } u_i(t+1) = 1, \\ 0 & \text{if } \beta_i(t)x_{i,n}(t) = 1 \wedge \gamma_{i,n}(\Phi(t)) \geq \gamma_{\text{th}}, \\ \beta_i(t), & \text{otherwise.} \end{cases} \quad (4.15)$$

which can be rewritten as

$$\beta_i(t+1) = u_i(t+1) + \beta_i(t)(1 - x_{i,n}(t))(1 - u_i(t+1)). \quad (4.16)$$

For the sake of tractability, the AoI can be explained by the following [104]:

$$A_i(t+1) = 1 + x_{i,n}(t)\beta_i(t)z_i(t) + (1 - x_{i,n}(t)\beta_i(t))A_i(t) \quad (4.17)$$

$$\gamma_{i,n}(\Phi(t)) \geq x_{i,n}(t)\beta_i(t)\gamma_{\text{th}}, \quad (4.18)$$

4.4 Problem Formulation

In this section, we leverage the communication model and the AoI definition presented in the previous sections to formulate a joint optimization of packets scheduling and RIS configuration to minimize the AoI of the system.

4.4.1 Problem Formulation

To ensure the freshness of the received information at each destination, we aim to minimize the expected sum AoI for the I streams over the time horizon of \mathcal{T} . Let \mathcal{X} and \mathcal{R} denote the sets of the scheduling policies and the RIS configurations over the time horizon \mathcal{T} , which are defined, respectively, as

$$\mathcal{X} = \{x_{i,n}(t) | \forall t \in \mathcal{T}, i \in \mathcal{I}, n \in \mathcal{N}\}, \quad (4.19)$$

$$\mathcal{R} = \{\Phi(t) | \forall t \in \mathcal{T}\}. \quad (4.20)$$

Hence, the optimization problem can be formulated as:

$$\mathcal{OP} : \min_{\mathcal{X}, \mathcal{R}} \frac{1}{I} \frac{1}{T} \mathbb{E} \left[\sum_{t=1}^T \sum_{i=1}^I A_i(t) | A_i(0) = 0 \right], \quad (4.21a)$$

$$\text{s.t.} \quad (4.2), (4.3), (4.16) - (4.18),$$

$$\theta_f(t) \in [0, 2\pi), \quad \forall t \in \mathcal{T}, l \in \mathcal{L}, \quad (4.21b)$$

$$x_{i,n}(t) \in \{0, 1\}, \quad \forall t \in \mathcal{T}, i \in \mathcal{I}, n \in \mathcal{N}, \quad (4.21c)$$

In problem \mathcal{OP} , the objective function in (4.21a) seeks to minimize the expected sum AoI. On the other hand, constraint (4.2) ensures that no more than N traffic streams are scheduled for transmission in a given time-slot and constraint (4.3) guarantees that each traffic stream is scheduled on at most one frequency channel. Moreover,

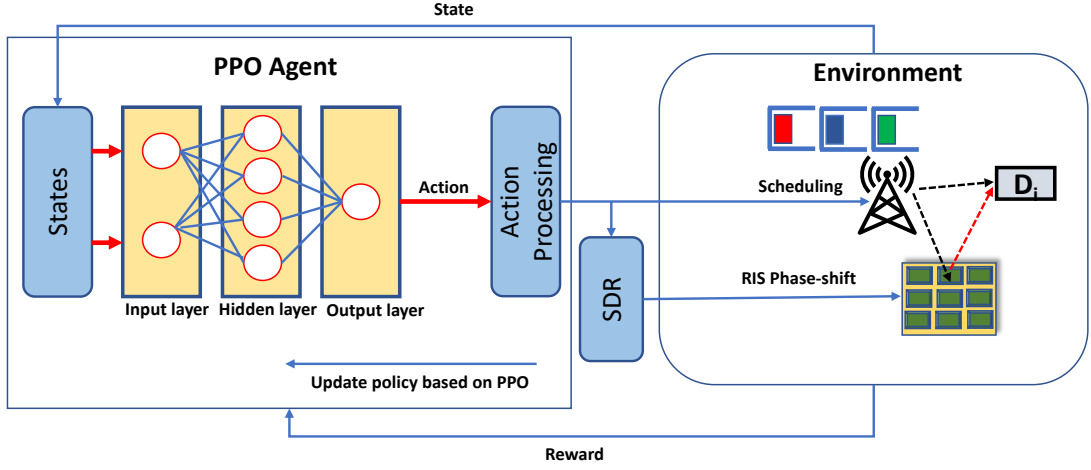


Figure 4.2: An illustration of the proposed solution.

constraint (4.16) shows the current status of the queue of each information stream at each time slot whether it is empty or has a packet available for transmission. In addition, constraints (4.17) and (4.18) ensure the correct evolution of AoI over the time horizon \mathcal{T} considering that the received SNR is above a certain threshold at each time slot. Furthermore, constraint (4.21b) restrains the range of the phase shift at each RIS element. Finally, constraint (4.21c) ensures the binarity of the traffic streams scheduling variables over the available frequency channels at each time slot. Given the uncertainties in the arrival of packets from each traffic stream at a given time-slot, \mathcal{OP} is a stochastic optimization problem over the time horizon \mathcal{T} . We further observe that \mathcal{OP} is a mixed-integer non-convex optimization problem which is difficult to be solved. This is due to the existence of both binary decision variables for packet scheduling and the RIS phase shift optimization. Therefore, we solve the \mathcal{OP} by using the concept of bi-level optimization [105].

4.4.2 Solution Approach

In this section, we present our roadmap to solve the joint scheduling and RIS phase shift optimization problem with the objective of minimizing the expected sum AoI. Leveraging the concept of bi-level optimization, we decompose the above problem into an outer traffic stream scheduling problem and an inner phase shift matrix optimization problem. The stochastic arrival of the traffic into each stream makes the outer problem quite challenging. Hence, we resort to DRL to observe the environment and train an agent that performs scheduling. While, the inner problem of phase shift matrix optimization is solved using SDR technique. The schematic illustration of our proposed solution approach is presented by Figure 4.2. We now discuss the two problems in detail:

4.4.2.1 Traffic streams scheduling problem

The outer problem aims to obtain the traffic stream scheduling having the RIS phase shift matrix obtained from the \mathcal{OP}_{inner} problem is modelled as an MDP. A DRL based on PPO algorithm is hereby proposed to determine the policy that governs the scheduling of traffic streams. The \mathcal{OP}_{outer} can be written as:

$$\mathcal{OP}_{outer} : \min_{\mathcal{X}} \frac{1}{I} \frac{1}{T} \mathbb{E} \left[\sum_{t=1}^T \sum_{i=1}^I A_i(t) | A_i(0) = 0 \right], \quad (4.22a)$$

$$\text{s.t.} \quad (4.2), (4.3), (4.16), (4.17), (4.21c)$$

$$\mathcal{R} = \mathcal{OP}_{Inner}, \quad (4.22b)$$

An MDP is generally defined as a 4-tuple $(\mathbf{S}, \mathbf{Y}, \mathbf{R}, \mathbf{P})$, where: \mathbf{S} is a finite set of all possible states $s(t)$ at any time-slot t , where $s(t) \in \mathbf{S}$; \mathbf{Y} is a set of all feasible actions $a(t)$ at any time-slot t , where $a(t) \in \mathbf{Y}$; \mathbf{R} is the reward distribution, given by a measurable function $P(r(t)|s(t), a(t))$, which grants immediate reward $r(t) \in \mathbf{R}$ after

an action $a(t) \in \mathbf{Y}$ has been chosen in a state $s(t) \in \mathbf{S}$ at time-slot t ; \mathbf{P} is a Markovian transition model, where $P(s(t+1)|s(t), a(t)), s(t), s(t+1) \in \mathbf{S}, a(t) \in \mathbf{Y}$ represents the probability of going from state $s(t)$ to state $s(t+1)$ with action $a(t)$. We will next elaborate the state, action and reward functions under the MDP framework as under:

- **State \mathbf{S} :** The system state at time t is defined as $s(t) = (\mathbf{A}(t), \boldsymbol{\beta}(t), \mathbf{Z}(t))$, where $s(t) \in \mathbf{S}$. The $\mathbf{A}(t) = (A_1(t), A_2(t), \dots, A_I(t))$ is a vector of size I containing the AoI of all traffic streams at time-slot t , $\boldsymbol{\beta}(t) = (\beta_1(t), \beta_2(t), \dots, \beta_I(t))$ is a vector of size I containing the indicator that traffic streams have packets available for transmission and $\mathbf{Z}(t) = (Z_1(t), Z_2(t), \dots, Z_I(t))$ is the system time related to the I streams at time slot t .
- **Action \mathbf{Y} :** An action $a(t)$ is executed at each time-slot t denoted by $a(t) \in \mathbf{Y}$ consists of channel allocation decisions. The $a(t)$ is a vector of size α , where α represents the number of channels to be assigned to users.
- **Reward \mathbf{R} :** The immediate reward $r(t)$ at time slot t is the negative summation of AoI, $r(t) = -\sum_{i=1}^I A_i(t)$, where $r(t) \in \mathbf{R}$. Considering the objective of minimizing the expected sum AoI, the RL-agent aims to optimize the scheduling decision that leads to minimize the AoI.

Algorithm 1 presents our proposed approach with DRL exploiting the PPO to develop the agent. The agent based on PPO is usually implemented in Actor-Critic framework. We now summarize the steps of algorithm. The agent first initializes a random sampling policy and a value function for neural networks as given by (line 3 and line 4). Further, at each episode, the agent observes the environment which is composed of current AoI of all the destinations, the current system time in each queue

up to t slot. Then at each time-slot, the agent selects an action which is a vector carrying the channels in a specific order to be mapped with the traffic streams that have a packet available for transmission. The action results to invoke the SDR (Algorithm 2) in order to configure the RIS phases shift matrix to maximize the channel gain. Eventually, the time step reward is calculated which is the negative sum of age of information of all the streams. Once the set of samples have been gathered and rewards have been computed, the agent determines the advantage function (line 15) which is the resultant of the difference of the expected value function from the actual reward. This is to note that the advantage estimate helps the system to analyze how good it is performing based on its normal estimate function value. Regarding the complexity, based on [104], the total computational complexity of DRL frameworks such as PPO algorithm can be expressed as the number of multiplications: $O(\sum_{p=1}^{P-1} n_p \cdot n_{p-1})$, where n_p is the number of neural units in the p -th hidden layer.

4.4.2.2 SDR for RIS phase shift coefficients

Referring to the definition of AoI given in Section (4.3), if no successful status update is delivered, the age will increase linearly with the time axis. Therefore, if the updated packets of a stream are scheduled by the BS but the corresponding channels do not satisfy the SNR constraints, the total AoI in T time-slots will increase. Therefore, the phase shifts of the reflective elements should be configured to maximize the SNR of the channels corresponding to the selected streams. The SDR technique is applied to obtain $\boldsymbol{\theta}$ that can maximize the overall channel gain.

$$\mathcal{OP}_{inner}: \max_{\boldsymbol{\theta}} |\mathbf{h}_{b \rightarrow R, n}^H(t) \boldsymbol{\Phi}(t) \mathbf{h}_{R \rightarrow i, n}(t) + h_{b \rightarrow i, n}(t)|^2 \quad (4.23a)$$

s.t.

$$0 \leq \theta_l(t) \leq 2\pi, \quad \forall l \in \llbracket 1, L \rrbracket \quad (4.23b)$$

Algorithm 4 Proposed solution approach for minimizing the expected sum AoI

- 1: **Input:** Number of users (I), Number of time-slots (T), Learning Rate, Episodes K , threshold (γ_{th}).
 - 2: **Output:** User scheduling, Resource allocation and Phase shift matrix.
 - 3: Initialize policy π with random parameter θ
 - 4: Initial value function V with random parameters ϕ
 - 5: **for** $k \leftarrow 1 : K$ **do**
 - 6: **for** $t \leftarrow 1 : T$ **do**
 - 7: Get $(\mathbf{A}(t), \boldsymbol{\beta}(t), \mathbf{Z}(t))$ from the environment.
 - 8: sample action $a(t) \sim \pi_{\theta_{old}}$.
 - 9: Take action $a(t)$ that specifies the channels (in a specific order).
 - 10: Obtain the resource allocation by mapping the top N traffic streams that have a packet available for transmission.
 - 11: Configure $\Phi(t)$ that maximizes the SNR of the mapped users to the respective channels using SDR approach using Algorithm 2.
 - 12: Perform the feasibility check to determine if SNR threshold constraint is satisfied.
 - 13: Get relevant reward $r(t)$ and $s(t+1)$.
 - 14: Store $(s(t), a(t), r(t), s(t+1))$ as one transition in the experience replay.
 - 15: Compute advantage estimate \hat{A} for all epochs.
 - 16: Optimize surrogate loss function using Adam optimizer.
 - 17: Update current policy $\pi_{\theta_{old}} \leftarrow \pi_{\theta}$.
-

Let us define, $\mathbf{v} = [v_1, v_2, \dots, v_L]^H$, where $v_l = e^{j\theta_l}$, $\forall l$. Thus, the constraints in (4.23b) are equivalent to the unit-modulus constraints, i.e., $|v_l|^2 = 1 \forall l \in L$. By applying the change of variables, $\mathbf{h}_{b \rightarrow R, n}^H(t) \Phi(t) \mathbf{h}_{R \rightarrow i, n}(t)$ can be represented as $\mathbf{v}^H \mathbf{W}(t)$, where $\mathbf{W}(t) = \text{diag}(\mathbf{h}_{b \rightarrow R, n}^H(t)) \mathbf{h}_{R \rightarrow i, n}(t)$. Thus, we have

$$|\mathbf{h}_{b \rightarrow R, n}(t) \Phi(t) \mathbf{h}_{R \rightarrow i, n}(t) + h_{b \rightarrow i, n}(t)|^2 = |\mathbf{v}^H \mathbf{W}(t) + h_{b \rightarrow i, n}(t)|^2 \quad (4.24)$$

An expression of overall channel gain denoted by \mathcal{Z} can be given as:

$$\begin{aligned} \mathcal{Z} &= |\mathbf{v}^H \mathbf{W}(t) + h_{b \rightarrow i, n}(t)|^2, \\ &= \mathbf{v}^H \mathbf{W}(t) \mathbf{W}^H(t) \mathbf{v} + h_{b \rightarrow i, n}(t) \mathbf{W}^H(t) \mathbf{v} \\ &\quad + \mathbf{v}^H \mathbf{W}(t) h_{b \rightarrow i, n}(t) + |h_{b \rightarrow i, n}(t)|^2 \end{aligned} \quad (4.25)$$

Algorithm 5 Design of Phase Shift Matrix via SDR

- 1: **Input:** Number of users, Number of RIS elements
 - 2: **Output:** Phase shift matrix, i.e. Φ .
 - 3: Initialize the maximum generation of candidate random vector as ξ
 - 4: Solve the relaxed SDR problem (4.27).
 - 5: **if** $\text{rank}(\mathbf{V}) = 1$ **then**
 - 6: With the obtained \mathbf{V} , calculate the eigenvalue ω and eigen vector \mathbf{u} according to $\mathbf{V}\mathbf{u} = \omega\mathbf{u}$.
 - 7: Update the value of the phase-shift matrix $\Phi^* := \text{diag}(\sqrt{\omega\mathbf{u}})$.
 - 8: **else**
 - 9: obtain the eigenvalue decomposition using Eq. (4.28)
 - 10: **for** $x \leftarrow 1 : \xi$ **do**
 - 11: Generate a Gaussian random vector \mathbf{r}_x , i.e., $\mathbf{r}_x \sim CN(0; I_{F+1})$
 - 12: Obtain a candidate solution Θ_x using Eq. (4.29) and Eq. (4.30).
 - 13: find the optimal $\Theta^* := \Theta_x$ that maximizes the combined channel gain for all users.
-

The above equation can be written as follows

$$\mathcal{Z} = \bar{\mathbf{v}}^H \Phi \bar{\mathbf{v}} + |h_{b \rightarrow i, n}(t)|^2, \quad (4.26)$$

where

$$\Phi = \begin{bmatrix} \mathcal{W}(t)\mathcal{W}^H(t) & \mathcal{W}(t)h_{b \rightarrow i, n}(t) \\ h_{b \rightarrow i, n}(t)\mathcal{W}^H(t) & 0 \end{bmatrix}$$

,

$$\bar{\mathbf{v}} = \begin{bmatrix} \mathbf{v} \\ 1 \end{bmatrix}$$

Note that $\bar{\mathbf{v}}^H \Phi \bar{\mathbf{v}} = \text{tr}(\Phi \bar{\mathbf{v}} \bar{\mathbf{v}}^H)$. Additionally, we define $\mathbf{V} = \mathbf{v} \bar{\mathbf{v}}^H$, which needs to satisfy $\text{rank}(\mathbf{V})=1$ and $\mathbf{V} \geq 0$. This rank constraint ($\text{rank}(\mathbf{V})=1$) is non-convex [35].

By dropping this constraint, the problem \mathcal{OP}_{inner} can be rewritten as:

$$\mathcal{P1}: \max_{\Phi} \mathcal{Z}(\Phi) \quad (4.27a)$$

s.t.

$$\mathbf{V} \geq 0, \quad (4.27b)$$

$$[\mathbf{V}]_{L,L} = 1. \quad (4.27c)$$

After the proposed transformation, the above problem can be solved by any convex optimization solver such as CVX[35]. Generally, the optimal \mathbf{V} obtained by solving problem $\mathcal{P1}$ does not satisfy the rank one constraint. This implies that the optimal solution of the $\mathcal{P1}$ only serves as an upper bound for the problem \mathcal{OP}_{inner} . Therefore, other steps are needed to construct a rank one solution. The rank one solution is hence achieved by applying the Gaussian randomization scheme. We now describe it in detail. Firstly, we obtain the eigenvalue decomposition of \mathbf{V} as

$$\mathbf{V} = \mathbf{U}\mathbf{\Sigma}\mathbf{U}^H, \quad (4.28)$$

where $\mathbf{U} = [u_1, u_2, \dots, u_{L+1}]$ is a unitary matrix and $\mathbf{\Sigma} = \text{diag}(\omega_1, \omega_3, \dots, \omega_{L+1})$ is a diagonal matrix, respectively. Next, a random vector is generated as follows,

$$\bar{\mathbf{v}} = \mathbf{U}\mathbf{\Sigma}^{1/2}\mathbf{r}, \quad (4.29)$$

where \mathbf{r} is a random vector that follows a circularly symmetric complex Gaussian (CSCG) distribution with a zero mean and a co-variance matrix equal to the identity matrix of order $L + 1$, denoted by I_{L+1} i.e., $\mathbf{r} \sim CN(0; I_{L+1})$. Furthermore, we generate the scalar \mathbf{v}

$$\mathbf{v} = \exp \left[j \arg \left(\frac{[\bar{\mathbf{v}}]_{1:L}}{[\bar{\mathbf{v}}]_{L+1}} \right) \right], \quad (4.30)$$

where $[\bar{\mathbf{v}}]_{1:L}$ represents the vector with first L elements in \mathbf{v} . It is significant to highlight that the SDR approach followed by a large number of Gauss randomization can guarantee a minimum accuracy of $\pi/4$ of the optimal objective value [35]. The core details of the phase shift matrix optimization is given by Algorithm 2. Regarding the complexity of Algorithm 2, obtaining the phase-shift matrix is a semi-definite programming (SDP) problem which can be solved by the interior point method and its order of computational complexity with m SDP constraints that contain an $n \times n$ positive semi-definite matrix is given as $\mathcal{O}(\sqrt{n} \log(1/\epsilon)(mn^3 + m^2n^2 + m^3))$, where $\epsilon > 0$ is the solution accuracy [52]. The approximate computational complexity to solve SDP can be written as $\mathcal{O}(\log(1/\epsilon)(L^{4.5}))$ with $m = L$ and $n = L + 1$. Meanwhile, let w be the maximal number of generated Gaussian random vectors and T_{GR} is the complexity of performing one Gaussian random iteration. Hence, the approximate complexity of obtaining phase shift matrix can be written as $\mathcal{O}(\log(1/\epsilon)(L^{4.5} + wT_{GR}))$.

4.5 Simulation and Numerical Analysis

In this section, we present a series of simulations to evaluate the performance of the proposed algorithm. The simulation parameters are first presented, followed by the adopted benchmark schemes and then the results and discussions.

4.5.1 Simulations Setup

We consider a 3-D area where a BS is communicating with a set of spatially dispersed destinations through an RIS. We assume that the global coordinate system (X, Y, Z) is Cartesian. As shown in Figure 4.3, the BS is located at $(0, 0, H_b)$ and

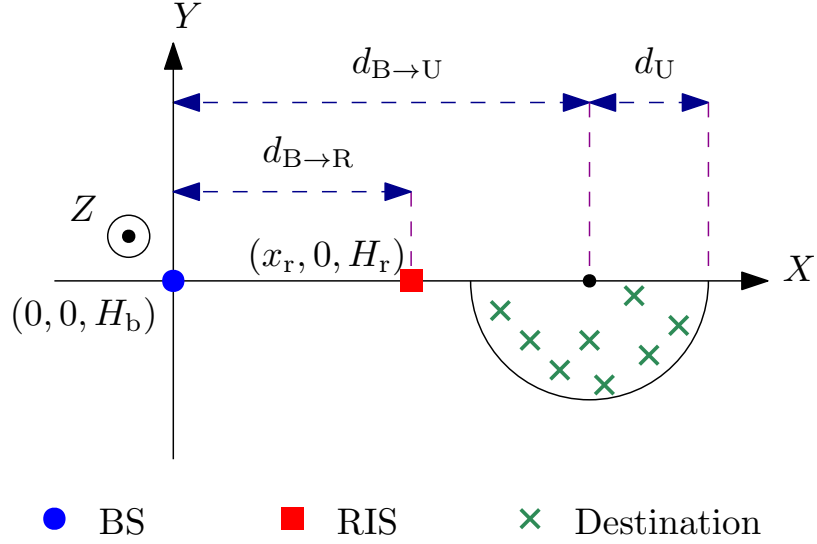


Figure 4.3: Distance model.

the RIS is located at $(x_r, 0, H_r)$, where $x_r = d_{B,R}$ is the distance from the BS to the RIS, and H_b and H_r are the heights of the transmit antenna of the BS and of the RIS, respectively. In addition, multiple destinations are randomly distributed at the ground level within a given area in the network, where for all $i \in \mathcal{I}$, the locations of destinations are $(x_i, y_i, 0)$. Precisely, based on Figure 4.3, the coordinates of the i th destination, for all $i \in \mathcal{I}$, are given by

$$\begin{aligned}
 x_i &= d_U \cos(\theta_i) + d_{B,U}, \\
 y_i &= d_U \sin(\theta_i) + d_{B,U},
 \end{aligned} \tag{4.31}$$

where d_U is the radius of the area where the destinations are located, $d_{B,U}$ is the distance from the BS to the center of this area and, $\theta_i \in [\pi, 2\pi]$ is a polar angle. Unless otherwise indicated, all the simulation parameters are given by Table 4.1.

4.5.2 Benchmark Schemes

To the best of our knowledge, there is no existing approach that aims to solve the problem of minimizing the age of information in RIS-assisted wireless networks

Parameter	Values
Total number of time slots, T	100
Arrival rate, λ	0.5
Activation functions	Softmax and Tanh
Number of Neurons	64
Number of Hidden layers for Networks	3
Learning Rate	0.002
$d_{B,U}$	200 m
d_U	10 m
$d_{B,R}$	200 m
H_b	10 m
H_r	10 m
σ^2	-110 dBm
η_{bR}	-2.2
η_{Ri}	-2.2
η_{bi}	-3.5
Rician factors (K1, K2)	2 dB
Optimizer technique	Adam
Clip function, ϵ	0.2
Total number of Epochs	3000
γ_0	-20dB
γ_{th}	45dB

Table 4.1: Simulation parameters.

by optimizing the scheduling of existing traffic streams and the design of the RIS configuration considering the impacts of the stochastic arrivals of the packets and the multi-user scheduling. Thus, for the sake of comparison, we develop three other baseline schemes in order to assess the performance of the proposed scheme.

4.5.2.1 Greedy Scheduling with SDR (GS-SDR)

In this scheme, the scheduling problem is solved using a greedy approach, whereas the RIS configuration problem is solved using the SDR approach. The greedy scheduling approach is explained as follows. At each time-slot $t \in \mathcal{T}$, the traffic streams are first ranked based on their current AoI. The top N streams are selected to get scheduled and the RIS phase shift matrix optimization is performed to maximize the

SNR of these selected streams. If the obtained SNR satisfies the given threshold, the selected streams are assumed to be scheduled and the corresponding age is calculated accordingly. However, the scheduling decisions are taken irrespective of the knowledge that the queue of the selected streams are empty or not. In case, if there is no status update packet in the selected stream’s queue, a time-slot is lost.

4.5.2.2 Round-Robin Scheduling with SDR (RRS-SDR)

This algorithm is based on round-robin scheme, where at each time-slot, the BS alternately selects an input stream $i \in \mathcal{I}$, starting from the first stream, to upload its status update packet to the destination node. The RIS configuration optimization is performed to maximize the channel gain of the scheduled streams. However, and similar to the GS-SDR baseline, the scheduling decisions are taken irrespective of the knowledge that the queue of the selected streams are empty or have packets to deliver

4.5.2.3 DRL with Random Phase-Shift Matrix (DRL-RPM)

In this approach, the proposed DRL algorithm is used to obtain the scheduling of the traffic streams. However, the RIS configuration is not optimally designed and instead, a random RIS phase shift matrix is employed.

4.5.3 Results and Discussions

We first attempt to observe the behavior of the DRL agent and to verify the convergence of the proposed algorithm. As depicted in Figure 4.4, the cumulative reward, which is the negative of the minimum average sum AoI, is significantly improving as the number of iterations, or episodes, is increasing. Basically, it can be observed from this figure that the proposed PPO algorithm starts to converge after 3000 iterations. In the next experiment, the impact of varying the size of the RIS (number of ele-

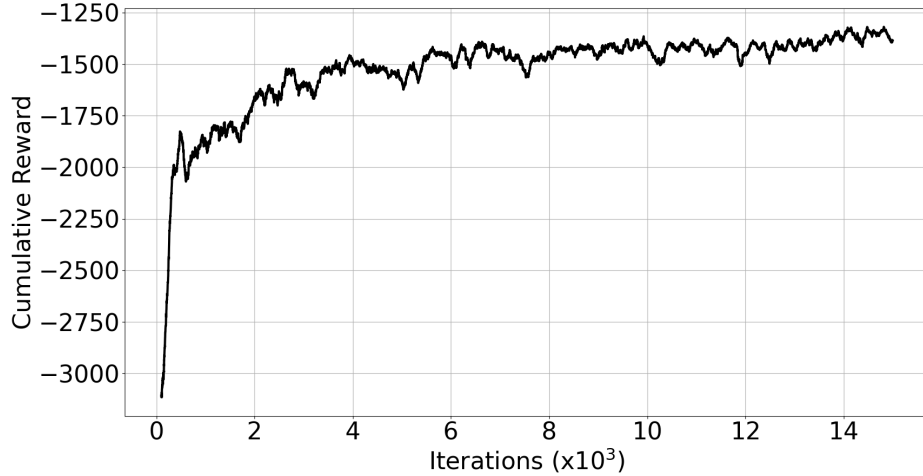
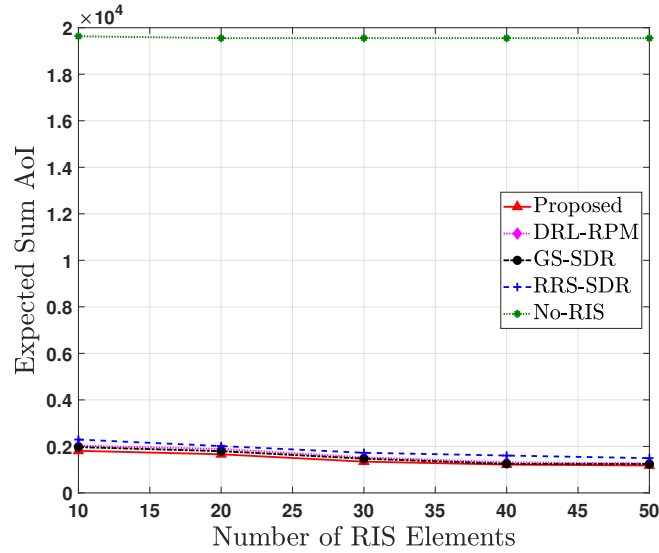


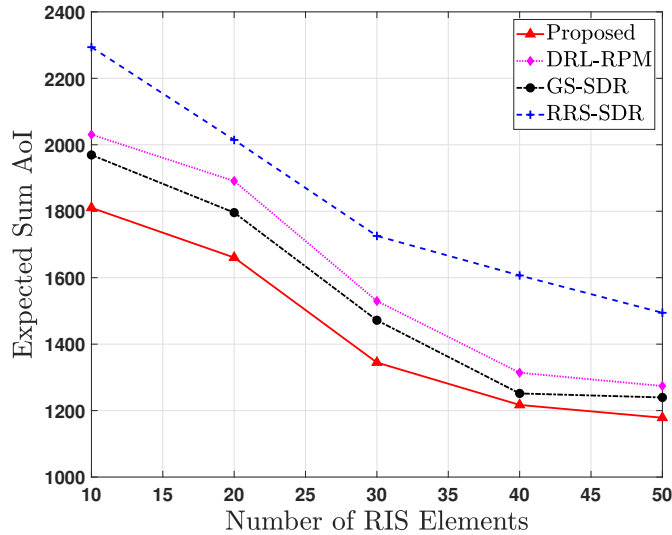
Figure 4.4: Accumulated reward vs. iterations.

ments) on the expected sum AoI under the different schemes is analyzed as shown in Figure 4.5. The impact of RIS elements is simulated by varying the number of RIS elements from 10 to 50 with a step size of 10. It can be seen from Figure 4.5.a that the integration of the RIS has a significant impact on the AoI as compared to the case when RIS is not utilized, i.e., when the direct links from the BS to destinations are solely relied on to transmit time-sensitive information. Indeed, this shows that the RIS can significantly improve the channel quality of the scheduled users, which subsequently results in a high success rate of packets delivery. We observed that the curves of the expected sum age of information for all schemes decrease as the number of RIS elements increase. Obviously, the channel quality of the potential scheduled users can be greatly enhanced by increasing the number of RIS elements as it improves the chances of successful delivery at the destination and eventually end up decreasing the AoI. From Figure 4.5.b, one can remark that the proposed algorithm achieves the lowest expected sum AoI compared to other benchmark approaches. For example, when the RIS elements is 50, the expected sum AoI obtained by the proposed algorithm is around 22% lower than the one obtained by the RRS-SDR approach. This is

due to the fact that the proposed PPO-based approach leverages the learning of the packet arrivals of the traffic streams and adjusts the RIS configuration accordingly for the streams that have packets to transmit. However, the other approaches do not consider this important factor which eventually results in worse age performance.



(4.5.a)



(4.5.b) [Zoomed view of (a).]

Figure 4.5: Impact of number of RIS elements on the AoI.

Although the expected sum AoI of the proposed algorithm is decreased by around

35% when the number of RIS elements are increased from 10 to 50 elements, one can further note from Figure 4.5 that the decrease in the AoI is not linear with the number of RIS elements, where the decrease in the AoI is not sharp when the number of elements are increased from 40 to 50, which is 3% in this case. This can be explained as increasing the number of RIS elements helps to improve the channel gains which eventually leads to satisfy the SNR threshold constraint. However, once it is satisfied, increasing number of RIS elements may not further bring the AoI down. We also observe that the GS-SDR scheme performs better than all other approaches except the proposed approach. Indeed, the greedy approach opts to schedule the streams with the worst AoI by ranking the streams with their AoI. However, since the scheduling decisions are taken irrespective of whether the scheduled stream has a packet available for transmission or not, a waste of resources occurs, which lowers the efficiency of the method. Unlike that, our method learns the presence of packets for scheduling and it is able to attain better performance through more informed scheduling decisions.

We next analyze the impact of a variable network load on the AoI, which is depicted in Figure 4.6, where the impact of increasing the network load on the AoI is investigated. The impact of increasing the load is simulated by varying the arrival rate of the packets from 0.1 to 0.5, with a step size of 0.1. The results are plotted for the expected sum AoI versus the arrival rate. The time-horizon used for this experiment is $T = 100$ time slots. As learnt from the theory of AoI, frequent information updates along with their successful delivery results in keeping the information fresh at a destination. Precisely, a low arrival rate leads to an increase in the expected AoI. However, as the arrival rate increases, more fresh packets arrive to the system and replace the old ones. Hence, under proper propagation environment through the RIS and a proper packets scheduling, the AoI decreases when the packets arrival rate increases. These facts are validated by Figure 4.6, where we observe that the curves

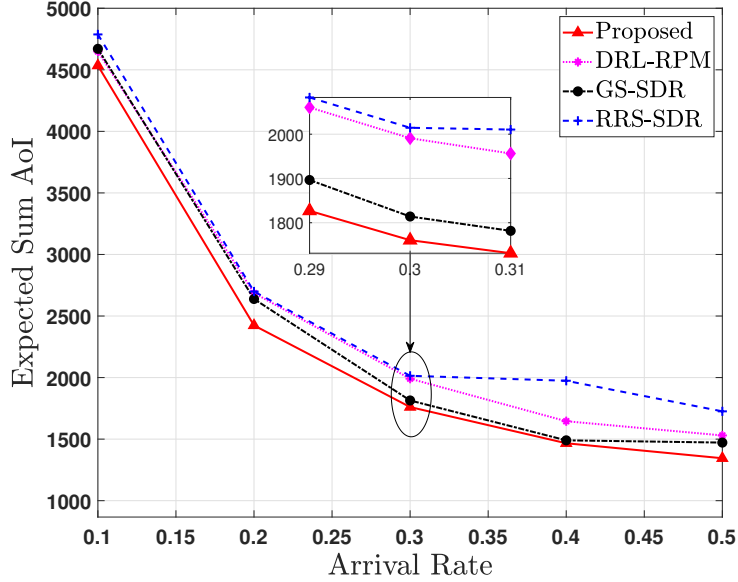


Figure 4.6: Impact of arrival rate on the AoI.

of the expected AoI for all the schemes decrease as the arrival rate increases. On top of this, our proposed method achieves the lowest AoI as compared to the other methods. For example when the arrival rate is increased from 0.1 to 0.5, the expected sum age is decreased by 70% for the proposed method. We also observe that the GS-SDR scheme performs better than the RR-SDR and the DRL-RPM schemes even when the arrival rate is low. The reason is related to its scheduling policy and RIS phase shift matrix optimization approach, since the GS-SDR scheme aims to schedule the streams that give the largest decrease in the sum AoI, and hence, results overall in a lower age than the other baseline approaches.

Figure 4.7 illustrates the impact of the RIS location from the perspective of the BS and the destinations. As delineated by Figure 4.7, the distance from the BS to the RIS, $d_{B,R}$ is varied starting by placing it next to the BS (at 1m distance) then increasing the distance up to 200m with an increment of 50m. Some interesting observations can be collected here. First, since the destinations are at least 200m apart from the BS, the direct link from the BS to each destination is expected to

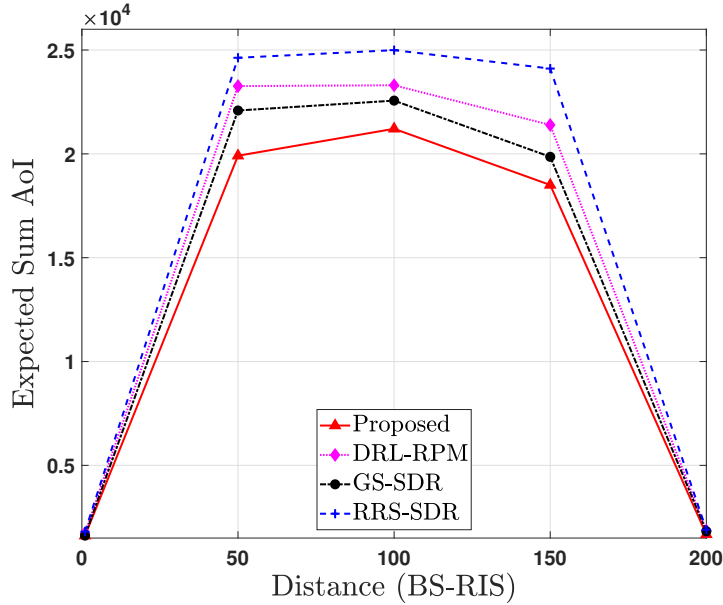
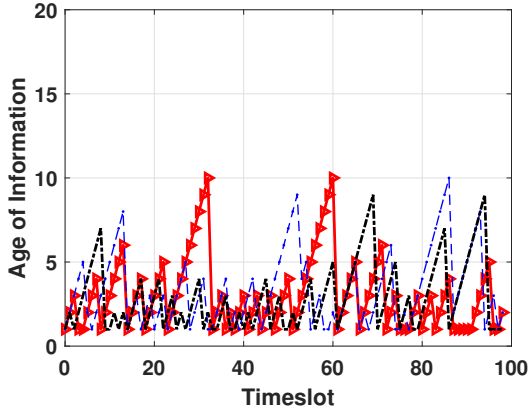


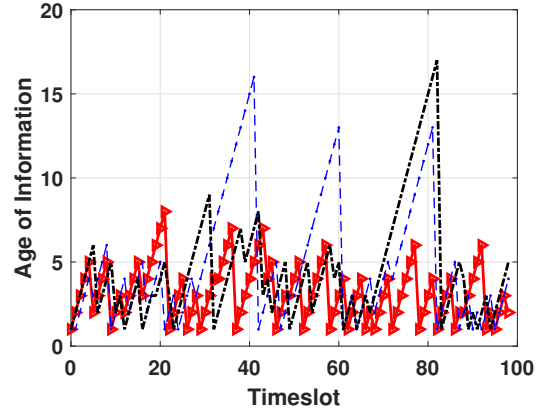
Figure 4.7: Impact of the position of RIS on the AoI

undergo severe fading which will result in very high AoI values for the case where the RIS is not used. The same has been experienced through simulations. Next, with the integration of the RIS, the quality of the transmitted signals can be greatly improved, which will eventually result in decreasing the AoI. It has been observed that, when the RIS is placed very close to the BS while the destinations were at least at 200m away from the BS, the AoI values were considerably low. The reason being that is, since the direct link was not sufficient to successfully transmit the information to the respective destinations, the RIS played its role and with a well designed phase shift matrix, the resultant AoI was low for all methods that employed RIS. On top of this, our proposed approach performed better than other baseline approaches.

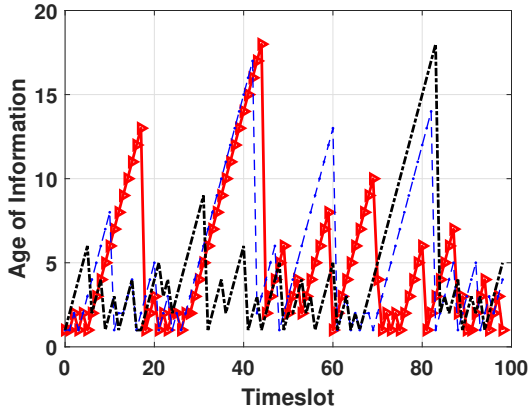
It can be seen that as the RIS is placed neither close to BS, nor close to destinations, the resultant AoI values start to increase for all approaches. Once, the RIS is installed close to the destinations, a significant improvement in terms of decreasing AoI against the No-RIS case can be provided. Again, the proposed approach outperforms the other baseline approaches. As explained earlier, the proposed approach



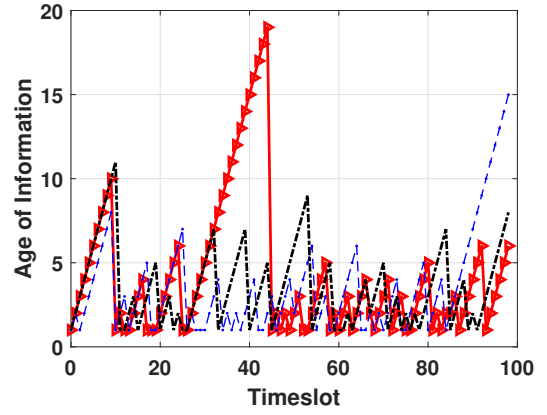
(4.8.a) Proposed



(4.8.b) GS-SDR



(4.8.c) RRS-SDR



(4.8.d) DRL-RPM

Figure 4.8: The performance comparison of different algorithms for a sample of three traffic streams.

takes advantage of the learning of the packets arrivals and also uses the SDR to efficiently configure the phase shift matrix of the RIS in order to maximize the SNR of the scheduled streams, which eventually results in reducing the AoI. To summarize, a well reasoned placement of the RIS can definitely lead to improving the overall system performance. The obtained results are in accordance with [52] which confirms that the best location for the RIS is either besides the BS or the users of interest.

Finally, to understand the impact of different scheduling and phase shift optimization techniques on the AoI evolution over time, the AoI evolution is presented in Figure 4.8 for all the algorithms. For a fair comparison, we have simulated a system

where $I = 5$ traffic streams are competing to forward their information update packets to the destinations and 3 traffic streams are selected to determine their AoI evolution over time. Figure 4.8 depicts that the AoI evolution is substantially different for the different methods. It can be observed that with the proposed approach, the AoI of all the streams is considerably smaller than those of the baseline methods. This is due to the fact that, as previously explained, the DRL agent learns how to schedule the traffic streams with packets to transmit such that the SNR on the selected channel is high enough to make the transmissions successful, which eventually reduces the AoI. However, the baseline approaches may undergo transmission failures due to inefficient scheduling, which results in packets' loss and re-transmission by the BS that increases the age. On the one hand, as delineated by Figure 4.8(b)-(d), it can be seen that baseline approaches significantly decrease the AoI for some streams.

Furthermore, the AoI gets significantly increased to the maximum for other streams. This is because (i) the RRS-SDR schedules the traffic streams in a round robin fashion irrespective of looking at the current AoI or the arrival time of the packets in the queue, (ii) the DRL-RPM utilizes the RIS agent to learn to do scheduling but without a proper RIS configuration, which may not achieve the required SNR for the selected streams and results in poor performance, and (iii) despite trying to schedule the streams with the worst AoI in each time-slot and properly configuring the RIS for the selected streams, the GS-SDR is limited due to the fact that it does scheduling attempt without having any knowledge about the arrival of packets. That's why, optimizing the RIS phase shifts alone may not guarantee that the scheduled stream would also have a packet to transmit and would increase the AoI.

4.6 Conclusion

This chapter investigates the role of RIS in transmitting the status update messages of multiple traffic streams to their respective destinations in order to keep the information fresh. The time-stamped status-update messages arrive to the BS with a stochastic arrival process and are selected following a scheduling policy to be forwarded to their respective destinations with the aid of RIS. We have formulated an optimization problem to find the efficient scheduling policy that minimizes the expected sum AoI evaluating the combined impact of stochastic packet arrivals, scheduling policy and RIS phase shift. The formulated optimization problem is a mixed integer non-convex optimization problem, which is difficult to solve. To circumvent the high-coupled optimization variables, we decompose the original problem into an outer traffic stream scheduling problem and an inner RIS phase-shift matrix problem. For the outer problem, owing to its complexity and stochastic nature of packet arrivals, we resort to deep reinforcement learning solution where the traffic stream scheduling is modeled as a MDP, and PPO is invoked to solve it. On the other hand, the inner problem to determine the RIS configuration is solved through SDR. Numerical results demonstrate the effectiveness of the proposed algorithm, which was also verified through extensive comparisons with other algorithmic solutions.

Chapter 5

AoI Optimization In RIS-Assisted NOMA/C-NOMA Based IoT Networks

5.1 Motivation and Contributions

The ever-increasing massive connectivity and spectral efficiency requirements of IoT applications brought forward NOMA as a promising scheme. To enhance the network performance in terms of AoI, it is imperative to serve as many users as possible while achieving their required Quality of Service (QoS). This can potentially be done by invoking NOMA in the proposed network model on account of its superior spectral efficiency performance against its contemporary OMA techniques [72]. Moreover, the integration of NOMA, cooperative relaying techniques and D2D communication, which is known as cooperative NOMA (C-NOMA), has been proposed to reinforce the performance of NOMA systems [78].

Recent investigations aiming to unleash the full potentials of NOMA towards optimizing the AoI in real-time applications unveiled that the timely delivery of information update messages can be severely compromised by the impact of the wireless channels [106, 107]. In a realistic sense, the highly random and uncontrollable behaviour of wireless communication environments impede the timely delivery of information update messages. By leveraging RIS, a strong channel between the source and destination can be constructed.

Motivated by the above, we aim in this chapter to investigate the envisioned benefits of integrating RIS in NOMA-based systems. The main contributions of this work are as under:

1. We formulate a joint RIS phase-shift matrix, IoTD-clustering policy, and IoTD transmit power optimization problem with the objective of minimizing the average sum AoI.
2. The formulated problem is a mixed integer non-convex problem, which is difficult to solve. In order to tackle this issue, we first obtain the RIS phase-shift

matrix that maximizes the minimum channel gains of all weak NOMA IoTDs. Afterwards, the original problem is reformulated as a bi-level optimization problem, comprising an outer IoTD clustering problem and an inner power allocation problem. The inner problem is a feasibility condition problem in which we derive the feasible range for the IoTD transmit power. Meanwhile, the outer problem is a classical linear assignment problem, which is solved through a one-to-one matching game.

3. As an extension to NOMA, we explored the cooperative communication and investigated how much performance gain in terms of AoI reduction can be brought by the RIS-enabled uplink C-NOMA system compared to the conventional C-NOMA and OMA system without RIS?.

5.2 AoI optimization in RIS-assisted NOMA based IoT networks

5.2.1 System Model

We consider the uplink IoT network depicted in Figure 5.1, which consists of one BS and $2I$ IoTDs that provide time-stamped status update information to the BS. The time is divided into time-slots with a slot index $t \in \mathcal{T}$, where $\mathcal{T} = \{1, 2, \dots, T\}$, such that T denotes the time horizon of this discrete-time system. Moreover, let $\mathcal{I} = \{1, 2, \dots, 2I\}$ denote the set of IoTDs. The IoTDs are divided into two disjoint sets with equal size I based on their channel gains [108]. The first set, denoted by \mathcal{S} , contains the I IoTDs with the highest channel gains, which are referred to as strong IoTDs. On the other hand, the second set, denoted by \mathcal{W} , contains the I IoTDs with the lowest channel gains, which are referred to as weak IoTDs. Due to

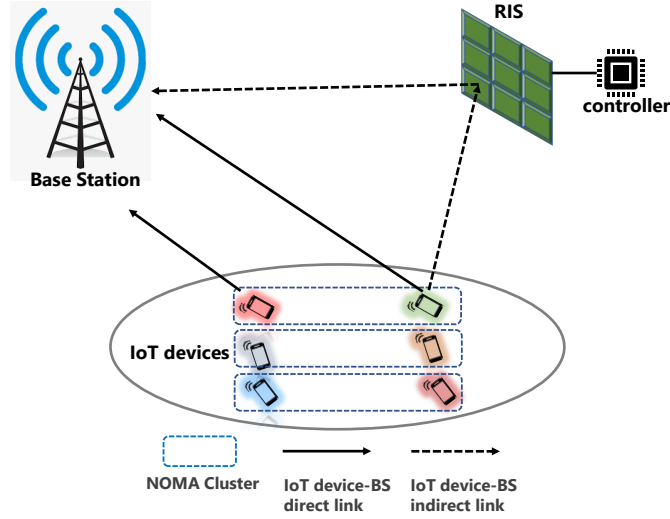


Figure 5.1: An illustration of the system model.

impurities and the obstacles of the wireless propagation environment, the existence of a strong direct line-of-sight (LoS) communication link between each weak IoT device and the BS is difficult to obtain. For this purpose, an RIS equipped with L reflecting elements is assumed to be deployed in order to assist the uplink transmission from the weak NOMA IoTs to the BS by passively relaying the status update information to the BS. The BS continuously controls the phase-shift of the reflecting elements in order to maintain the required quality of service of the weak IoTs. Let $\Phi(t) = \text{diag}(\exp[j\theta(t)]) \in \mathbb{C}^{L \times L}$ be the RIS's diagonal phase-shift matrix in the t th time-slot, where $\theta(t) = [\theta_1(t), \dots, \theta_L(t)]$ and, for all $l \in L$, $\theta_l(t) \in [0, 2\pi)$ is the phase-shift of the l th reflecting element of the RIS. Note that once the RIS phase-shift matrix is obtained, the disjoint sets of IoTs \mathcal{W} and \mathcal{S} are reconstructed by sorting the IoTs based on their updated channel gains. The $2I$ IoTs are grouped into I disjoint clusters by pairing exactly one strong IoT from \mathcal{S} with exactly one IoT from \mathcal{W} . Each cluster communicates with the BS using the uplink NOMA scheme

¹The reason for considering two IoTs in each cluster is that employing a large number of IoTs in a cluster is impractical due to the complexity of the SIC process. Also, the signal processing latency may further be increased if a large number of IoTs are jointly served through a NOMA cluster which will impact the information freshness and hence is not suitable for the studied problem.

and FDMA is considered to avoid the inter-cluster interference similar to other works in the literature [108].

5.2.1.1 Channel Model and SINR Analysis

To properly illustrate the signal model at BS, a single NOMA cluster is considered. Consider a cluster of IoTDs $(s, w) \in \mathcal{S} \times \mathcal{W}$, where s and w represent the strong and weak IoTDs in the considered NOMA, respectively. The channel gain between the RIS and the BS is denoted by $\mathbf{h}_{R \rightarrow b}(t) \in \mathbb{C}^{L \times 1}$, between the weak IoTD w and the RIS is denoted by $\mathbf{h}_{w \rightarrow R}(t) \in \mathbb{C}^{L \times 1}$, and between IoTD x and the BS, for $x \in \{s, w\}$, by $h_{x \rightarrow b}(t) \in \mathbb{C}$. All channel gains consist of both the small-scale and the large-scale fading, which are given as $\mathbf{h}_{R \rightarrow b}(t) = \hat{\mathbf{h}}_{R \rightarrow b}(t) \Delta_{R \rightarrow b}$, $\mathbf{h}_{w \rightarrow R}(t) = \hat{\mathbf{h}}_{w \rightarrow R}(t) \Delta_{w \rightarrow R}$, and $h_{x \rightarrow b}(t) = \hat{h}_{x \rightarrow b}(t) \Delta_{x \rightarrow b}$, for $x \in \{s, w\}$, where $\hat{\mathbf{h}}_{R \rightarrow b}(t)$, $\hat{\mathbf{h}}_{w \rightarrow R}(t)$, and $\hat{h}_{x \rightarrow b}(t)$ represent the small-scale fading coefficients between the RIS and the BS, between the weak IoTD w and the RIS, and between the IoTD $x \in \{s, w\}$ and the BS respectively. The signals of strong IoTDs that are reflected by the RIS are neglected due to the substantial path loss [109]. The large-scale fading coefficients $\Delta_{R \rightarrow b}$, $\Delta_{w \rightarrow R}$, and $\Delta_{x \rightarrow b}$, for $x \in \{s, w\}$, are modeled as $\Delta_{R \rightarrow b} = \sqrt{\gamma_0 d_{R \rightarrow b}^{-\eta_{R \rightarrow b}}}$, $\Delta_{w \rightarrow R} = \sqrt{\gamma_0 d_{w \rightarrow R}^{-\eta_{w \rightarrow R}}}$ and $\Delta_{x \rightarrow b} = \sqrt{\gamma_0 d_{x \rightarrow b}^{-\eta_{x \rightarrow b}}}$, where γ_0 is the path-loss average channel power gain at a reference distance $d_0 = 1\text{m}$, η_k , for $k \in \{R \rightarrow b, w \rightarrow R, x \rightarrow b\}$ is the path-loss exponent of the wireless link k , while d_k represents the distance for the communication link k . The small scale fading of the direct links between the IoTDs and the BS is modeled as a Rayleigh fading with a zero mean and a unit variance [46]. Meanwhile, the communication links between the RIS and the BS and between the weak IoTD w and the RIS are considered to have LoS components. These links experience a small-scale fading that is modeled as a Rician fading. Hence, the small-scale fading between the BS and RIS is given as [46]

$$\hat{\mathbf{h}}_{R \rightarrow b}(t) = \sqrt{\frac{K_1}{K_1 + 1}} \tilde{\mathbf{h}}_{R \rightarrow b}(t) + \sqrt{\frac{1}{K_1 + 1}} \bar{\mathbf{h}}_{R \rightarrow b}(t), \quad (5.1)$$

where K_1 is the Rician factor, and $\tilde{\mathbf{h}}_{R \rightarrow b}(t)$ and $\bar{\mathbf{h}}_{R \rightarrow b}(t)$ are the deterministic LoS and Rayleigh fading components. Note that, the $\hat{\mathbf{h}}_{w \rightarrow R}(t)$ can be obtained similarly.

Let $p_s(t)$ and $p_w(t)$ denote the transmit power of the IoTD s and w in cluster (s, w) at time-slot t , respectively. In uplink NOMA, the BS receives the signals from the IoTDs s and w , respectively. Then, it sequentially applies SIC to decode the signals of both IoTDs, where the decoding order is determined based on the channel gains of the IoTDs. In fact, the BS starts by decoding the signal of the strong IoTD s while considering the signal of the weak IoTD w as an interference. Consequently, the received SINR of IoTD s at the BS in time-slot $t \in T$ can be expressed as

$$\gamma_s(t) = \frac{p_s(t) |h_{s \rightarrow b}(t)|^2}{p_w(t) |\mathbf{h}_{w \rightarrow R}(t) \mathbf{\Phi}(t) \mathbf{h}_{R \rightarrow b}^H(t) + h_{w \rightarrow b}(t)|^2 + \sigma^2}, \quad (5.2)$$

where σ^2 is the variance of zero-mean additive Gaussian noise. Afterwards, the decoded signal of the strong IoTD s is removed from the received signal at the BS and, then, the signal of IoTD w will be decoded without any interference. Hence, the SINR of the IoTD w at the BS in time-slot $t \in T$ can be expressed as

$$\gamma_w(t) = \frac{p_w(t) |\mathbf{h}_{w \rightarrow R}(t) \mathbf{\Phi}(t) \mathbf{h}_{R \rightarrow b}^H(t) + h_{w \rightarrow b}(t)|^2}{\sigma^2}. \quad (5.3)$$

5.2.1.2 AoI Modeling

For all $i \in \mathcal{I}$ and $t \in \mathcal{T}$, we denote the AoI of the i th IoTD at the BS in t th time-slot as $A_i(t)$. A successful delivery of a packet at the BS in a given time slot t is conditioned on the case that the SINR of the channel between the IoTD and the BS is above a given threshold denoted as γ_{th} . Precisely, if a packet of the i th IoTD is

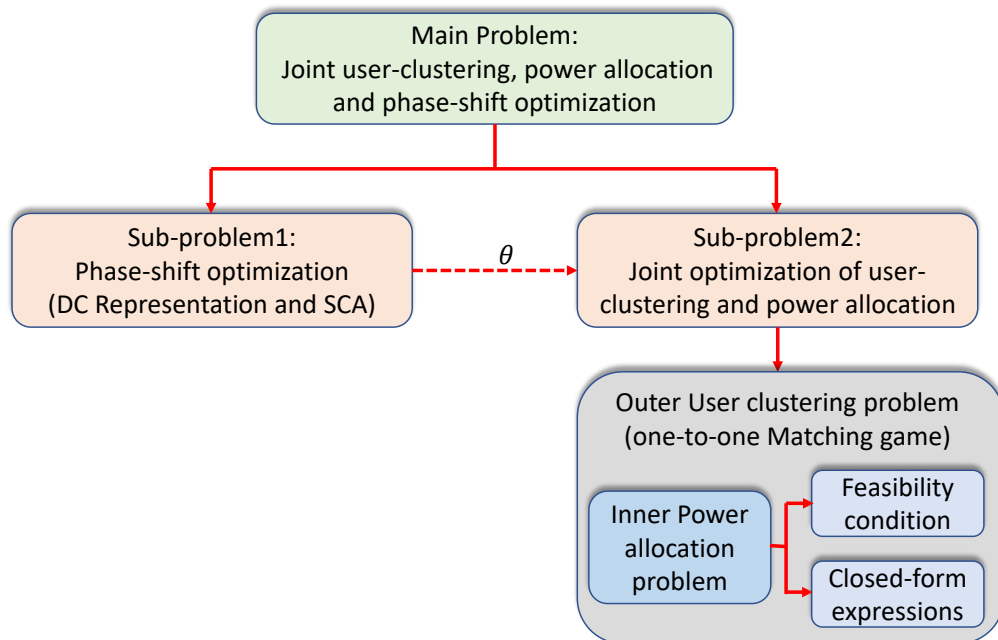


Figure 5.2: Problem decomposition and solution flow.

successfully delivered at the BS, the corresponding AoI in the same time-slot is given by $A_i(t) = 1$. Conversely, if the transmission remains unsuccessful, the AoI value will increase by 1, i.e., $A_i(t) = A_i(t - 1) + 1$. In this work, and similar to [107], a *generate at will* model is considered, where a packet is generated at the start of a time-slot and the transmission occurs in the same time-slot. The evolution of AoI of the i th IoTD is given by

$$A_i(t) = \begin{cases} 1, & \text{if } U(I - i)\gamma_s(t) + \\ & U(i - I)\gamma_w(t) \geq \gamma_{\text{th}}, \\ A_i(t - 1) + 1, & \text{otherwise,} \end{cases} \quad (5.4)$$

$U(x)$ is a unit step function ($= 1$ if $x \geq 0$, 0 otherwise).

5.2.2 Problem Formulation and Solution Approach

To ensure the information freshness at the BS, we aim to minimize the average sum AoI of all IoTDS over the entire observation interval $[0, T]$, which is given by [110]

$$A(T) = \frac{1}{T} \sum_{t < T} \left[\frac{1}{2I} \sum_{s \in \mathcal{S}} \sum_{w \in \mathcal{W}} \left\{ A_s(t) + A_w(t) \right\} b_{s,w}(t) \right], \quad (5.5)$$

In the context of our system model, since the generate-at-will model is adopted, a packet is assumed to be generated when it is requested by the BS. Based on this, the preset goal translates into minimizing the sum AoI at each time slot $t \in \{1, 2, \dots, T\}$ with respect to the sets of strong and weak IoTDS. To do so, we optimize the sum AoI with respect to the RIS phase-shift matrix Φ , the IoTDS transmit power $(\mathbf{p}_w, \mathbf{p}_s)$, and the clustering decision variable \mathbf{B} at each time slot $t \in \{1, 2, \dots, T\}$, which can be modelled as the following optimization problem

$$\mathcal{OP}: \min_{\substack{\mathbf{B}, \Phi, \\ \mathbf{p}_w, \mathbf{p}_s}} \left[\frac{1}{2I} \sum_{s \in \mathcal{S}} \sum_{w \in \mathcal{W}} \left\{ A_s(t) + A_w(t) \right\} b_{s,w}(t) \right] \quad (5.6a)$$

$$\text{s.t.} \quad \theta_l(t) \in [0, 2\pi), \quad \forall l \in \mathcal{L}, t \in T, \quad (5.6b)$$

$$b_{s,w}(t) \in \{0, 1\}, \quad \forall w \in \mathcal{W}, s \in \mathcal{S}, t \in \mathcal{T}, \quad (5.6c)$$

$$\sum_{s=1}^I b_{s,w}(t) \leq 1, \quad \forall w \in \mathcal{W}, t \in \mathcal{T}, \quad (5.6d)$$

$$\sum_{w=1}^I b_{s,w}(t) \leq 1, \quad \forall s \in \mathcal{S}, t \in \mathcal{T}, \quad (5.6e)$$

$$p_w(t), p_s(t) \leq P_{\max}, \quad \forall s \in \mathcal{S}, w \in \mathcal{W}, t \in T, \quad (5.6f)$$

where the objective function in (6a) targeting to minimize the sum AoI at each time slot $t \in \{1, 2, \dots, T\}$, $b_{s,w}(t) \in \{0, 1\}$ is the clustering decision variable, i.e., $b_{s,w}(t) = 1$ indicates that IoTDS $s \in \mathcal{S}$ is paired with IoTDS $w \in \mathcal{W}$ at time-slot t ,

and $b_{s,w}(t) = 0$, otherwise, P_{\max} is the IoTD power budget, $\mathbf{B} = \{b_{s,w} | (s, w) \in \mathcal{SW}\}$, $\mathbf{p}_w = \{p_w | w \in \mathcal{W}\}$, and $\mathbf{p}_s = \{p_s | s \in \mathcal{S}\}$. Constraints (5.6d) and (5.6e) ensure that each strong IoTD $s \in \mathcal{S}$ is paired with at most one weak IoTD $w \in \mathcal{W}$ and vice versa. Finally, (5.6f) ensures that the IoTD transmit power does not exceed its power budget. It can be easily seen that the formulated optimization problem \mathcal{OP} is an mixed-integer nonlinear programming problem due to the coexistence of the binary clustering matrix \mathbf{B} and the continuous variables $(\boldsymbol{\theta}, \mathbf{p}_w, \mathbf{p}_s)$, and therefore, it is difficult to solve directly.

5.2.2.1 Solution Approach

One can observe from problem \mathcal{OP} that it is difficult to obtain the optimal power control, the optimal IoTD clustering and the optimal RIS phase-shift matrix jointly. Consequently, we first obtain the RIS phase-shift matrix that maximizes the minimum channel gains of the weak IoTDs. Afterwards, the obtained RIS phase-shift matrix is injected into the original problem \mathcal{OP} and the resulting problem then becomes a joint IoTD clustering and power control problem which is solved using the concept of bi-level optimization.

5.2.2.2 RIS Phase-Shift Matrix

The RIS phase-shift matrix optimization problem is given as

$$\mathcal{OP}1: \max_{\boldsymbol{\Phi}} \min_{w \in \mathcal{W}} |\mathbf{h}_{w \rightarrow R}(t) \boldsymbol{\Phi}(t) \mathbf{h}_{R \rightarrow b}^H(t) + h_{w \rightarrow b}(t)|^2 \quad (5.7a)$$

$$\text{s.t. } \theta_l(t) \in [0, 2\pi), \quad \forall l \in \mathcal{L}, t \in T. \quad (5.7b)$$

Here, we introduce an auxiliary variable ζ to solve phase-shift optimization problem.

The resulting problem can be then re-written as

$$\mathcal{OP}2 : \max_{\zeta, \Phi(t)} \zeta \quad (5.8a)$$

$$\text{s.t.} \quad |\mathbf{h}_{w \rightarrow R}(t) \Phi(t) \mathbf{h}_{R \rightarrow b}^H(t) + h_{w \rightarrow b}(t)|^2 \geq \zeta,$$

$$\forall w \in \mathcal{W}, t \in \mathcal{T}, \quad (5.8b)$$

$$\theta_l(t) \in [0, 2\pi), \quad \forall l \in \mathcal{L}, t \in \mathcal{T}. \quad (5.8c)$$

Now, we reformulate the above problem into a rank-one constrained optimization problem via change of variables and matrix lifting. Let $\mathbf{v} \triangleq [v_1, v_2, \dots, v_L]^H$, where $v_l = e^{j\theta_l}$ for all $l \in \mathcal{L}$. Thus, for all $l \in \mathcal{L}$, the constraint $\theta_l(t) \in [0, 2\pi)$ is equivalent to the unit-modulus constraints, i.e., $|v_l|^2 = 1$. By applying the change of variables $\mathbf{h}_{w \rightarrow R}(t) \Phi(t) \mathbf{h}_{R \rightarrow b}^H(t) = \mathbf{v}^H \mathbf{Q}(t)$, where $\mathbf{Q}(t) = \text{diag}(\mathbf{h}_{R \rightarrow b}^H(t)) \mathbf{h}_{w \rightarrow R}(t)$, we obtain $|\mathbf{h}_{w \rightarrow R}(t) \Phi(t) \mathbf{h}_{R \rightarrow b}^H(t) + h_{w \rightarrow b}(t)|^2 = |\mathbf{v}^H \mathbf{Q}(t) + h_{w \rightarrow b}(t)|^2 = \bar{\mathbf{v}}^H \Theta \bar{\mathbf{v}} + |h_{w \rightarrow b}(t)|^2 = \text{tr}(\Theta \bar{\mathbf{v}} \bar{\mathbf{v}}^H) + |h_{w \rightarrow b}(t)|^2$, where

$$\Theta = \begin{bmatrix} \mathbf{Q}(t) \mathbf{Q}^H(t) & \mathbf{Q}(t) h_{w \rightarrow b}(t) \\ h_{w \rightarrow b}(t) \mathbf{Q}^H(t) & 0 \end{bmatrix}, \quad \bar{\mathbf{v}} = \begin{bmatrix} \mathbf{v} \\ 1 \end{bmatrix}. \quad (5.9)$$

Now, let $\mathbf{V} \triangleq \mathbf{v}\bar{\mathbf{v}}^H$, which needs to satisfy $\text{rank}(\mathbf{V}) = 1$ and $\mathbf{V} \geq 0$. Consequently, $\mathcal{OP}2$ can be rewritten as follows:

$$\mathcal{OP}3: \max_{\mathbf{V}, \zeta} \zeta \quad (5.10a)$$

$$\text{s.t. } \text{tr}(\Theta\mathbf{V}) + |h_{w \rightarrow b}(t)|^2 \geq \zeta, \quad (5.10b)$$

$$\mathbf{V} \geq 0, \quad (5.10c)$$

$$[\mathbf{V}]_{l,l} = 1, \quad \forall l \in \llbracket 1, L+1 \rrbracket, \quad (5.10d)$$

$$\text{rank}(\mathbf{V}) = 1, \quad (5.10e)$$

where (5.10e) is still non-convex. To resolve this issue, the rank-one constraint (5.10e) is represented in the difference-of-convex (DC) form [46][111]. As specified by matrix norm theory, for a positive semi-definite (PSD) matrix \mathbf{V} with $\text{tr}(\mathbf{V}) > 0$, we have

$$\text{rank}(\mathbf{V}) = 1 \iff \|\mathbf{V}\|_* - \|\mathbf{V}\|_2 = 0, \quad (5.11)$$

where the nuclear norm, $\|\mathbf{V}\|_*$, equals to the summation of all singular value of matrix \mathbf{V} and the spectral norm $\|\mathbf{V}\|_2$ equals to the largest singular value of \mathbf{V} . Thus, the objective in $\mathcal{OP}3$ can be re-written by adding a term of rank-one penalty as

$$\max_{\mathbf{V}, \zeta} \zeta - \varsigma(\|\mathbf{V}\|_* - \|\mathbf{V}\|_2), \quad (5.12)$$

where $\varsigma > 0$ is a penalty parameter. The DC formulation for (5.12) is non-convex. However, based on its structure, an efficient algorithm can be developed by utilizing the successive convex approximation (SCA). Precisely, in the i^{th} iteration of SCA, the optimization problem can be represented as

$$\max_{\mathbf{V}, \zeta} \zeta - \varsigma(\|\mathbf{V}\|_* - (\|\mathbf{V}^i\|_2 + \text{Re}(\text{tr}((\partial_{\mathbf{V}^i}\|\mathbf{V}\|_2)(\mathbf{V} - \mathbf{V}^i))))) , \quad (5.13)$$

where \mathbf{V}^i is a matrix that represents the value of \mathbf{V} at the i^{th} iteration. The sub-gradient of the spectral norm at \mathbf{V}^i can be computed as $\partial_{\mathbf{V}^i} \|(\mathbf{V})\|_2 = ss^H$ [111], where s is the singular vector that corresponds to the largest singular value of \mathbf{V}^i .

5.2.2.3 Bi-Level Optimization

We assume that phase-shift matrix is obtained and served as an input to problem \mathcal{OP} . It can be observed from \mathcal{OP} that the AoI function is independent from the pairing variable \mathbf{B} and it is only a function of the power control policy (see eq. (5.4)). Precisely, let the set of optimal IoT-D clustering and power control scheme, i.e., the solutions of the problem \mathcal{OP} , be denoted by $\{(b_{s,w}^*(t), p_s^*(t), p_w^*(t)), s, w \in \mathcal{S} \times \mathcal{W}\}$. For all $s, w \in \mathcal{S} \times \mathcal{W}$, if $b_{s,w}^*(t) = 0$, then $(p_s^*(t), p_w^*(t)) = (0, 0)$. However, if $b_{s,w}^*(t) = 1$, then $(p_s^*(t), p_w^*(t))$ should be the optimal solutions for the power control policy of IoT-Ds s and w . In order to facilitate the SIC process at the BS, the strong IoT-D is assumed to transmit at the maximum power P_{\max} . Meanwhile, the transmit power for weak IoT-D needs to be optimized. Therefore, for all $(s, w) \in \mathcal{S} \times \mathcal{W}$, if we assume that the IoT-Ds are paired together and that we obtain the optimal power allocation $p_w^*(t)$, then problem \mathcal{OP} will simply become a linear assignment that determines the optimal pairing policy $(b_{s,w}^*)_{(s,w) \in \mathcal{S} \times \mathcal{W}}$. Here, for all $(s, w) \in \mathcal{S} \times \mathcal{W}$, since we aim to determine the optimal power allocation that satisfies the SINR threshold for each pair of IoT-Ds such that the AoI is minimized, we can reduce the feasible set of the power control of problem \mathcal{OP} to the set of the power allocation that minimize the sum of AoI of each pair of IoT-Ds. Consequently, problem \mathcal{OP} can be re-written as:

$$\mathcal{OP}_{outer}: \min_{\mathbf{B}} \left[\frac{1}{2I} \sum_{s \in \mathcal{S}} \sum_{w \in \mathcal{W}} \{A_s(t) + A_w(t)\} b_{s,w}(t) \right] \quad (5.14a)$$

$$\text{s.t.} \quad (5.6c), (5.6d), (5.6e), \quad (5.14b)$$

where $p_w^*(t)$ can be obtained by solving the following feasibility check optimization problem

$$\mathcal{OP}_{inner} : \text{Find } \mathbf{p}_w \quad (5.15a)$$

$$\text{s.t. } p_w(t), p_s(t) \leq P_{\max}, \quad \forall w \in \mathcal{W}, s \in \mathcal{S}, t \in \mathcal{T}, \quad (5.15b)$$

$$\gamma_s(t) \geq \gamma_{\text{th}}, \quad \forall s \in \mathcal{I}, t \in \mathcal{T}, \quad (5.15c)$$

$$\gamma_w(t) \geq \gamma_{\text{th}}, \quad \forall w \in \mathcal{I}, t \in \mathcal{T}, \quad (5.15d)$$

for each pair of IoTDS $(s, w) \in \mathcal{S} \times \mathcal{W}$. Consequently, \mathcal{OP}_{inner} is a power allocation problem for a given cluster of IoTDS and it defines the set of feasible solutions for problem \mathcal{OP}_{outer} , which is a linear assignment problem. Nonetheless, \mathcal{OP}_{inner} needs to be solved for all possible combinations of IoTDS $(s, w) \in \mathcal{S} \times \mathcal{W}$. Therefore a computationally efficient approach is presented to solve \mathcal{OP}_{inner} in the following section.

5.2.2.4 Power Control

Let us consider the pair of NOMA IoTDS $(s, w) \in \mathcal{S} \times \mathcal{W}$. The goal here is to obtain a possible value of the power allocation for the weak IoTDS w , i.e., p_w , that satisfies the SINR constraints of IoTDS s and w when paired together.

$$\gamma_s(t) \geq \gamma_{\text{th}}, \quad (5.16a)$$

$$\gamma_w(t) \geq \gamma_{\text{th}}. \quad (5.16b)$$

From the SINRs expressions in (5.2) and (5.3), one can conclude that the SINRs constraints in (5.16) are satisfied if and only if

$$p_w^{\min} \leq p_w^{\max}, \quad (5.17)$$

where p_w^{\min} and p_w^{\max} are expressed, respectively, as

$$p_w^{\max} = \min \left(\frac{p_s |h_{s \rightarrow b}^n(t)|^2 - \gamma_{\text{th}} \sigma^2}{\gamma_{\text{th}} |\mathbf{h}_{w \rightarrow R}(t) \Phi(t) \mathbf{h}_{R \rightarrow b}^H(t) + h_{w \rightarrow b}(t)|^2}, P_{\max} \right), \quad (5.18a)$$

$$p_w^{\min} = \frac{\gamma_{\text{th}} \sigma^2}{|\mathbf{h}_{w \rightarrow R}(t) \Phi(t) \mathbf{h}_{R \rightarrow b}^H(t) + h_{w \rightarrow b}(t)|^2}. \quad (5.18b)$$

Based on this, any random value of the power p_w within the range $[p_w^{\min}, p_w^{\max}]$ is a feasible value for problem \mathcal{OP}_{inner} . After obtaining the optimal power allocation for each possible NOMA cluster along with its corresponding sum AoI, we apply the one-to-one matching game [112] to obtain the optimal clustering configuration.. Moreover, if both IoTDs in a cluster are unable to satisfy SINR threshold, one of the two IoTDs may be served if it satisfies the SINR. However, the preference is given to one with the worst AoI.

5.2.2.5 Complexity Analysis

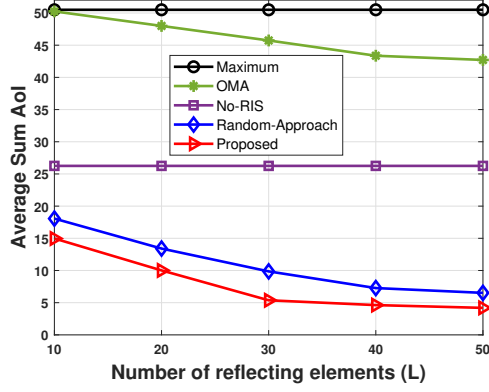
After obtaining the closed form expression of the power, the computational complexity of obtaining the total transmit power is approximately $\mathcal{O}(1)$. We then employ the one-to-one matching algorithm, which has a time complexity of $\mathcal{O}(I^2)$. On the other hand, the phase shift matrix problem is a semi-definite programming problem with approximate computational complexity $\mathcal{O}(\log(1/\epsilon)(L^{4.5})[46]$.

5.2.3 Simulation and Numerical Analysis

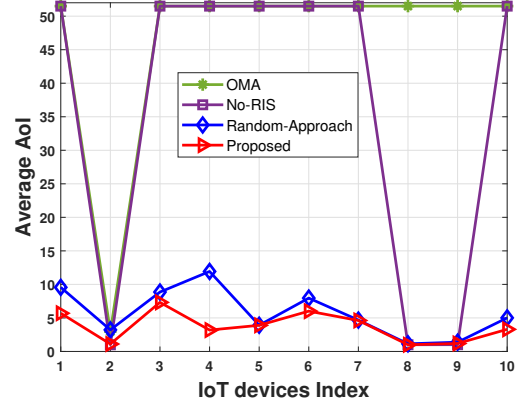
We consider a 3-D area that consists of one BS, one RIS and a set of IoTDs. We assume that the global coordinate system (X, Y, Z) is Cartesian. The BS is located at $(0, 0, H_b)$ and the RIS is located at $(d_{R \rightarrow b}, 0, H_r)$, where $d_{R \rightarrow b}$ is the distance from RIS to the BS, and H_b and H_r are the heights of the transmit antenna of the BS and of the RIS, respectively. In addition, multiple IoTDs are randomly distributed

at the ground level, where for all $i \in \mathcal{I}$, the locations of IoT-Ds are $(x_i, y_i, 0)$. The coordinates of the strong IoT-Ds which are randomly located within a circular area centered at the BS and with radius d^s , are given by $x_i^s = d^s \cos(\theta_i^s)$ and $y_i^s = d^s \sin(\theta_i^s)$, where $\theta_i^s \in [0, 2\pi]$ is a polar angle. Similarly, the coordinates of the weak IoT-Ds are given by $x_i^w = d_i^w \cos(\theta_i^w) + d_{R \rightarrow b}$ and $y_i^w = d_i^w \sin(\theta_i^w)$. The total number of time-slots $T = 100$ and number of IoT-Ds $I = 20$, while the communication parameters are taken as $d_i^s = 10\text{m}$, $d_i^w = 10\text{m}$, $d_{R \rightarrow b} = 150\text{m}$, $\sigma^2 = -110\text{dBm}$, $\eta_{R \rightarrow b} = -2.2$, $\eta_{w \rightarrow R} = -2.2$, $\eta_{s \rightarrow b} = \eta_{w \rightarrow b} = -3.5$, $K_1 = 2$, $H_b = H_r = 10\text{m}$, $\gamma_{\text{th}} = 45\text{dB}$. In order to evaluate the effectiveness of the proposed algorithm, we compare its performance with three baselines schemes as follows: (i) OMA, where at most I IoT-Ds can be served in each time-slot, (ii) a random-approach which creates clusters of 2-IoTDs through a random selection of one IoT-D from each \mathcal{S} and \mathcal{W} sets. The RIS phase-shift matrix is also obtained randomly in this scheme, and (iii) an approach where IoT-D clustering is obtained through one-to-one matching but RIS is not considered to be deployed to enhance the channel quality of the weak IoT-Ds.

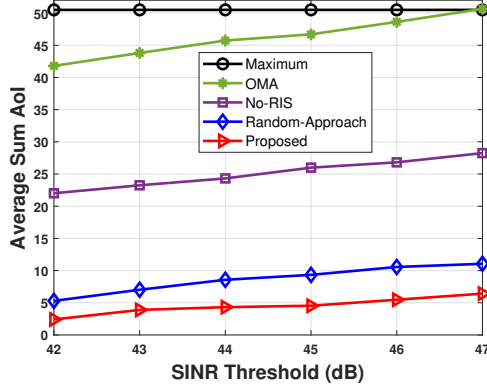
Figure 5.3(a) depicts the impact of the size of the RIS on the average sum AoI. It can be seen that the RIS has a significant impact on the AoI and increasing the number of the RIS elements results in decreasing the AoI for all schemes. This is evident since the RIS helps to improve the channel quality of the weak IoT-Ds which leads to augmenting the likelihood of pairing with strong IoT-Ds and eventually ends up decreasing the AoI. In addition, we observe that the proposed algorithm achieves the lowest sum AoI compared to the other approaches. Particularly, the proposed scheme achieves around 90.18%, 84.02%, and 35.72% decrease in the average AoI with 50 RIS elements compared to the OMA, No-RIS and the random-approach, respectively. It can be observed that the random-approach is more effective than OMA since based on NOMA principle, it tries to increase the number of served IoT-Ds by creating clusters



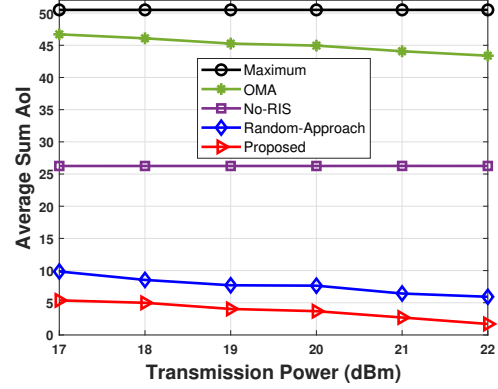
(5.3.a) Impact of number of RIS elements.



(5.3.b) Average age per IoT device.



(5.3.c) Impact of SINR Threshold on AoI.



(5.3.d) Impact of Power on AoI.

Figure 5.3: Performance evaluation.

of IoTDS to be served in the same resource block. However, the proposed approach with efficient clustering and RIS configuration outperforms the all other approaches. We plot the average AoI for a set of IoTDS in Figure 5.3(b). The average age of IoTDS i in time T is calculated by $\frac{1}{T} \sum_{t=0}^T A_i^t, \forall i$. It can be seen that the proposed method has a lower average sum AoI per IoTDS compared to the other approaches. Moreover, the average AoI gap is relatively high among different schemes, which highlights the significance of the efficient RIS configuration, IoTDS clustering and power allocation. Figure 5.3(c) depicts the impact of the SINR threshold on the average sum AoI. It can be seen that, as the SINR threshold increases, the average sum AoI starts increasing for all the schemes. However, the proposed method achieves the lowest sum AoI

compared to the others. OMA again achieves the worst AoI values which reinforces that being able to serve large number of IoTDs with optimization of both the RIS configuration and the IoTD clustering is important to achieve the required freshness of information. Finally, Figure 5.3(d) shows the impact of the maximum transmit power per IoTD on the average sum AoI. It can be observed that when the IoTD transmit power increases, the SINR increases and, hence, the AoI decreases.

5.2.4 Extension to Multi-RIS Setting

As an extension to the system model investigated in Section 5.2.1, we propose integrating multiple RISs in order to enhance the quality of the wireless channels and the timeliness performance of uplink NOMA-based IoT network. In this setup, another dimension that needs to be optimized is IoTDs assignment to the RIS's. Figure 5.4 illustrates the system model, where a set of RISs denoted by $\mathcal{N} = \{1, 2, \dots, N\}$ is assumed to be deployed to enhance the uplink transmission from the weak IoTDs to the BS, where each RIS is equipped with L reflecting elements. Whereas, similar to the system model given in Section 5.2.1, the RIS-empowered uplink IoT network consists of one BS and $2I$ IoTDs ($I \in \mathbb{N}$). We assume that each weak IoTD $w \in \mathcal{W}$ is served by a set of RISs denoted by Ω_w , i.e., $1 \leq |\Omega_w| \leq N$. Furthermore, let $\mathbf{\Omega} = \{\Omega_1, \Omega_2, \dots, \Omega_I\}$ be the set of all RISs assignments.

Literally, it seems a good solution to let all the IoTDs $w \in \mathcal{W}$ be served by the N RISs. However, such a solution amplifies the cost of prodigious channel estimation complexity. In fact, if all RISs are allowed to serve all the IoTDs, the total number of required channel estimations is equal to the product of the number of IoTDs and the sum of the elements of all RISs. Therefore, the computational time of the channel estimation process becomes extremely high since the channel estimation process is a complex and time-consuming problem. On the other hand, if each IoTD $w \in \mathcal{W}$ is

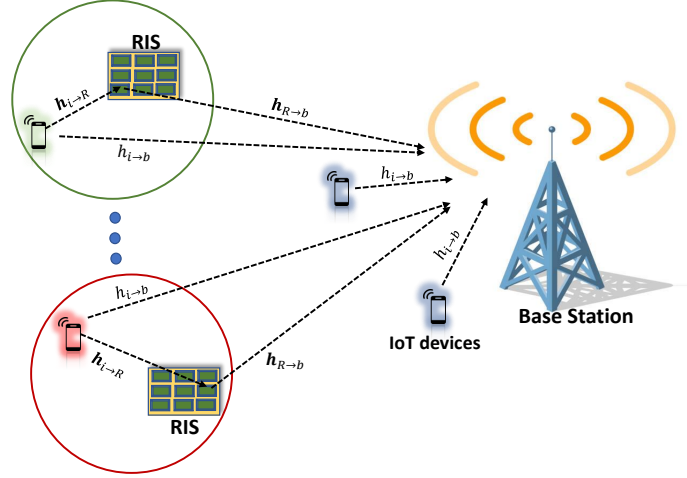


Figure 5.4: An illustration of the system model.

restricted to be served by only one RIS to reduce the channel estimation complexity, the required QoS constraints may not be achieved. Based on this, a more flexible solution is required in order to avoid the two aforementioned extreme cases. Hence, the question that arises here is the following: *what is the best assignment strategy that maximizes the benefits brought by the RISs to the weak IoTDs?*. To answer this question, we assume that each weak IoTD is associated to k RISs, with $1 \leq k \leq N$. Now, as per [52, 113], the users get the highest channel gains when they are located in close proximity to the RIS. Thus, each weak IoTD is assigned to its k nearest RISs.

Following the discussions in 5.2, we only provide the equations of the received SINR of IoTD s and IoTD w at the BS in time-slot $t \in T$ can be expressed as (5.19), and (5.20) respectively. It is worth mentioning that the BS receives the signal of the weak IoTD through the direct link, the assigned RISs to this weak IoT (first summation in the numerator of (5.20)), and the non-assigned RISs (second summation in the numerator of (5.20)).

$$\zeta_s(t) = \frac{p_s(t)|h_{s \rightarrow b}(t)|^2}{p_w(t)|h_{w \rightarrow b}(t) + \sum_{n \in \mathcal{N}} h_{w \rightarrow R_{(w,n)}}(t) \mathbf{\Phi}_n(t) \mathbf{h}_{R_n \rightarrow b}^H(t)|^2 + \sigma^2} \quad (5.19)$$

$$\zeta_w(t) = \frac{p_w(t) \left| \sum_{n \in \Omega_w} h_{w \rightarrow R_{(w,n)}}(t) \Phi_n(t) \mathbf{h}_{R_n \rightarrow b}^H(t) + \sum_{n' \in (\Omega \setminus \Omega_w)} \mathbf{h}_{w \rightarrow R_{(w,n)}}(t) \Phi_{n'}(t) \mathbf{h}_{R_n \rightarrow b}^H(t) \right|^2}{\sigma^2} \quad (5.20)$$

Considering a pair of NOMA IoTDS $(s, w) \in \mathcal{S} \times \mathcal{W}$, the goal is to obtain a possible value of the power allocation for the weak user w , i.e., p_w , that satisfies the SINR constraints of IoTDS s and w when paired together, which is given as follows.

$$\zeta_s(t) \geq \zeta_{\text{th}} \text{ and } \zeta_w(t) \geq \zeta_{\text{th}}. \quad (5.21)$$

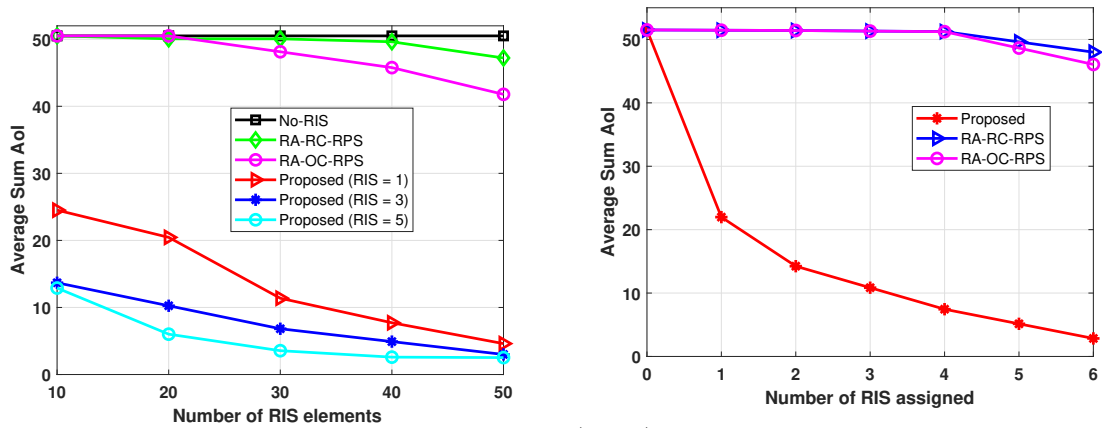
From the SINRs expressions in (5.19) and (5.20), it can be concluded that the SINRs constraints in (5.21) are satisfied if and only if

$$p_w^{\min} \leq p_w^{\max}, \quad (5.22)$$

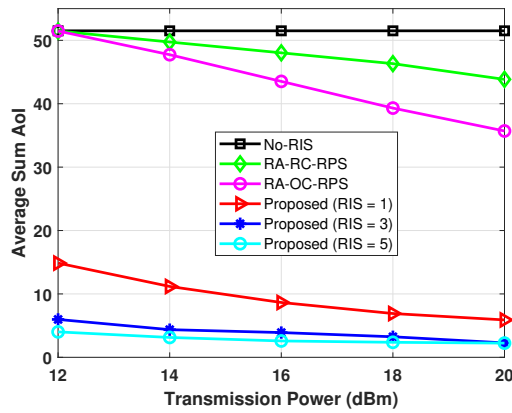
where p_w^{\max} and p_w^{\min} are expressed by (5.23) and (5.24) respectively. Consequently, any value of the power p_w within the range $[p_w^{\min}, p_w^{\max}]$ is a feasible value for \mathcal{OP}_{inner} .

$$p_w^{\max} = \min \left(\frac{p_s |h_{s \rightarrow b}^n(t)|^2 - \zeta_{\text{th}} \sigma^2}{\zeta_{\text{th}} \left| \sum_{n \in \mathcal{N}} h_{w \rightarrow R_{(w,n)}}(t) \Phi_n(t) \mathbf{h}_{R_n \rightarrow b}^H(t) \right|^2}, P_{\max} \right), \quad (5.23)$$

$$p_w^{\min} = \frac{\zeta_{\text{th}} \sigma^2}{\left| h_{w \rightarrow b}(t) + \sum_{n \in \Omega_w} h_{w \rightarrow R_{(w,n)}}(t) \Phi_n(t) \mathbf{h}_{R_n \rightarrow b}^H(t) + \sum_{n' \in (\Omega \setminus \Omega_w)} \mathbf{h}_{w \rightarrow R_{(w,n)}}(t) \Phi_{n'}(t) \mathbf{h}_{R_n \rightarrow b}^H(t) \right|^2}. \quad (5.24)$$



(5.5.a) Impact of number of elements per RIS. (5.5.b) Impact of number of assigned RISs on AoI.



(5.5.c) Impact of Power on AoI.

Figure 5.5: Performance evaluation.

5.2.5 Results and Discussions

Fig. 5.5(a) depicts the impact of the size of the RISs on the average sum AoI. The total number of RISs are set to five in this experiment whereas each IoT is served by one, three and five RISs. It can be seen that the RIS has a significant impact on the AoI and increasing the number of the RIS elements results in decreasing the AoI. This is evident since the RIS helps to improve the channel quality of the weak IoTs which leads to augmenting the likelihood of pairing with strong IoTs and eventually ends up decreasing the AoI. In addition, we observe that the proposed algorithm

achieves the lowest sum AoI compared to the other approaches. Particularly, the proposed scheme achieves around 94.43%, 92.8%, and 93.65% decrease in the average AoI when three RISs (each having 50 RIS elements) are assigned to each weak IoT as compared to the No-RIS, RA-OC-RPS and RA-RC-RPS case respectively. In addition, we note that if the number of RIS elements are small, IoTs should be assigned to more than one RISs to achieve a lower average sum AoI. Moreover, it can be observed that having three assigned RISs gets very similar AoI reduction as of assigning five RISs with large number of RIS elements, i.e., 50. Note that this insight could help network operators to decide on the number of RISs to be deployed in the network with their respective sizes in terms of RIS elements.

Fig. 5.5(b) illustrates the average sum AoI that is achieved by varying the number of RISs assigned to each weak IoT. As can be observed, the average sum AoI attains its maximum value when no RIS has been utilized. As the number of assigned RISs is increased, the average sum AoI starts declining. We can see a sharp decrease in the AoI curve (around 57.4% decrease) when a single RIS is assigned as compared to no-RIS assignment case. However, the gap in AoI reduction starts reducing as more number of RISs are assigned (e.g., around 24.4% decrease when the number of assigned RISs increases from 5 to 6). Moreover, both the other schemes with random assignment and random phase shift matrix attains the highest AoI.

Fig. 5.5(c) plots the average sum AoI against the maximum transmit power per IoT. The total number of RISs are kept as five in this experiment with each RIS having 30 elements. It is demonstrated that increasing the power directly increases the SINR, and thus, results in reducing the AoI. Nevertheless, our proposed approach outperforms others to a large extent. Moreover, the importance of the optimal clustering when relying on random RIS configuration can also be noted. The AoI achieved by the random clustering gets around 18.56% higher than the one with the optimal

clustering with power budget of each user = 20dBm. Finally, it always pays off to increase the number of RIS assignment. However, it can be compensated with the increase of the IoTs transmit power.

5.2.6 Conclusion

We explored the integration of RIS (single and multiple RISs) in uplink NOMA-based IoT networks to preserve information freshness. An optimization problem is formulated to minimize the average sum AoI. To tackle this, RIS configuration problem is solved first using the DC approach. Then, the joint IoT-clustering and power control problem is decomposed into disjoint IoT-clustering and power-control. One-to-One matching approach is adopted to solve the IoT-clustering sub-problem while the feasible transmit power range is obtained for the power-control sub-problem. Numerical results demonstrate that the proposed method has superior performance.

5.3 AoI Optimization In RIS-Assisted C-NOMA Based IoT Networks

5.3.1 System Model

We consider the RIS-empowered uplink C-NOMA based IoT network as depicted in Figure 5.6, which consists of one BS, one strong UE denoted as UE_s and one weak UE denoted as UE_w . As per the NOMA principle, both UEs are served simultaneously within the same time/frequency resource block to provide their status update information to the BS. We assume that each UE and the BS are equipped with one transmit and one receive antenna. Let $[0, T]$ be the observation interval of the system, where T represents the total observation duration. The observation interval is

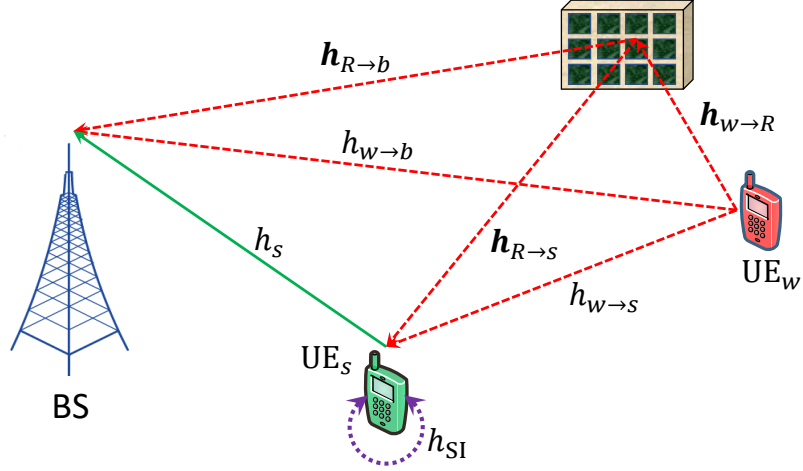


Figure 5.6: RIS-assisted uplink C-NOMA based IoT network.

divided into slots with a slot index $t \in \{1, 2, \dots, T\}$. To enhance the performance of UE_w , we allow UE_s to act as a full duplex (FD) decode and forward (DF) relay that assists UE_w to upload its information to the BS.² UE_s first decodes UE_w 's signal that is received on the D2D link and then combines it with its own signal into a superimposed signal using SC, which is finally transmitted to the BS. Based on the above description, the transmission of UE_s occurs on the direct link $UE_s \rightarrow BS$, whereas, the information updates of UE_w arrives at the BS through the direct link $UE_w \rightarrow BS$ and through the cooperative link $UE_w \rightarrow UE_s \rightarrow BS$. To alleviate the effects of the impurities and obstacles of the wireless propagation environment, an RIS equipped with L reflecting elements is assumed to be deployed close to UE_w in order to improve its transmission to the BS and to enhance the performance of the D2D communication link from UE_w to UE_s .

²In this work, we have considered the full-duplex (FD) relaying mode, in which the data reception from UE_w to UE_s and the data transmission from UE_s to the BS occur both in the same time-slot with the cost of inducing self interference (SI) at UE_s [114], [115]. Moreover, we realize that a processing delay is involved to decode the message of UE_w at UE_s even though it operates in FD mode. However, similar to [79], we consider that this delay is negligible as compared to the total transmission duration.

5.3.1.1 Channel Model and SINR Analysis

Let $\mathbf{h}_{R \rightarrow b}(t) \in \mathbb{C}^{L \times 1}$, $\mathbf{h}_{R \rightarrow s}(t) \in \mathbb{C}^{L \times 1}$, $\mathbf{h}_{w \rightarrow R}(t) \in \mathbb{C}^{L \times 1}$, $h_{w \rightarrow s}(t) \in \mathbb{C}$, $h_{w \rightarrow b}(t) \in \mathbb{C}$, and $h_s(t) \in \mathbb{C}$ be the channel coefficients of the communication links from the RIS to the BS, from the RIS to UE_s, from UE_w to the RIS, from UE_w to UE_s, from UE_w to the BS, and from UE_s to the BS, respectively. In addition, let h_{SI} be the channel coefficient of the self-interference (SI) experienced at UE_s. Based on this, the channel coefficient of the cascaded channel from UE_w to the BS is given by $h_w(t) = (h_{w \rightarrow b}(t) + \mathbf{h}_{R \rightarrow b}^H \Phi(t) \mathbf{h}_{w \rightarrow R}(t))$ and the channel coefficient of the cascaded channel from UE_w to UE_s is given by $h_{w,s}(t) = (h_{w \rightarrow s}(t) + \mathbf{h}_{R \rightarrow s}^H \Phi(t) \mathbf{h}_{w \rightarrow R}(t))$, where $\Phi(t) = \text{diag}(\exp[j\boldsymbol{\theta}(t)]) \in \mathbb{C}^{L \times L}$ is the RIS's diagonal phase-shift matrix in the t th time-slot, such that $\boldsymbol{\theta}(t) = [\theta_1(t), \dots, \theta_L(t)]$, in which, for all $l \in L$, $\theta_l(t) \in [0, 2\pi)$ is the phase-shift of the l th reflecting element of the RIS.

As illustrated in Figure 5.6, UE_w transmits its own signal toward the BS and UE_s. In addition, each transmission of UE_w will result in two signals to be received at the BS and at UE_s. The first signal is due to the direct transmission and the second signal comes from the reflection from the RIS. Upon receiving the signal of UE_w on D2D channel at each time slot, UE_s will decode it first and the resulting decoded signal will be superimposed on the signal of UE_s by applying SC for onward transmission to the BS. As a result, the received signal at the BS due to the transmissions of both UE_s and UE_w and the received signal at UE_s due to the transmission of UE_w are expressed, respectively, as

$$y_B(t) = h_s(t)(\sqrt{\alpha_s}x_s + \sqrt{\alpha_w}x_w)\sqrt{p_s} + h_w(t)\sqrt{\beta_w p_w}x_w + w_b(t), \quad (5.25)$$

$$y_{w \rightarrow s}(t) = h_{w,s}(t)\sqrt{\beta_w p_w}x_w + h_{SI}(\sqrt{\alpha_s}x_s + \sqrt{\alpha_w}x_w)\sqrt{p_s} + w_s(t), \quad (5.26)$$

where x_s and x_w are the signals of UE_s and UE_w, respectively, p_s and p_w denote

the maximum transmit power of UE_s and UE_w, respectively, $\alpha_s, \alpha_w \in [0, 1]$ are the power control coefficients allocated by UE_s to transmit its own message and the message of UE_w in the relaying phase, respectively, $\beta_w \in [0, 1]$ is the power control coefficient allocated by UE_w to transmit its own message, and $w_s, w_b \sim \mathcal{CN}(0, \sigma^2)$ are the additive white Gaussian noises experienced at UE_s and UE_w, respectively, where each has a zero mean and a variance σ^2 .

According to NOMA principle, the BS will first decode x_w by treating x_s as interference upon receiving the superimposed signal. With that goal, the BS will employ maximum-ratio combination (MRC) to combine the signal that is directly transmitted by UE_w with the superimposed signal that is directly transmitted by UE_s in order to decode x_w . Once achieved, x_w will be subtracted from the total received signal at the BS to obtain x_s [79]. Based on this, the SINR at the BS to decode the signal of UE_s, the SINR at the BS to decode the signal of UE_w after applying MRC, and the SINR at UE_s to decode the signal of UE_w in time slot t can be expressed, respectively, as

$$\gamma_s(t) = \alpha_s(t)p_s\delta_s, \quad (5.27)$$

$$\gamma_{w,\text{MRC}}(t) = \frac{\beta_w(t)p_w\delta_w + \alpha_w(t)p_s\delta_s}{\alpha_s(t)\delta_s(t)p_s + 1}, \quad (5.28)$$

$$\gamma_{w,s}(t) = \frac{\beta_w(t)p_w\delta_{w,s}}{\delta_{SI}(\alpha_s + \alpha_w)p_s + 1}, \quad (5.29)$$

where $\delta_s = \frac{|h_s(t)|^2}{\sigma^2}$, $\delta_w = \frac{|h_w(t)|^2}{\sigma^2}$, $\delta_{w,s} = \frac{|h_{w,s}(t)|^2}{\sigma^2}$, $\delta_{SI} = \frac{h_{SI}^2(t)}{\sigma^2}$. As mentioned above, the BS is receiving and combining two copies of the message x_w of UE_w through two different links, one from UE_w and one from UE_s. However, this combination is successful if and only if the copy transmitted from UE_s is truly the exact message x_w of UE_w, i.e., if and only if UE_s is able to decode the message x_w of UE_w. Therefore, the SINR required to decode the signal of UE_w at the BS is constrained by the SINR at UE_s to decode the message x_w of UE_w. Consequently, the SINR required to decode

the signal of UE_w at the BS is the minimum of the SINR at the BS to decode the transmission of UE_w after applying MRC and the SINR at UE_s to decode the message of UE_w, i.e., $\gamma_w(t) = \min\{\gamma_{w,\text{MRC}}(t), \gamma_{w,s}(t)\}$.

5.3.1.2 AoI Modeling

We denote the AoI of both UE_s and UE_w in time-slot t as $A_s(t)$ and $A_w(t)$, respectively. A successful transmission at the BS, which occurs when the SINR is above a given threshold γ_{th} , will bring the AoI for each UE to 1 [116]. Otherwise, if the transmission remains unsuccessful, the AoI value will increase linearly by 1 [116]. In this work, we consider a *generate-at-will* model similar to [117]. In the context of our system model, a packet is requested at the beginning of each time-slot and the transmission occurs within the same time-slot. The evolution of AoI of the i th UE, for all $i \in \{s, w\}$, is given as

$$A_i(t) = \begin{cases} 1, & \text{if } \gamma_i(t) \geq \gamma_{th}, \\ A_i(t-1) + 1, & \text{otherwise,} \end{cases} \quad (5.30)$$

where it is assumed that $A_i(0) = 0$.

5.3.2 Problem Formulation and Solution Approach

5.3.2.1 Problem Formulation

To ensure the information freshness at the BS for the proposed IoT network, our aim is to minimize the average sum AoI over the entire observation interval $[0, T]$, which is given by [110]

$$A(T) = \frac{1}{2T} \sum_{t=1}^T (A_s(t) + A_w(t)), \quad (5.31)$$

In the context of our system model, since the generate-at-will model is adopted, a packet is assumed to be generated when it is requested by the BS. Based on this, the preset goal translates into minimizing the sum AoI at each time slot $t \in \{1, 2, \dots, T\}$ with respect to the strong and weak UEs. To do so, we optimize the sum AoI with respect to the RIS phase-shift matrix Φ , the power control coefficients (α_w, α_s) , and the power allocation factor (β_w) at each time slot $t \in \{1, 2, \dots, T\}$, which can be modelled as the following optimization problem

$$\mathcal{OP}: \min_{\substack{\Phi, \beta_w \\ \alpha_s, \alpha_w}} \frac{1}{2} (A_s(t) + A_w(t)) \quad (5.32a)$$

$$\text{s.t. } \theta_l(t) \in [0, 2\pi), \quad \forall l \in L, \quad (5.32b)$$

$$0 \leq \alpha_s(t), \alpha_w(t), \beta_w(t) \leq 1. \quad (5.32c)$$

$$\alpha_s(t) + \alpha_w(t) \leq 1. \quad (5.32d)$$

The objective function in (5.32a) targets to minimize the sum AoI at each time slot $t \in \{1, 2, \dots, T\}$. The constraint (5.32b) restrains the phase-shift range at each RIS element, whereas the constraint (5.32c) and (5.32d) ensure that the power transmitted by UE_s and UE_w does not exceed their individual power budget.

5.3.2.2 Solution Approach

It can be observed from problem \mathcal{OP} that it is difficult to jointly obtain the optimal RIS phase-shift matrix and the optimal power control. Consequently, we resort to first obtaining the RIS phase-shift matrix that improves the channel gains on the desired links. Following that, the obtained RIS phase-shift matrix is injected into the original problem \mathcal{OP} and the resulting problem turns out to be a power control problem. Based on this, we discuss in the following sections the solution approaches of the phase-shift and the power control sub-problems.

5.3.2.3 RIS Phase-Shift Matrix

As discussed earlier, since UE_s acts as a DF relay, the SINR achieved at the BS to decode the message of UE_w is the minimum of the SINR at the BS to decode the signal of UE_w after applying MRC $\gamma_{w,\text{MRC}}(t)$ and the SINR at which UE_s decodes UE_w $\gamma_{w,s}(t)$. Therefore, the performance of the weak UE is limited by the lowest SINR between these two links. In this situation, we are trying to enhance the performance of the weakest link between the two, which comes through by enhancing the channel gain of the link between UE_s and UE_w and between the BS and UE_w . Precisely, our goal with the RIS phase-shift matrix optimization problem is to maximize the minimum channel conditions such that the performance of both links gets improved. Based on this, the RIS phase-shift matrix optimization problem is given as

$$\mathcal{OP}_{\text{PS}} : \max_{\Phi} \min \{ \delta_w(\theta), \delta_{w,s}(\theta) \} \quad (5.33a)$$

$$\text{s.t. (5.32b)}. \quad (5.33b)$$

which can be transformed as

$$\mathcal{OP}_{\text{PS}}^1 : \max_{\zeta, \Phi(t)} \zeta \quad (5.34a)$$

$$\text{s.t. } \min (|h_{w,s}|^2, |h_w|^2) \geq \zeta, \forall t \in \mathcal{T}, \quad (5.34b)$$

$$\theta_l(t) \in [0, 2\pi), \forall l \in L, t \in T. \quad (5.34c)$$

The problem in (5.34) will be reformulated into a rank-one constrained optimization problem via change of variables and matrix lifting. Let $\mathbf{v} \triangleq [v_1, v_2, \dots, v_L]^H$, where $v_l = e^{j\theta_l}$ for all $l \in L$. Thus, for all $l \in L$, the constraint $\theta_l(t) \in [0, 2\pi)$ is equivalent to the unit-modulus constraints, i.e., $|v_l|^2 = 1$. By applying the change of variables $\mathbf{h}_{R \rightarrow b}^H \Phi(t) \mathbf{h}_{w \rightarrow R}(t) = \mathbf{v}^H \mathbf{Q}(t)$, where $\mathbf{Q}(t) = \text{diag}(\mathbf{h}_{R \rightarrow b}^H(t)) \mathbf{h}_{w \rightarrow R}(t)$ and

$\mathbf{h}_{R \rightarrow s}^H(t) \Phi(t) \mathbf{h}_{w \rightarrow R}(t) = \mathbf{v}^H \Psi(t)$, where $\Psi(t) = \text{diag}(\mathbf{h}_{R \rightarrow n}^H(t)) \mathbf{h}_{w \rightarrow R}(t)$, we obtain $|\mathbf{h}_{R \rightarrow b}^H \Phi(t) \mathbf{h}_{w \rightarrow R}(t) + h_{w \rightarrow b}(t)|^2 = |\mathbf{v}^H \mathbf{Q}(t) + h_{w \rightarrow b}(t)|^2 = \bar{\mathbf{v}}^H \Theta_{w \rightarrow b} \bar{\mathbf{v}} + |h_{w \rightarrow b}(t)|^2 = \text{tr}(\Theta_{w \rightarrow b} \bar{\mathbf{v}} \bar{\mathbf{v}}^H) + |h_{w \rightarrow b}(t)|^2$ and $|\mathbf{h}_{R \rightarrow s}^H \Phi(t) \mathbf{h}_{w \rightarrow R}(t) + h_{w \rightarrow s}(t)|^2 = |\mathbf{v}^H \Psi(t) + h_{w \rightarrow s}(t)|^2 = \bar{\mathbf{v}}^H \Theta_{w \rightarrow s} \bar{\mathbf{v}} + |h_{w \rightarrow s}(t)|^2 = \text{tr}(\Theta_{w \rightarrow s} \bar{\mathbf{v}} \bar{\mathbf{v}}^H) + |h_{w \rightarrow s}(t)|^2$,

where

$$\Theta_{w \rightarrow b} = \begin{bmatrix} \mathbf{Q}(t) \mathbf{Q}^H(t) & \mathbf{Q}(t) h_{w \rightarrow b}(t) \\ h_{w \rightarrow b}(t) \mathbf{Q}^H(t) & 0 \end{bmatrix}, \quad (5.35)$$

$$\Theta_{w \rightarrow s} = \begin{bmatrix} \Psi(t) \Psi^H(t) & \Psi(t) h_{w \rightarrow s}(t) \\ h_{w \rightarrow s}(t) \Psi^H(t) & 0 \end{bmatrix}, \quad \bar{\mathbf{v}} = \begin{bmatrix} \mathbf{v} \\ 1 \end{bmatrix}. \quad (5.36)$$

Now, let $\mathbf{V} \triangleq \bar{\mathbf{v}} \bar{\mathbf{v}}^H$, which needs to satisfy $\text{rank}(\mathbf{V}) = 1$ and $\mathbf{V} \geq 0$. This rank one constraint is non-convex [52]. By dropping this constraint, problem $\mathcal{OP}_{\text{PS}}^1$ can be rewritten as

$$\mathcal{OP}_{\text{PS}}^2 \max_{\mathbf{V}, \zeta} \zeta \quad (5.37a)$$

$$\text{s.t. } \text{tr}(\Theta_{w \rightarrow b} \mathbf{V}) + |h_{w \rightarrow b}(t)|^2 \geq \zeta, \quad (5.37b)$$

$$\text{tr}(\Theta_{w \rightarrow s} \mathbf{V}) + |h_{w \rightarrow s}(t)|^2 \geq \zeta, \quad (5.37c)$$

$$\mathbf{V} \geq 0, \quad (5.37d)$$

$$[\mathbf{V}]_{L,L} = 1. \quad (5.37e)$$

The proposed transformation turns the problem into a convex optimization problem that can be solved through any convex optimization solver, e.g., CVX [52]. However, if the obtained phase-shift matrix does not satisfy the rank-one constraint, GR method can be applied to construct a rank-one solution as explained in [52].

5.3.2.4 Power Control

Since the phase-shift matrix Φ is already obtained, problem \mathcal{OP} turns out to a feasibility-check problem and the feasibility conditions for the power control coefficients can be obtained by solving the following problem.

$$\mathcal{OP}_{\text{PC}} : \text{ Find } [\beta_w(t), \alpha_w(t), \alpha_s(t)] \quad (5.38a)$$

$$\text{s.t. } 0 \leq \beta_w(t), \alpha_w(t), \alpha_s(t) \leq 1, \quad t \in \mathcal{T}, \quad (5.38b)$$

$$\min(\gamma_s(t), \gamma_w(t)) \geq \gamma_{\text{th}}, \quad (5.38c)$$

$$\alpha_s(t) + \alpha_w(t) \leq 1. \quad (5.38d)$$

In the following, we will derive the optimal solution of problem \mathcal{OP}_{PC} . Since $0 \leq \alpha_s(t) \leq 1$, then $\gamma_s(t) \geq \gamma_{\text{th}}$ if and only if $\alpha_s^{\min} \leq \alpha_s(t) \leq \alpha_s^{\max}$, where $\alpha_s^{\min} = \frac{\gamma_{\text{th}}}{p_s \delta_s(t)}$ and $\alpha_s^{\max} = 1$. Hence, the first feasibility condition of problem \mathcal{OP}_{PC} is $\alpha_s^{\min} \leq \alpha_s^{\max}$. In this case, the feasibility region of $\alpha_s(t)$ is the interval $[\alpha_s^{\min}, \alpha_s^{\max}]$. Second, $\gamma_w(t) \geq \gamma_{\text{th}}$ if and only if $\gamma_{w,\text{MRC}}(t) \geq \gamma_{\text{th}}$ and $\gamma_{w,s}(t) \geq \gamma_{\text{th}}$. Based on their expressions, $\gamma_{w,\text{MRC}}(t)$ and $\gamma_{w,s}(t)$ are increasing functions with respect to $\beta_w(t)$ and decreasing functions with respect to $\alpha_s(t)$. Hence, in order to satisfy both inequalities, the optimal value of $\beta_w(t)$ is 1 and the optimal value of $\alpha_s(t)$ is α_s^{\min} . In this case, since $0 \leq \alpha_w(t) \leq 1$, the inequalities $\gamma_{w,\text{MRC}}(t) \geq \gamma_{\text{th}}$ and $\gamma_{w,s}(t) \geq \gamma_{\text{th}}$, along with the constraint in (14d) are satisfied if and only if $\alpha_w^{\min} \leq \alpha_w(t) \leq \alpha_w^{\max}$, where

$$\alpha_w^{\min} = \max \left(0, \frac{\gamma_{\text{th}} \alpha_s^{\min} p_s \delta_s(t) + \gamma_{\text{th}} - p_w \delta_w(t)}{p_s \delta_s(t)} \right), \quad (5.39a)$$

$$\alpha_w^{\max} = \min \left(1 - \alpha_n^{\min}(t), \frac{p_w \delta_{s,w} - \gamma_{\text{th}} \delta_{SI} \alpha_n^{\min}(t) p_s - \gamma_{\text{th}}}{p_s \delta_{SI} \gamma_{\text{th}}} \right). \quad (5.39b)$$

Hence, the second feasibility condition of problem \mathcal{OP}_{PC} is $\alpha_w^{\min} \leq \alpha_w^{\max}$. In this case, any random value of $\alpha_w(t)$ within the interval $[\alpha_w^{\min}, \alpha_w^{\max}]$ is optimal for problem

Table 5.1: Simulation parameters.

Parameter	Value	Parameter	Value	Parameter	Value
$\eta_{R \rightarrow b}$	2.2	$\eta_{w \rightarrow R}$	2.2	$\eta_{s \rightarrow b}$	3.5
$\eta_{w \rightarrow b}$	4	$\eta_{R \rightarrow s}$	3	$\eta_{w \rightarrow s}$	4
γ_0	-30dB	p_w, p_s	20dBm	K_1	3dB
σ_2	-100dB	T	100	-	-

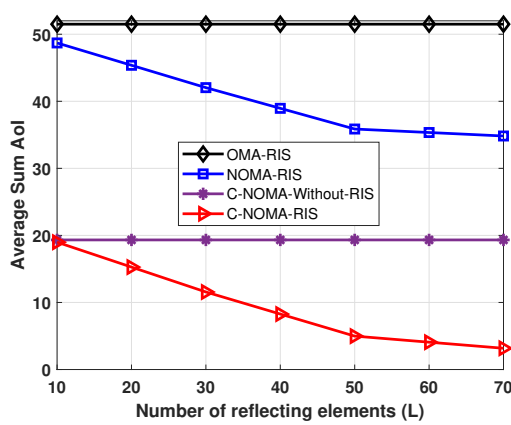
\mathcal{OP}_{PC} . However, the wisest solution of problem \mathcal{OP}_{PC} is the one that provides the lowest energy consumption at the near user. In this case, the optimal solution of $\alpha_w(t)$ is α_w^{min} .

5.3.2.5 Complexity Analysis

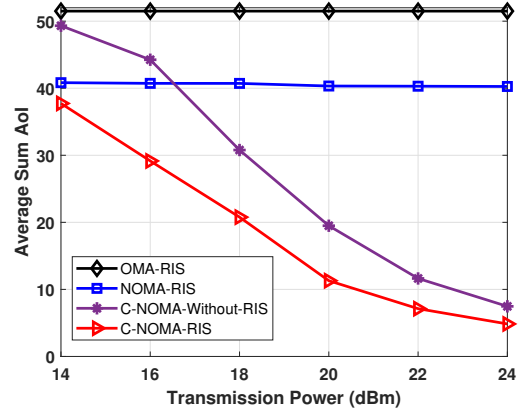
We discuss here the computational complexity of the proposed solution. After obtaining the closed form expression of the power, the computational complexity of obtaining the total transmit power is approximately $\mathcal{O}(1)$. On the other hand, the phase shift matrix problem is a semi-definite programming problem whose complexity along with applying GR is approximately $\mathcal{O}(\log(1/\epsilon)(L^{4.5} + xT_{GR}))$ [118].

5.3.3 Simulation Results

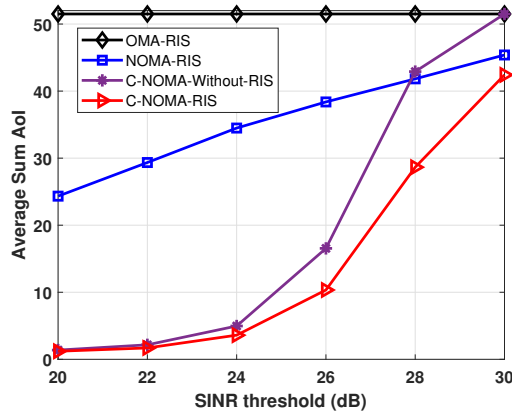
We assume that the global coordinate system (X, Y, Z) is Cartesian. The BS is located at $(0\text{m}, 10\text{m}, 0\text{m})$, the RIS is located at $(80\text{m}, 10\text{m}, 0\text{m})$, and UE_s and UE_w are located at $(40\text{m}, 0\text{m}, 0\text{m})$ and $(80\text{m}, 0\text{m}, 0\text{m})$, respectively. All the channel gains are assumed to consist of both the small-scale and the large-scale fading. The large-scale fading is modeled as $\sqrt{\gamma_0 d_k^{-\eta_k}}$, where γ_0 is the path-loss average channel power gain at a reference distance $d_0 = 1\text{m}$, η_k is the path-loss exponent, while d_k represents the distance for the communication link $k \in \{R \rightarrow b, w \rightarrow R, s \rightarrow b, w \rightarrow b, R \rightarrow s, w \rightarrow s\}$. The small scale fading of the direct links between UE_s/UE_w and the BS is modeled as a Rayleigh fading with a zero mean and a unit variance [52]. Meanwhile, for all $b \in \{R \rightarrow b, w \rightarrow R, R \rightarrow s\}$, the communication link b is considered to have LoS



(5.7.a) Impact of number of RIS elements.



(5.7.b) Impact of maximum transmit power per UE.



(5.7.c) Impact of SINR Threshold on AoI.

Figure 5.7: Performance evaluation

components. This link experiences a small-scale fading that is modeled as a Rician fading given as $\sqrt{\frac{K_1}{K_1+1}}\tilde{\mathbf{h}}_b(t) + \sqrt{\frac{1}{K_1+1}}\bar{\mathbf{h}}_b(t)$ where K_1 is the Rician factor, and $\tilde{\mathbf{h}}_b(t)$ and $\bar{\mathbf{h}}_b(t)$ are the deterministic LoS and Rayleigh fading components [52]. Finally, the simulation parameters are listed as Table 5.1. In order to evaluate the effectiveness of the proposed RIS-aided C-NOMA scheme, we compare its performance with other baseline schemes as follows: (i) Uplink NOMA with RIS, (ii) RIS-aided OMA and (iii) C-NOMA without RIS. Figure 5.7(a) depicts the impact of the size of the RIS on the average sum AoI. First, it can be observed that the RIS has a significant impact on the AoI and increasing the RIS elements results in the AoI reduction at large. This

is evident as the RIS helps to improve the channel quality for UE_w , which leads to satisfy the QoS and to decrease the AoI. However, the C-NOMA transmission complemented with the RIS gain achieves the lowest AoI as compared to all other schemes. Precisely, C-NOMA with RIS achieves around 83.60%, 90.90%, and 93.85% decrease in the average AoI with 70 RIS elements compared to the C-NOMA without RIS, NOMA, and the OMA respectively, which makes RIS-aided C-NOMA transmission a prominent solution for real-time applications that have stringent requirements of information freshness. Figure 5.7(b) plots the average sum AoI against the maximum transmit power per UE. The number of RIS elements are 30 in this experiment. It is demonstrated that increasing the power directly increases the SINR, and thus, results in reducing the AoI. Nevertheless, C-NOMA with RIS outperforms C-NOMA without RIS and NOMA to a large extent. In fact, when the power budget is very small, i.e., 14dBm, C-NOMA and NOMA with RIS give very close performance, although C-NOMA outperforms NOMA but the AoI reduction gap is small. However, as the power increases, the performance gap starts increasing and reaches to around 87.95% lower AoI obtained by C-NOMA with RIS over NOMA with power of 24dBm.

Finally, we evaluate the AoI performance with different SINR threshold values as shown in Figure 5.7(c). It can be observed that the RIS-aided C-NOMA scheme achieves the lowest sum AoI compare to other counterparts, even with the large threshold values. Precisely, the RIS-enabled C-NOMA gives a significant performance over RIS-enabled NOMA scheme, which implies that the cooperation helps to meet the SINR requirement and, hence, leads to a decrease in the average sum AoI. Also, the C-NOMA without RIS performs worst than the NOMA scheme at high value of SINR threshold. This is because that SI discourages the near user to transmit with high power, and hence, the probability of achieving the QoS constraint is low.

5.3.4 Conclusion

In this chapter, the integration of RIS and C-NOMA in uplink IoT networks has been investigated to optimize the freshness of information. An optimization problem has been formulated to minimize the average sum AoI by optimizing the UEs' transmit power and the RIS configuration. A closed-form solution has been derived for the power control sub-problem and the SDR approach was adopted for the RIS configuration sub-problem. Simulation results demonstrate that our proposed RIS-empowered uplink C-NOMA scheme achieves higher AoI-reduction compared to all baseline schemes.

Chapter 6

Conclusions and Future Research

Directions

6.1 Conclusion

The upcoming generations of wireless networks are envisioned to offer massive connectivity, high throughput, reliable and low-latency communication. This technological revolution is anticipated to unfold a myriad of propitious applications and services such as intelligent transportation systems, augmented reality, industry 4.0, and so forth. These disruptive applications possess stringent requirements of fresh and timely information updates to make crucial decisions. Therefore, in order to fully realize this digital transformation, reliability and timeliness in delivering information must be ensured for these real-time applications. Towards achieving this goal, this dissertation demonstrated multiple solutions and frameworks linked to the realization of timely delivery of information updates for time-sensitive applications, with the assistance of novel technologies and architectures. First, we studied the impact of MEC towards minimizing the AoI. We considered a downlink IoT network that consists of a BS and serves traffic streams from multiple IoT devices. The expected sum AoI was optimized considering the joint impact of random arrivals and unreliable channel conditions. Second, we utilize RIS to diminish the propagation induced impairments of the wireless environments so that a strong channel can be constructed between the sources and the destinations towards achieving the lower AoI. We formulated an optimization problem considering the joint impact of user scheduling and phase-shift matrix optimization. The original problem was decomposed into an outer traffic stream scheduling problem and an inner RIS phase-shift matrix problem. For the outer problem, a deep reinforcement learning based solution was proposed where the traffic stream scheduling is modeled as an MDP and PPO is invoked to solve it. To solve the inner problem, we leveraged SDR approach. Third, we examine the integration of RIS and uplink NOMA scheme to analyze the potential benefits of NOMA over traditional OMA schemes in terms of AoI reduction. In this context, an optimization

problem was formulated to optimize the RIS configuration, the transmit power of IoTDs and their clustering policy. We leveraged bi-level optimization approach to solve power allocation and clustering problem where optimal closed form expressions were derived for power allocation. Finally, we presented a novel RIS-enabled uplink C-NOMA system and investigated its performance gain in terms of AoI reduction against the conventional uplink NOMA and OMA schemes with and without RIS. Simulation results demonstrate that our proposed RIS-empowered uplink C-NOMA scheme achieves higher AoI-reduction compared to all baseline schemes.

6.2 Future Research Directions

Although, this dissertation addressed several research challenges realizing the timeliness requirement of IoT applications by proposing novel architectural solutions, there still exist some interesting research directions that need to be addressed in the future.

- In Chapter 3, a concrete analytical characterization of AoI was provided with an MEC node deployed at the BS to expedite the processing of packets of different traffic streams. In the considered system model, MEC node could process one packet at a time assuming that a single VNF application is running inside MEC node. Future research should focus on extending this framework to realize more dynamic applications by considering multiple VNFs, each running different applications with different processing capabilities. This will make MEC node to serve multiple users carrying different types of requests with different processing requirements in a given time-slot. In such case, resource management at VNFs level should be investigated.

- In Chapter 4, information freshness in RIS-assisted static environment was explored. However, RIS can be mounted on UAVs to achieve ubiquitous wireless connectivity and upgraded network capacity. The RIS-enabled UAVs solution will be more viable than conventional terrestrial (fixed) RISs from the deployment's point of view. The fixed RISs are usually deployed on facades of buildings, which is challenging from the perspective of site acquisition in urban landscape. Moreover, moving towards a dynamic environment, destinations could be the vehicles with different velocities. The higher mobility of vehicles will definitely complicate the design of scheduling and RIS configuration approach, whereas UAVs trajectory is another dimension to be optimized in this setting and will be investigated in a future work.
- In Chapter 5, the integration of RIS in uplink single-input-single-output (SISO) NOMA and C-NOMA based IoT networks was investigated towards the goal of enhancing information freshness. Future work can extend the existing system model of NOMA/C-NOMA system with single antenna at the BS to a more realistic multi-antennas model. In such case, the use of multiple antennas at the BS may benefit in terms of serving multiple C-NOMA pairs of users simultaneously within the same frequency band without any interference between the different pairs. This can be achieved by performing zero-forcing (ZF) beamforming to cancel the inter-pair interference. The challenges in this work will be regarding the acquisition of the channel state information (CSI) of all the links (i.e., between each antenna and the IoT), the design of the optimal ZF precoding matrix jointly with the IoTs pairing policy and the RIS phase shift matrix optimization.

Another future work towards achieving the high spectral efficiency and massive connectivity of IoTs is to investigate other multiple access schemes, such

as, rate splitting multiple access (RSMA). Rate splitting is envisioned as an appealing paradigm for non-orthogonal transmission. More specifically, for interference management and multiple access strategies in 6G networks. RSMA is envisioned to achieve the entire capacity region of the multiple access channel by enabling successive decoding [119]. The user messages are splitted into common and private parts at the transmitter and thus interference is partially decoded and the rest of it is treated as a noise. Precisely, in uplink RSMA system, each user transmits a superposition of two messages with different power levels and the BS uses SIC to decode the received messages (the decoding order for both the private and common messages may be different at the BS for each user) . In this context, optimization of power management and message decoding order is a challenge that needs to be handled for uplink RSMA systems.

Bibliography

- [1] T. Taleb et al. Paper on 6G networking [white paper]. (6G research visions, no. 6). <http://urn.fi/urn:isbn:9789526226842>, 2020.
- [2] Meryem Simsek et al. 5G-enabled tactile internet. *IEEE Journal on Selected Areas in Communications*, 34(3):460–473, 2016.
- [3] Asad Waqar Malik et al. Symbiotic robotics network for efficient task offloading in smart industry. *IEEE Transactions on Industrial Informatics*, 17(7):4594–4601, 2020.
- [4] A. Kosta et al. Age of information: A new concept, metric, and tool. *Foundations and Trends in Networking*, 12(3):162–259, 2017.
- [5] Sanjit Kaul et al. Real-time status: How often should one update? In *IEEE INFOCOM*, pages 2731–2735, 2012.
- [6] A. Alabbasi et al. Joint information freshness and completion time optimization for vehicular networks. *IEEE Trans. Serv. Comput.*, 2020.
- [7] Shuhang Zhang et al. Age of information in a cellular internet of UAVs: Sensing and communication trade-off design. *IEEE Transactions on Wireless Communications*, 19(10):6578–6592, 2020.

- [8] M. Bastopcu et al. Information freshness in cache updating systems. *arXiv preprint arXiv:2004.09475*, 2020.
- [9] M. Emara et al. MEC-enhanced information freshness for safety-critical C-V2X communications. *arXiv preprint arXiv:2003.02495*, 2020.
- [10] I. Kadota et al. Minimizing the age of information in wireless networks with stochastic arrivals. *IEEE Trans. Mobile Comput.*, 2019.
- [11] Praful D Mankar, Zheng Chen, Mohamed A Abd-Elmagid, Nikolaos Pappas, and Harpreet S Dhillon. Throughput and age of information in a cellular-based IoT network. *IEEE Transactions on Wireless Communications*, 20(12):8248–8263, 2021.
- [12] S. Zhang et al. Low-latency and fresh content provision in information-centric vehicular networks. *IEEE Trans. Mobile Comput.*, pages 1–1, 2020.
- [13] S. Abedin et al. Data freshness and energy-efficient UAV navigation optimization: A deep reinforcement learning approach. *arXiv preprint arXiv:2003.04816*, 2020.
- [14] H. Huimin et al. AoI-minimal trajectory planning and data collection in UAV-assisted wireless powered IoT networks. *IEEE Internet Things J.*, 2020.
- [15] S. Zhang et al. Towards fresh and low-latency content delivery in vehicular networks: An edge caching aspect. In *IEEE WCSP*, pages 1–6, 2018.
- [16] Xuying Zhou et al. Age of information aware content resale mechanism with edge caching. *IEEE Transactions on Communications*, pages 1–1, 2021.
- [17] Zhenyu Liu et al. Age of information-based scheduling for wireless device-to-device communications using deep learning. In *IEEE WCNC*, pages 1–6, 2021.

- [18] Mingyan Li et al. Age-of-information aware scheduling for edge-assisted industrial wireless networks. *IEEE Transactions on Industrial Informatics*, 17(8):5562–5571, 2021.
- [19] A. Maatouk et al. On the age of information in a CSMA environment. *IEEE/ACM Transactions on Networking*, 28(2):818–831, 2020.
- [20] R.D. Yates et al. The age of information: Real-time status updating by multiple sources. *IEEE Trans. Inf. Theory*, 65(3):1807–1827, 2018.
- [21] Y. Hsu. Age of information: Whittle index for scheduling stochastic arrivals. In *IEEE International Symposium on Information Theory (ISIT)*, pages 2634–2638, 2018.
- [22] Chengzhang Li et al. Minimizing age of information under general models for IoT data collection. *IEEE Transactions on Network Science and Engineering*, 2019.
- [23] Howard H. Yang et al. Understanding age of information in large-scale wireless networks. *IEEE Transactions on Wireless Communications*, 20(5):3196–3210, 2021.
- [24] Y. Mao et al. A survey on mobile edge computing: The communication perspective. *IEEE Commun. Surveys Tuts.*, 19(4):2322–2358, 2017.
- [25] W. Feng et al. Joint offloading and computing optimization in wireless powered Mobile-edge computing systems. *IEEE Trans. Wireless Commun.*, 17(3):1784–1797, 2017.
- [26] L. Chen-Feng et al. Latency and reliability-aware task offloading and resource allocation for mobile edge computing. In *Proc. IEEE GLOBECOM Workshops*, pages 1–7, 2017.

- [27] M. Jia et al. Heuristic offloading of concurrent tasks for computation-intensive applications in mobile cloud computing. In *Proc. IEEE INFOCOM*, pages 352–357. IEEE, 2014.
- [28] Q. Kuang et al. Age-of-information for computation-intensive messages in mobile edge computing. In *Proc. IEEE WCSP*, pages 1–6, 2019.
- [29] L. Liu et al. Timely updates in MEC-assisted status update systems: Joint task generation and computation offloading scheme. *China Communications*, 17(8):168–186, 2020.
- [30] Long Liu et al. Optimizing information freshness in MEC-assisted status update systems with heterogeneous energy harvesting devices. *IEEE Internet of Things Journal*, 2021.
- [31] A. Zakeri et al. A unified framework for joint energy and AoI optimization via deep reinforcement learning for NOMA MEC-based networks. *arXiv preprint arXiv:2011.00436*, 2020.
- [32] Qiaobin Kuang et al. Age-of-information for computation-intensive messages in mobile edge computing. In *11th International Conference on Wireless Communications and Signal Processing (WCSP)*, pages 1–6, 2019.
- [33] Zhaolong Ning et al. Mobile edge computing enabled 5g health monitoring for internet of medical things: A decentralized game theoretic approach. *IEEE Journal on Selected Areas in Communications*, 39(2):463–478, 2021.
- [34] Rui Han et al. Age of information and performance analysis for UAV-Aided IoT systems. *IEEE Internet of Things Journal*, pages 1–1, 2021.
- [35] Q. Wu and R. Zhang. Intelligent reflecting surface enhanced wireless network

- via joint active and passive beamforming. *IEEE Transactions on Wireless Communications*, 18(11):5394–5409, 2019.
- [36] W. Tang et al. Wireless communications with reconfigurable intelligent surface: Path loss modeling and experimental measurement. *IEEE Transactions on Wireless Communications*, pages 1–1, 2020.
- [37] Y. Chen et al. Reconfigurable intelligent surface assisted device-to-device communications. *IEEE Transactions on Wireless Communications*, pages 1–1, 2020.
- [38] Z. Yang et al. Beamforming design for multiuser transmission through reconfigurable intelligent surface. *IEEE Transactions on Communications*, pages 1–1, 2020.
- [39] S. Atapattu et al. Reconfigurable intelligent surface assisted two-way communications: Performance analysis and optimization. *IEEE Transactions on Communications*, 68(10):6552–6567, 2020.
- [40] S. Hong et al. Artificial-noise-aided secure MIMO wireless communications via intelligent reflecting surface. *IEEE Transactions on Communications*, 68(12):7851–7866, 2020.
- [41] Moataz Samir et al. Optimizing age of information through aerial reconfigurable intelligent surfaces: A deep reinforcement learning approach. *arXiv preprint arXiv:2011.04817*, 2020.
- [42] Yue Xiu et al. Reconfigurable intelligent surfaces aided mmWave NOMA: Joint power allocation, phase shifts, and hybrid beamforming optimization. *IEEE Transactions on Wireless Communications*, 20(12):8393–8409, 2021.

- [43] Yiqing Li et al. Joint beamforming design in multi-cluster MISO NOMA reconfigurable intelligent surface-aided downlink communication networks. *IEEE Transactions on Communications*, 69(1):664–674, 2020.
- [44] Gang Yang et al. Reconfigurable intelligent surface-assisted non-orthogonal multiple access. *IEEE Transactions on Wireless Communications*, 20(5):3137–3151, 2021.
- [45] Jiakuo Zuo et al. Intelligent reflecting surface enhanced millimeter-wave NOMA systems. *IEEE Communications Letters*, 24(11):2632–2636, 2020.
- [46] Mohamed Elhattab et al. RIS-Assisted Joint Transmission in a Two-Cell Downlink NOMA Cellular System. *IEEE J. Sel. Areas Commun.*, 40(4):1270–1286, 2022.
- [47] Tianwei Hou et al. Reconfigurable intelligent surface aided NOMA networks. *IEEE J. Sel. Areas Commun.*, 38(11):2575–2588, 2020.
- [48] Chenyu Wu et al. Coverage Characterization of STAR-RIS Networks: NOMA and OMA. *IEEE Commun. Lett.*, 25(9):3036–3040, 2021.
- [49] Zhe Zhang et al. Improving Physical Layer Security for Reconfigurable Intelligent Surface Aided NOMA 6G Networks. *IEEE Trans. Veh. Technol.*, 70(5):4451–4463, 2021.
- [50] Min Fu et al. Intelligent reflecting surface for downlink non-orthogonal multiple access networks. In *2019 IEEE Globecom Workshops (GC Wkshps)*, pages 1–6. IEEE, 2019.
- [51] Jiakuo Zuo et al. Reconfigurable Intelligent Surface Assisted Cooperative Non-Orthogonal Multiple Access Systems. *IEEE Trans. Commun.*, 69(10):6750–6764, 2021.

- [52] Mohamed Elhattab et al. Reconfigurable intelligent surface enabled full-duplex/half-duplex cooperative non-orthogonal multiple access. *IEEE Transactions on Wireless Communications*, 2021.
- [53] Ali Muhammad et al. Minimizing Age of Information in Multi-Access Edge Computing-assisted IoT Networks. *IEEE Internet of Things Journal*, pages 1–1, 2021.
- [54] Ali Muhammad et al. Leveraging Reconfigurable Intelligent Surface to Minimize Age of Information in Wireless Networks. In *Proc. IEEE ICC*, Seoul, South Korea, May 2022.
- [55] Ali Muhammad et al. Age of Information Optimization in a RIS-Assisted Wireless Network. *IEEE Trans. Network and Service Management*, 2021.
- [56] Ali Maatouk et al. Minimizing the age of information: NOMA or OMA? In *Proc. IEEE INFOCOM WKSHPs*, Paris, France, May 2019.
- [57] A. Muhammad et al. Optimizing Age of Information in RIS-Empowered Uplink Cooperative NOMA Networks. 2022.
- [58] A. Muhammad et al. Optimizing Information Freshness in RIS-assisted NOMA-based IoT Networks. 2022.
- [59] A. Muhammad et al. Optimizing Information Freshness Leveraging Multi-RISs in NOMA-based IoT Networks . In *2022 IEEE Global Communications Conference (GLOBECOM)*, 2022.
- [60] Mohamed A. Abd-Elmagid et al. AoI-Optimal Joint Sampling and Updating for Wireless Powered Communication Systems. *IEEE Transactions on Vehicular Technology*, 69(11):14110–14115, 2020.

- [61] Abd-Elmagid et al. On the role of age of information in the Internet of Things. *IEEE Commun. Magazine*, 57(12):72–77, 2019.
- [62] ETSI. Multi-access edge computing (MEC). [online] available: <https://www.etsi.org/technologies/multi-access-edge-computing>, 2020.
- [63] Pawani Porambage, Jude Okwuibe, Madhusanka Liyanage, Mika Ylianttila, and Tarik Taleb. Survey on multi-access edge computing for internet of things realization. *IEEE Communications Surveys & Tutorials*, 20(4):2961–2991, 2018.
- [64] Bin Cao, Long Zhang, Yun Li, Daquan Feng, and Wei Cao. Intelligent offloading in multi-access edge computing: A state-of-the-art review and framework. *IEEE Communications Magazine*, 57(3):56–62, 2019.
- [65] S. Gong et al. Toward smart wireless communications via intelligent reflecting surfaces: A contemporary survey. *IEEE Communications Surveys & Tutorials*, 22(4):2283–2314, 2020.
- [66] Ludek Subrt and Pavel Pechac. Intelligent walls as autonomous parts of smart indoor environments. *IET communications*, 6(8):1004–1010, 2012.
- [67] Qingqing Wu, Shuowen Zhang, Beixiong Zheng, Changsheng You, and Rui Zhang. Intelligent reflecting surface-aided wireless communications: A tutorial. *IEEE Transactions on Communications*, 69(5):3313–3351, 2021.
- [68] Marco Di Renzo et al. Smart radio environments empowered by reconfigurable intelligent surfaces: How it works, state of research, and the road ahead. *IEEE Journal on Selected Areas in Communications*, 38(11):2450–2525, 2020.
- [69] Qingqing Wu and Rui Zhang. Towards Smart and Reconfigurable Environment: Intelligent Reflecting Surface Aided Wireless Network. *IEEE Communications Magazine*, 58(1):106–112, 2020.

- [70] Shimin Gong et al. Toward smart wireless communications via intelligent reflecting surfaces: A contemporary survey. *IEEE Communications Surveys & Tutorials*, 22(4):2283–2314, 2020.
- [71] Darian Pérez-Adán, Óscar Fresnedo, José P González-Coma, and Luis Castedo. Intelligent Reflective Surfaces for Wireless Networks: An Overview of Applications, Approached Issues, and Open Problems. *Electronics*, 10(19):2345, 2021.
- [72] Xin Liu et al. Uplink resource allocation for NOMA-based hybrid spectrum access in 6G-enabled cognitive Internet of Things. *IEEE Internet of Things Journal*, 8(20):15049–15058, 2020.
- [73] Jinyong Cheon and Ho-Shin Cho. Power allocation scheme for non-orthogonal multiple access in underwater acoustic communications. *Sensors*, 17(11):2465, 2017.
- [74] Ferdi Kara et al. On the error performance of cooperative-NOMA with statistical CSIT. *IEEE Commun. Lett.*, 23(1):128–131, 2018.
- [75] Md Shipon Ali, Hina Tabassum, and Ekram Hossain. Dynamic user clustering and power allocation for uplink and downlink non-orthogonal multiple access (NOMA) systems. *IEEE access*, 4:6325–6343, 2016.
- [76] Phúc Hũu et al. A low-complexity framework for joint user pairing and power control for cooperative NOMA in 5G and beyond cellular networks. *IEEE Trans. Commun.*, 68(11):6737–6749, 2020.
- [77] Yuanwei Liu, Shuowen Zhang, Xidong Mu, Zhiguo Ding, Robert Schober, Nao-fal Al-Dhahir, Ekram Hossain, and Xuemin Shen. Evolution of NOMA Toward Next Generation Multiple Access (NGMA) for 6G. *IEEE Journal on Selected Areas in Communications*, 40(4):1037–1071, 2022.

- [78] Zhiguo Ding et al. Cooperative non-orthogonal multiple access in 5G systems. *IEEE Commun. Lett.*, 19(8):1462–1465, 2015.
- [79] Yingying Zhang et al. Performance analysis of a novel uplink cooperative NOMA system with full-duplex relaying. *IET Communications*, 12(19):2408–2417, 2018.
- [80] Dehuan Wan et al. Non-orthogonal multiple access for cooperative communications: Challenges, opportunities, and trends. *IEEE Wireless Communications*, 25(2):109–117, 2018.
- [81] Linglong Dai et al. A survey of non-orthogonal multiple access for 5G. *IEEE communications surveys & tutorials*, 20(3):2294–2323, 2018.
- [82] Qing He, Di Yuan, and Anthony Ephremides. Optimal link scheduling for age minimization in wireless systems. *IEEE Transactions on Information Theory*, 64(7):5381–5394, 2017.
- [83] Igor Kadota et al. Scheduling algorithms for optimizing age of information in wireless networks with throughput constraints. *IEEE/ACM Transactions on Networking*, 27(4):1359–1372, 2019.
- [84] Sami Kekki et al. MEC in 5G networks. *ETSI White Paper No. 28*, 2018.
- [85] Sanjit K. Kaul et al. Status updates through queues. In *46th Annual Conference on Information Sciences and Systems (CISS)*, pages 1–6, 2012.
- [86] Moataz Samir et al. Online altitude control and scheduling policy for minimizing aoi in UAV-assisted IoT wireless networks. *IEEE Transactions on Mobile Computing*, 2020.

- [87] Bo Zhou and Walid Saad. Joint status sampling and updating for minimizing age of information in the internet of things. *IEEE Transactions on Communications*, 67(11):7468–7482, 2019.
- [88] Vishrant Tripathi and Sharayu Moharir. Age of Information in Multi-Source Systems. In *IEEE Global Communications Conference*, pages 1–6, 2017.
- [89] Bejjipuram Sombabu and Sharayu Moharir. Age-of-information based scheduling for multi-channel systems. *IEEE Transactions on Wireless Communications*, 19(7):4439–4448, 2020.
- [90] Shaoling Hu and Wei Chen. Balancing data freshness and distortion in real-time status updating with lossy compression. In *IEEE (INFOCOM WKSHPS)*, pages 13–18, 2020.
- [91] Daniel Jaramillo-Ramírez et al. Coordinated multi-point transmission with imperfect CSI and other-cell interference. *IEEE Transactions on Wireless Communications*, 14(4):1882–1896, 2015.
- [92] Parag Aggarwal and Vivek Ashok Bohara. Analytical characterization of dual-band multi-user MIMO-OFDM system with nonlinear transmitter constraints. *IEEE Transactions on Communications*, 66(10):4536–4549, 2018.
- [93] Bo Zhou, Walid Saad, Mehdi Bennis, and Petar Popovski. Risk-aware optimization of age of information in the internet of things. In *ICC 2020-2020 IEEE International Conference on Communications (ICC)*, pages 1–6. IEEE, 2020.
- [94] Xianfu Chen et al. Age of information aware radio resource management in vehicular networks: A proactive deep reinforcement learning perspective. *IEEE Transactions on wireless communications*, 19(4):2268–2281, 2020.

- [95] M. Samir et al. UAV trajectory planning for data collection from time-constrained IoT devices. *IEEE Trans. Wireless Commun.*, 19(1):34–46, 2019.
- [96] Yuanbin Chen et al. QoS-driven spectrum sharing for reconfigurable intelligent surfaces (RISs) aided vehicular networks. *IEEE Transactions on Wireless Communications*, 20(9):5969–5985, 2021.
- [97] Vasilis Maglogiannis et al. Experimental V2X Evaluation for C-V2X and ITS-G5 Technologies in a Real-Life Highway Environment. *IEEE Trans. Netw. Service Manag.*, 2021.
- [98] Shivani Dhok et al. Non-Linear Energy Harvesting in RIS-assisted URLLC Networks for Industry Automation. *IEEE Transactions on Communications*, 69(11):7761–7774, 2021.
- [99] Wanli Ni et al. Resource allocation for multi-cell IRS-aided NOMA networks. *IEEE Transactions on Wireless Communications*, 20(7):4253–4268, 2021.
- [100] Mohamed Elhattab et al. RIS-Assisted Joint Transmission in a Two-Cell Downlink NOMA Cellular System. *IEEE Journal on Selected Areas in Communications*, 2022.
- [101] Zhen-Qing He et al. Cascaded channel estimation for large intelligent metasurface assisted massive MIMO. *IEEE Wireless Communications Letters*, 9(2):210–214, 2019.
- [102] Li Wei et al. Channel estimation for RIS-empowered multi-user MISO wireless communications. *IEEE Transactions on Communications*, 69(6):4144–4157, 2021.

- [103] Antzela Kosta et al. Non-linear age of information in a discrete time queue: Stationary distribution and average performance analysis. In *IEEE International Conference on Communications (ICC)*, pages 1–6, 2020.
- [104] Moataz Samir et al. Online altitude control and scheduling policy for minimizing aoi in uav-assisted iot wireless networks. *IEEE Transactions on Mobile Computing*, pages 1–1, 2020.
- [105] Jonathan F Bard. *Practical bilevel optimization: algorithms and applications*, volume 30. Springer Science & Business Media, 2013.
- [106] Benedetta Picano et al. Aging and Delay Analysis Based on Lyapunov Optimization and Martingale Theory. *IEEE Trans. Veh. Technol.*, 70(8):8216–8226, 2021.
- [107] Qian Wang et al. Optimizing Information Freshness via Multiuser Scheduling With Adaptive NOMA/OMA. *IEEE Trans. Wireless Commun.*, 21(3):1766–1778, 2022.
- [108] Phúc Hũu et al. A Low-Complexity Framework for Joint User Pairing and Power Control for Cooperative NOMA in 5G and Beyond Cellular Networks. *IEEE Trans. Commun.*, 68(11):6737–6749, 2020.
- [109] Zhiguo Ding et al. On the impact of phase shifting designs on IRS-NOMA. *IEEE Wireless Commun. Lett.*, 9(10):1596–1600, 2020.
- [110] Biplav Choudhury et al. AoI-minimizing Scheduling in UAV-relayed IoT Networks. In *IEEE MASS*, Denver, CO, USA, Oct 2021.
- [111] Min Fu et al. Reconfigurable Intelligent Surface Empowered Downlink Non-Orthogonal Multiple Access. *IEEE Trans. Commun.*, 69(6):3802–3817, 2021.

- [112] D. Gale and L. S. Shapley. College admissions and the stability of marriage. *The American Mathematical Monthly*, 69(1):9–15, 1962.
- [113] Jiakuo Zuo et al. Resource Allocation in Intelligent Reflecting Surface Assisted NOMA Systems. *IEEE Transactions on Communications*, 68(11):7170–7183, 2020.
- [114] Gang Liu et al. Hybrid half-duplex/full-duplex cooperative non-orthogonal multiple access with transmit power adaptation. *IEEE Transactions on Wireless Communications*, 17(1):506–519, 2017.
- [115] Xinwei Yue et al. Spatially random relay selection for full/half-duplex cooperative NOMA networks. *IEEE Trans. Commun.*, 66(8):3294–3308, 2018.
- [116] Rajat Talak et al. Improving age of information in wireless networks with perfect channel state information. *IEEE/ACM Trans. Networking*, 28(4):1765–1778, 2020.
- [117] Rajshekhar Vishweshwar Bhat et al. Throughput maximization with an average age of information constraint in fading channels. *IEEE Trans. Wireless Commun.*, 20(1):481–494, 2020.
- [118] A. Muhammad et al. Optimizing Information Freshness in RIS-assisted NOMA-based IoT Networks. *IEEE Transactions on Vehicular Technology*, 2022.
- [119] Zhaohui Yang, Mingzhe Chen, Walid Saad, Wei Xu, and Mohammad Shikh-Bahaei. Sum-rate maximization of uplink rate splitting multiple access (RSMA) communication. *IEEE Transactions on Mobile Computing*, 2020.